Title
Deciphering the Organization of Protein Complexes in Toxoplasma gondii using a Photoactivated Unnatural Amino Acid Crosslinking System

Author
Choi, Charles Paul

Publication Date
2019

Peer reviewed|Thesis/dissertation

UNIVERSITY OF CALIFORNIA

Los Angeles

Deciphering the Organization of Protein Complexes in *Toxoplasma gondii* using a Photoactivated Unnatural Amino Acid Crosslinking System

A dissertation submitted in partial satisfaction

of the requirements for the degree Doctor of Philosophy

in Molecular Biology

by

Charles Paul Choi

2019

ABSTRACT OF THE DISSERTATION

Deciphering the Organization of Protein Complexes in *Toxoplasma gondii* using a Photoactivated Unnatural Amino Acid Crosslinking System

by

Charles Paul Choi

Doctor of Philosophy in Molecular Biology

University of California, Los Angeles, 2019

Professor Peter John Bradley, Chair

The phylum Apicomplexa consists of obligate intracellular parasites, many of which are prevalent pathogens of medical and veterinary importance. *Toxoplasma gondii* is one of the most successful parasites in the world, estimated to infect one-third of the human population, and poses potentially life-threatening complications in immunocompromised individuals and during a primary infection of a developing fetus. *T. gondii* also serves as a model organism for other apicomplexans such as *Plasmodium* spp., the causative agent of malaria, due to its ease of culture, high rate of transformation, and a rich set of tools available for genetic manipulation.

A common structure found in this phylum is the inner membrane complex (IMC), which is made of both membrane and cytoskeletal components and lays underneath the plasma membrane to provide a framework for replication and motility. An intermediate filament layer confers rigidity and tensile strength to the cell and these filaments are believed to be composed of a family of

proteins called the alveolins. However, the exact organization of the proteins that make up this network is unknown and traditional methods for studying protein interactions are inadequate due to the detergent-insoluble nature of the IMC cytoskeleton.

Here, I successfully implement an unnatural amino acid (UAA) system in *T. gondii* using the photoactivated crosslinking UAA *p*-azidophenylalanine to study the IMC and other macromolecular complexes. This technique takes advantage of an orthogonal amber stop codon suppressor tRNA and cognate mutant aminoacyl-tRNA synthetase pair. In this system, the endogenous translational machinery directly incorporates Azi into the primary structure of a protein of interest. Upon exposure to ultraviolet light, Azi forms a covalent crosslinking between bait and prey proteins, enabling precise identification of the binding partner and overcoming the limitations of other protein interaction methods. Site-specific incorporation of Azi also maps the binding interface on the bait protein, providing structural information of the interaction.

After confirming that the requisite amber suppressor tRNA and aminoacyl-tRNA synthetase function properly and Azi can be used to crosslink protein complexes in the parasite, I applied this system towards IMC-localizing protein 1 (ILP1), which is a critical IMC protein involved in cytoskeletal integrity. I determine that ILP1 binds to three alveolins and one other cytoskeletal IMC protein, which is the first demonstration of interaction between components of the IMC intermediate filament network. I also explore the application towards a key protein complex that anchors the rhoptries, the secretory organelle that apicomplexans use to actively invade their host cell. This site-specific photoactivated UAA crosslinking system is a completely new approach to studying important protein complexes in *T. gondii* and provides new insight into apicomplexan biology.

The dissertation of Charles Paul Choi is approved.

David A. Campbell

Elissa A. Hallem

Kent L. Hill

James Akira Wohlschlegel

Peter John Bradley, Committee Chair

University of California, Los Angeles

2019

DEDICATION

To my family,

this doctorate is for you.

TABLE OF CONTENTS

LIST OF FIGURES

LIST OF TABLES

ACKNOWLEDGEMENTS

The work in this dissertation was performed in the laboratory of my mentor Professor Peter J. Bradley of the Molecular Biology Institute at UCLA. Perhaps it was by luck that I ended up working with him, but I could not have asked for a better mentor. Thank you for all the countless hours spent on advice, discussions, arguments, text revisions, presentation practice, jokes, but most importantly, sharing a beer at the end of a deadline. Thanks also to the past and present members of the Bradley lab, particularly Drs. Allen Chen and Santhosh Nadipuram, for your camaraderie and support. Thank you very much to the other members of my committee, Professors David Campbell, Elissa Hallem, Kent Hill, and James Wohlschlegel, for providing your precious time, insight, and resources to guide my project to where it is now.

Chapter 2 is a version of a manuscript currently in submission: Charles P. Choi, Andy S. Moon, Peter S. Back, Yasaman Jami-Alahmadi, Ajay A. Vashisht, James A. Wohlschlegel, and Peter J. Bradley. A photoactivatable crosslinking system in *Toxoplasma gondii* reveals organization of the parasite inner membrane complex. Andy Moon performed the initial immunoprecipitation of ILP1 and Peter Back generated antibodies used in the study. Yasaman Jami-Alahmadi, Ajay Vashisht, and the rest of the James Wohlschlegel lab performed the mass spectrometric analysis and were instrumental in identifying the unknown interactions. Peter Bradley was the principal investigator.

This work was supported by the Ruth L. Kirschstein National Research Service Award GM007185 and the Philip J. Whitcome Fellowship to Charles Choi. This work was also supported by NIH grant R01 AI123360 and R21 AI135661 to Peter Bradley, and NIH grant R01 GM089778 to James Wohlschlegel.

I could not have finished this long and arduous journey called higher education without the immense support of my parents, brother, grandparents, and relatives who have been sending their love across the country for the better part of a decade. Thank you to all the friends that I have known for that decade who have made Los Angeles my second home.

VITA

2009	Semifinalist Intel Science Talent Search
2013	Bachelor of Science, Chemical Engineering University of California, Los Angeles
2014-2015	Teaching Assistant Department of MIMG University of California, Los Angeles
2015-2016	Predoctoral Fellow Cellular and Molecular Biology Training Grant
2016-2018	Predoctoral Fellow Philip J. Whitcome Fellowship

Publications and Presentations

Singh, M., Choi, C. P., & Feigon, J. (2013). xRRM: a new class of RRM found in the telomerase La family protein p65. *RNA Biology*, 10(3), 353–359. https://doi.org/10.4161/rna.23608

Chen, A. L., Moon, A. S., Bell, H. N., Huang, A. S., Vashisht, A. A., Toh, J. Y., Lin, A. H., Nadipuram, S. M., Kim, E. W., Choi, C. P., et al. (2017). Novel insights into the composition and function of the Toxoplasma IMC sutures. *Cellular Microbiology*, *19*(4). https://doi.org/10.1111/cmi.12678

Adaptation of BioID for Examination of Rhoptry Organellar Positioning in *Toxoplasma gondii*. Poster presentation at the Southern California Eukaryotic Pathogen Symposium at UC Riverside, November 2014.

Crosslinking methods for examining protein interactions critical for invasion by *Toxoplasma gondii.* Poster presentation at the MBI Annual Retreat, April 2015.

Crosslinking methods for examining protein interactions critical for invasion by *Toxoplasma gondii,* Poster presentation at the Southern California Eukaryotic Pathogen Symposium at UC Riverside, November 2015.

The Mechanism of Apical Rhoptry Tethering in *Toxoplasma gondii*. Oral presentation at the MBI Student Seminar Series, January 2016.

Examining rhoptry protein interactions critical for invasion by *Toxoplasma gondii*. Poster presentation at the MBI Annual Retreat, April 2016.

Examining rhoptry protein interactions critical for invasion by *Toxoplasma gondii*. Poster presentation at the Southern California Eukaryotic Pathogen Symposium at UC Riverside, November 2016.

Studying Apical Rhoptry Tethering in *Toxoplasma* Using an Unnatural Amino Acid System. Oral presentation at the monthly UCLA Joint Parasitology Group Meeting, April 2017.

Studying Apical Rhoptry Tethering in *Toxoplasma* Using an Unnatural Amino Acid System. Oral presentation at the MBI Annual Retreat, April 2017.

Studying protein-protein interactions in *Toxoplasma* using a photocrosslinkable unnatural amino acid system. Poster presentation at Toxo14: The 14th biennial conference of the *Toxoplasma gondii* research community, June 2017.

A photocrosslinkable unnatural amino acid system to study the *Toxoplasma gondii* inner membrane complex. Oral presentation at the MBI Student Seminar Series, February 2018.

A photocrosslinkable unnatural amino acid system to study the *Toxoplasma gondii* inner membrane complex. Poster presentation at the MBI Annual Retreat, March 2018.

A photocrosslinkable unnatural amino acid system to study the *Toxoplasma gondii* inner membrane complex. Oral presentation at the MBI Recruitment Weekend, January 2019.

CHAPTER 1:

Introduction

1.1 – The Apicomplexan *Toxoplasma gondii*

1.1.1 - Significance

Toxoplasma gondii is one of the most successful parasites in the world. The sole member of its genus, it belongs to the phylum Apicomplexa, a broad group of parasitic organisms with substantial medical and zoonotic impact. Estimated to have infected at least one-third of the human population, it is acquired through the consumption of cyst forms present in inadequately cooked or raw meat from an infected animal or feline feces (Flegr et al., 2014). A primary infection can also be vertically transmitted from a pregnant mother to her developing child. Depending on many conditions such as eating habits, water purity, hygiene standards, and climate, the rates of infection vary widely, with as low as 3% in East Asian countries and up to ~70% in tropical areas of South American and African countries (Flegr et al., 2014). Compared to the United States (22.5%), countries where undercooked meat is commonly eaten, such as France (47%) and Germany (50%), exhibit elevated seroprevalence (Flegr et al., 2014; Jones et al., 2001).

Non-congenital infection is typically innocuous in healthy individuals, but clinical toxoplasmosis can manifest in certain scenarios. During an acquired acute infection, mild flu-like symptoms may occur as a normal course of adaptive immunity. In more severe cases, pulmonary toxoplasmosis results in atypical pneumonia, mimicking the more common etiologic agents *Mycoplasma pneumoniae* and *Chlamydia pneumoniae* (de Souza Giassi et al., 2014). While the chronic infection is normally rendered latent by a competent immune system, the immune privileged nature of the eye also enables necrotic proliferation of the parasite, causing retinal scarring and potential blindness (Holland et al., 2002). This ocular toxoplasmosis is estimated to affect 2% of all infected individuals, regardless of immune status (Holland, 2003; Jones et al., 2006). However, the most severe complication can arise from reactivation of a chronic infection

that has laid dormant for years in immunocompromised or immunosuppressed patients (CD4 count below 100/mL), where toxoplasmic encephalitis can lead to neurological complications or death (Luft & Remington, 1992). Historically, toxoplasmic encephalitis posed a substantial danger to AIDS patients, observed in 24% of cases in 1990 (Grant et al., 1990). However, with the advent of effective antiretroviral therapies, HIV-associated toxoplasmosis hospitalizations in the United States reduced from 10583 cases in 1995 down to 3643 cases in 2001, and 2985 cases in 2008 (Jones & Roberts, 2012). Nevertheless, toxoplasmic encephalitis remains the leading cause of brain mass lesions in AIDS patients (Marra, 2018). Prophylaxis for toxoplasmosis must also be considered for non-HIV immunodeficiencies such as lymphomas, related immunosuppressive chemotherapies, and even solid organ transplants (Khurana & Batra, 2016).

Congenital toxoplasmosis is most commonly developed when a pregnant mother contracts a primary *T. gondii* infection, although rare instances of a seropositive mother either becoming immunocompromised or infected with a more virulent strain have been reported (Maldonado et al., 2017). Chorioretinitis, intracranial calcifications, and hydrocephaly are common indicators for afflicted infants, while premature birth, miscarriage, or stillbirth may happen in severe cases. The gestational age of the fetus at the time of infection factors into the severity of the disease; first trimester infections, although rarer, are more devastating than those in the later trimesters (Lindsay & Dubey, 2011). The seroprevalence among women of childbearing age in the United States is estimated to be around 15%. Therefore, the remaining 85% of seronegative women are at risk of contracting a primary *Toxoplasma* infection during pregnancy and thus are at danger of transmitting congenital toxoplasmosis to their unborn child (Jones et al., 2001). Administration of antibiotics such as spiramycin or pyrimethamine-sulfadiazine to a newly infected mother is recommended to mitigate the incidence or effects of vertically transmitted toxoplasmosis

(Montoya & Liesenfeld, 2004). In France, due to the increased risk of *T. gondii* infection, monthly screens for seroconversion of at-risk mothers enables a rapid response to start treatment upon infection (Peyron et al., 2017). In summary, *T. gondii* is a globally prevalent opportunistic pathogen that poses potentially life-threatening risks if untreated.

1.1.2 - Discovery and history

First described in 1908 independently by Nicolle and Manceaux in the tissue of the gundi (*Ctenodactylus gundi*), a small desert rodent, and by Splendore in the tissue of a rabbit, this eukaryotic parasite was first called *Leishmania gondii* due to the presence of a large and small chromatin body, with the smaller of the two thought to be a *Leishmania* kinetoplast but now known to be the apicoplast organelle (Morrissette & Ajioka, 2009; Nicolle & Manceaux, 1908; Splendore, 1908). Subsequent morphological studies by the two groups eventually lead to the classification of this parasite as the new species *Toxoplasma gondii*, named after the unique shape (*toxon* being Greek for "bow") and the original source (gundi). The first human infection was described when *T. gondii* was cultured from postmortem central nervous system samples from a neonatal infant who suffered from seizures, respiratory issues, and chorioretinitis (Wolf et al., 1939). Discovery of the oocyst form of the parasite in the definitive cat host in the 1970s conclusively categorized *T. gondii* as a coccidian pathogen (Dubey, 2009). Since then, infections have been identified in hundreds of mammalian and avian species, indicating that any warm-blooded animal can serve as an intermediate host (Hill et al., 2005).

Genotyping of isolated strains of *T. gondii* resulted in the initial identification of three lineages in North America and Europe: types I, II, and III (Howe & Sibley, 1995). Type I is considered the most virulent genotype (LD_{100} of 1 parasite in a laboratory mouse infection) and

has been associated with the more severe presentations of toxoplasmosis while only composing around 20% of the 106 strains analyzed. The RH strain, first described by Albert Sabin and named after the child from which it was isolated, has become the *de facto* type I strain used in the laboratory and is the parent strain used in this dissertation (Sabin, 1941). Type II is the most commonly encountered genotype of *Toxoplasma* in human infection and is attributed to more muted yet still potentially life-threatening manifestations (Boothroyd & Grigg, 2002). These strains, with an LD_{50} of ~10^3 parasites in mice and an ability to form brain cysts (unlike the lab-adapted hypervirulent type I strains), are used for *in vivo* animal studies. Type III parasites are the least virulent genotype (LD_{50} of ~10^4) and mostly associated with animal infections (Lim et al., 2013). More recently, a new lineage designated type 12 has been defined as endemic to many animal species in North America (Khan et al., 2011). Phylogenetically divergent from type II, this new genotype nevertheless shares similar pathogenicity (i.e. moderate virulence and development of a dormant chronic infection). With the advent of improved serological testing, it has become clear that the global prevalence of particular genotypes has a substantial effect on clinical presentation. For example, type I and type III parasites are more prevalent in the United States, where there is a higher incidence of congenital toxoplasmosis-related prematurity and disease compared to European countries, where type II is the dominant lineage (McLeod et al., 2012). The first high-throughput gene mapping effort for *T. gondii* was the generation of expressed sequence tags (EST) from complementary DNA (cDNA) (Ajioka et al., 1998; Wan et al., 1996). Whole genome sequencing of the *T. gondii* type II strain ME49 followed and revealed a ~65 Mbp genome composed of 14 chromosomes (Khan et al., 2005). The online resource ToxoDB (http://ToxoDB.org) was initiated to organize the new genomic sequences and other rapidly progressing omics, and has proven to become an invaluable resource for the *T. gondii* research

community (Gajria et al., 2008; Kissinger et al., 2003). Since then, this database has been regularly updated with transcriptomics, RNA-Seq, and proteomic evidence to assemble a comprehensive archive of knowledge about *T. gondii* and closely related apicomplexans. During the span of my predoctoral work, useful datasets such as cell cycle expression profiles and a genome-wide CRISPR/Cas9 knockout screen had been instrumental in my experimental design (Behnke et al., 2010; Sidik et al., 2016).

1.1.3 – Life cycle

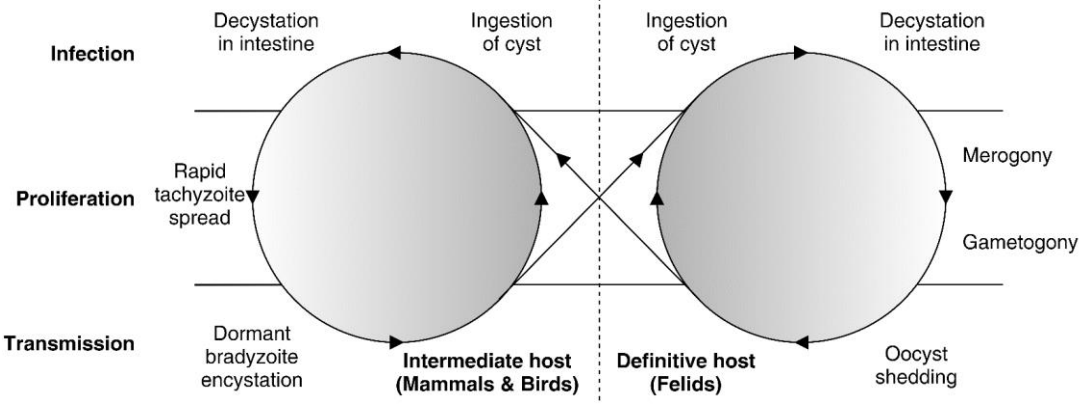

Figure 1-1. *Toxoplasma gondii* life cycle. *T. gondii* can infect a wide range of mammals and birds as intermediate hosts, but only felids can act as definitive hosts. Infection is acquired through ingestion of encysted forms of the parasite, either as dormant bradyzoite tissue cysts, or oocysts. In intermediate hosts, parasites invade intestinal epithelial cells, cross the epithelium, and proliferate to other regions of the body, such as the brain. Eventual suppression by the immune system induces formation of immune-evasive bradyzoite cysts. In the definitive host, parasites undergo sexual reproduction in the intestine and differentiate into oocysts, which are shed in the feces and are extremely resilient to environmental conditions.

T. gondii is facultatively heteroxenous, with both domestic and wild cats (family Felidae) acting as the definitive host and warm-blooded animals as intermediate hosts (Figure 1-1). In both cases, infection is caused by the ingestion of either bradyzoite ("slow growing") tissue cysts or feline-derived oocysts (Robert-Gangneux & Dardé, 2012). Both encysted forms are resistant to the

gastric environment of the stomach and rupture when they reach the intestines. The parasites which emerge from the oocysts are called sporozoites, while reactivated bradyzoites differentiate back into tachyzoites ("fast growing"). Although both sporozoites and tachyzoites are capable of intracellularly infecting host cells, it has been shown that sporozoites have comparatively more invasion-related secretory organelles, suggesting that this life stage is specialized for rapid infection (Dubey et al., 1998). In the cat gut, the parasite infects an intestinal epithelium cell and undergoes schizogony, where cytokinesis of a multinucleated schizont gives rise to merozoites (Sheffield, 1970). Subsequently, merozoites differentiate into micro (male) or macro (female) gametes and undergo sexual reproduction, giving rise to oocysts. The immature oocysts (the sole diploid life stage) are excreted in cat feces and undergo meiosis in the environment to become fully infective (Sibley et al., 2009). Millions of oocysts are shed within a short period of time following an infection and are incredibly resilient, unaffected by strong disinfectants such as bleach and being able to survive years in soil and water (Jones & Dubey, 2010).

In intermediate hosts, ingested oocysts or tissue cysts infect intestinal epithelial cells, but do not undergo the sexual reproduction process for reasons which are unknown (Robert-Gangneux & Dardé, 2012). Instead, the sporozoites and bradyzoites differentiate into tachyzoites, which repeatedly infect and replicate until the host cell is ruptured, in a race against the host immune system. They rapidly access other tissue by traveling paracellularly through the intestinal epithelium (Barragan & Sibley, 2002). Infection of motile cells like macrophages allow the parasite to disseminate throughout the body, reaching immune privileged sites such as the brain (Carruthers & Suzuki, 2007). IFN-γ-dependent immunity eventually suppresses the acute tachyzoite infection but also induces the formation of the immune-evasive bradyzoite tissue cysts,

resulting in a prolonged chronic infection that can persist for the life of the host (Skariah et al., 2010).

1.1.4 – Tachyzoite morphology and replication

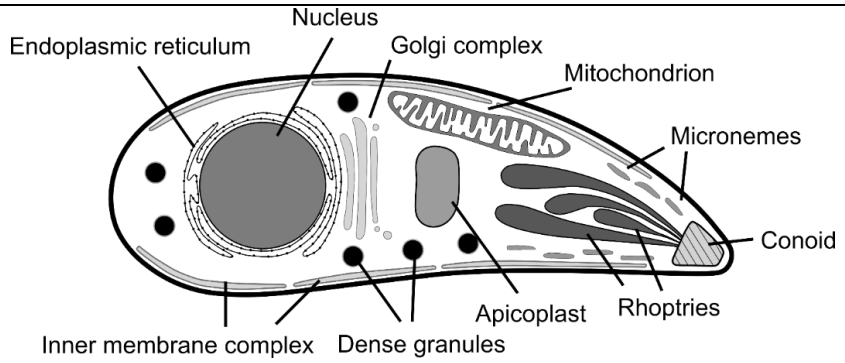

Figure 1-2. Morphology of a *Toxoplasma gondii* tachyzoite. In addition to having the normal eukaryotic organelles, *T. gondii* and other apicomplexans exhibit a unique secretory apparatus called the apical complex. The contents of the membrane-bound micronemes and rhoptries are released through this complex to initiate host cell invasion. Dense granules are then secreted to remodel the parasitophorous vacuole and modify host cell behavior. The inner membrane complex, which is the apicomplexan adaptation of the alveoli, is essential for motility and replication. Most apicomplexans also have an apicoplast, a plastid organelle involved in essential metabolic pathways.

The tachyzoite is the most widely studied life cycle stage of *T. gondii* due to the ease of cell culture, high genetic tractability, and rapid proliferation. Its morphology resembles a teardrop or banana shape and is roughly 5 μm long (Figure 1-2). All of the normal eukaryotic organelles are present: a nucleus containing a haploid genome is surrounded by an endoplasmic reticulum, with the Golgi apparatus situated immediately anterior to the nucleus, and a single mitochondrion (Joiner & Roos, 2002; Melo et al., 2000). However, as intracellular parasites, *T. gondii* and other apicomplexans have evolved several specialized organelles involved in host cell invasion and modulation of the host to optimize its intracellular niche.

The organization of the parasite cell is highly polarized, with the pointed apical end containing the densely packed secretory invasion machinery called the apical complex. This

intricate assembly of organelles enables the apicomplexan-specific process of active invasion and formation of a non-fusogenic parasitophorous vacuole (PV) in the host. The micronemes are small rod-shaped organelles containing numerous transmembrane adhesins that are released to the parasite plasma membrane to form a stable contact upon encountering a host cell (Soldati et al., 2001). The rhoptries are a bundle of approximately 8-10 individual club-shaped organelles also positioned at the apical end with a bulbous base and a narrow neck. The rhoptry necks are extended towards the extreme tip of the cell where they release their contents through the middle of a microtubule-based structure called the conoid (Dubey et al., 1998). The rhoptry proteins that are injected into the host membrane form the moving junction (MJ), a unique complex that serves as the anchor for penetration. Following successful invasion, the dense granules are released to modify the parasitophorous vacuole and hijack host cell function, making an environment suitable for parasite growth. The process of active invasion is reviewed in greater detail in section 1.2.

The apicoplast is a non-photosynthetic plastid organelle with a 35 kb genome located anterior to the Golgi apparatus. A vestige of endosymbiosis between a chromalveolate ancestor and red algae, the apicomplexan apicoplast has lost photosynthetic capabilities (Lim & McFadden, 2010). Nevertheless, this organelle remains essential for proper growth, serving as the site for fatty acid, isoprenoid, iron-sulfur cluster, and heme synthesis. Due to these important functions, this parasite-specific organelle has been a target for therapeutics (Mukherjee & Sadhukhan, 2016; Soldati, 1999).

The inner membrane complex (IMC) is a large structure composed of both membrane and supporting cytoskeletal layers that are situated directly underneath the plasma membrane. An evolution of the alveoli, or the layer of flattened membrane sacs that is a defining characteristic of the infrakingdom Alveolata, the IMC has been adapted to support the parasitic lifestyle of

apicomplexans (Gould et al., 2008). An accompanying intermediate filament network provides structural stability and tensile strength (Tremp et al., 2008). The IMC houses the glideosome, the actomyosin motor complex that is critical for both host cell seeking and invasion. In addition, it plays an essential role during replication, serving as a scaffold for daughter formation during a unique process of asexual reproduction called endodyogeny (Figure 1-3). The IMC is reviewed in greater detail in section 1.3.

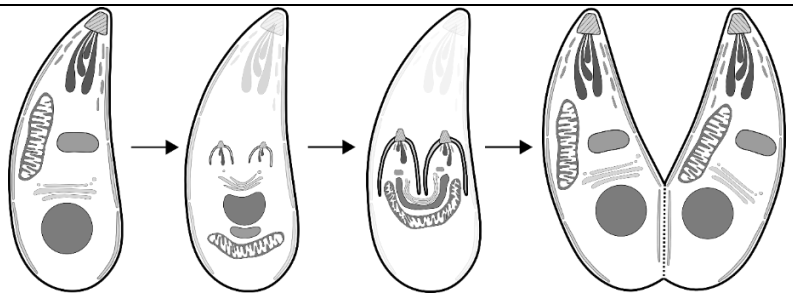

Figure 1-3. The asexual forms of *T. gondii* replicate by endodyogeny. When infecting an intermediate host, the asexual stages of *T. gondii* proliferate through a unique process where two daughters form internally in the maternal cytoplasm. Replication initiates with the formation of an IMC scaffold, which grows and serves as an organization center for the *de novo* production of invasion organelles (i.e. micronemes, rhoptries, and dense granules) and division of other organelles like the nucleus, apicoplast, and mitochondrion. As division progresses, the maternal secretory organelles and IMC are degraded. Developing daughter buds adopt the maternal plasma membrane and divide into two separate cells.

1.2 – Active host cell invasion

1.2.1 – Gliding motility and host cell attachment

Movement of apicomplexans is achieved through a unique process called gliding motility. Unlike their distant alveolate relatives, *T. gondii* lack cilia or flagella, except for the sexual microgamete stage. Instead, extracellular parasites secrete surface adhesins, which provide an anchor for the internal actomyosin motors of the glideosome to generate a pulling force through hydrolysis of ATP, either along surfaces or to forcibly enter a host cell. Movement by gliding is fairly rapid (1-10 μm/s) compared to ameboid motility (1-10 μm/min), suggesting that *T. gondii* may be able to avoid phagocytosis by an immune cell simply by being faster at invasion (Håkansson et al., 1999; Morisaki et al., 1995). This form of motility may also facilitate penetration of host epithelial barriers better than ciliary/flagellar propulsion. For example, parasites are able to utilize human intercellular adhesion molecule 1 (ICAM-1) on endothelial cells as a receptor for paracellular migration (Barragan et al., 2005; Gubbels & Duraisingh, 2012). The molecular mechanisms of the glideosome are reviewed in greater detail in section 1.3.2.

Host cell attachment signifies the first stage of active invasion by *T. gondii*. The initial contact is mediated, at least in part, by the SAG1-related sequence (SRS) surface antigens, a family of over 120 homologous GPI-anchored proteins that abundantly coat the outer surface of the parasite (Jung et al., 2004; Mineo et al., 1993; Wasmuth et al., 2012). Although these proteins were mainly thought to be responsible for eliciting a host immune response, one member, SAG3, was found to bind host heparan sulfate proteoglycans, which are ubiquitous cell surface markers, with low micromolar affinity (Jacquet et al., 2001). Following the initial low affinity attachment, the micronemes release their adhesins in a Ca^{2+}-dependent manner, establishing a strong connection at the apical region of the parasite and orienting the invasion machinery towards the host (Lovett

& Sibley, 2003). Many micronemal adhesins exhibit known ligand-binding domains, including thrombospondin-1 repeat, von Willebrand A, PAN/Apple, EGF-like, and lectin domains (Carruthers & Tomley, 2008). The multiplicity of distinct attachment proteins may be a contributing factor for the ability of *T. gondii* to infect a broad range of hosts (Soldati et al., 2001). The apical membrane antigen (AMA) proteins are a set of micronemal adhesins that interact with the rhoptry protein RON2 to form the MJ complex that drives active invasion (Lamarque et al., 2014).

1.2.2 – Rhoptries and the moving junction

The rhoptries contain proteins and lipids that are densely packed into a crystalline lattice and delimited into two regions (i.e. the neck and the bulb) despite a lack of any physical boundary (Bradley et al., 2005; Lebrun et al., 2014). Following host cell attachment, the contents are secreted into the host cell to initiate invasion. While the trigger for rhoptry exocytosis is unknown, the microneme protein MIC8 is essential for this process, suggesting a signaling cascade initiated by micronemal release (Kessler et al., 2008). Unlike micronemes, rhoptry secretion is not induced by elevated calcium levels (using the ionophore A23187), although recent work shows that it is dependent on the Ca^{2+}-sensing ferlin protein FER2 (Carruthers & Sibley, 1999; Coleman et al., 2018). In support of this, release of rhoptry proteins in *Plasmodium* merozoites has been linked to a return of calcium concentration to basal levels, which may function similarly in *T. gondii* (Singh et al., 2010).

The mechanism of rhoptry release has not been determined, but the prevailing model involves a porosome-like opening at the extreme apical tip of the plasma membrane surrounding the conoid (Jena, 2009; Nichols et al., 1983). While a single parasite has several rhoptry organelles,

only four rhoptry necks at most can fit within the hollow interior of the conoid, and only one rhoptry is believed to be able to interface with the porosome for release at a time (Paredes-Santos et al., 2012). Once secreted into the host, rhoptry proteins can be visualized as either soluble or packaged in membranous assemblies that originate from the lipidic material stored in the rhoptries (Boothroyd & Dubremetz, 2008; Håkansson et al., 2001).

A subset of proteins stored in the anteriorly located rhoptry neck (RONs) are released and assemble the MJ, a ring-shaped macrostructure embedded in the host plasma membrane that encircles the parasite as it rapidly invades (25-40 seconds) the host cell using force generated by the glideosome (Morisaki et al., 1995). The parasites enter the host cell by invaginating the host plasma membrane, but this process is distinct from the endocytic methods employed by other intracellular pathogens, as the MJ complex selectively excludes host transmembrane proteins to establish a PV that is non-fusogenic with the host endolysosomal system (Charron & Sibley, 2004; Mordue et al., 1999). One of the MJ proteins secreted into the host membrane, RON2, is a single-pass transmembrane protein with a short extracellular C-terminus that tightly interacts with the micronemal AMA1 ectodomain to form the link between parasite and host (Tonkin et al., 2011; Tyler & Boothroyd, 2011). RON4, RON5, and RON8 are soluble proteins tethered by the RON2 N-terminus to the cytoplasmic-face of the host plasma membrane and serve roles in stabilizing the complex and binding to host components. RON4 and RON5 have been shown to interact with human proteins ALIX, CIN85/CD2AP, and TSG101, which are involved in endosomal membrane remodeling and actin assembly, and are important for firmly anchoring the MJ to the host cytoskeleton (Guérin et al., 2017). RON8 functions similarly through a currently unknown mechanism, but has also been associated with proper scission of the nascent PV once the parasite is fully inside, possibly by mimicking or recruiting dynamins (Ferguson & De Camilli, 2012;

Straub et al., 2011). Elucidating other possible functions of these proteins is difficult, as disruption of one subunit causes either degradation or mislocalization of the others, implying that the core MJ complex is preformed and must be intact for correct trafficking to the rhoptry (Beck et al., 2014; Lamarque et al., 2014; M. Wang et al., 2017). This codependence is exhibited by RON2/4/5, which (along with AMA1) are conserved in Apicomplexa and played an early role in enabling a parasitic lifestyle, whereas RON8, a newer coccidian-only evolution, is an exception and does not impact biogenesis of the other MJ proteins (Besteiro et al., 2011; Straub et al., 2011).

1.2.3 – Host cell modulation, growth, and egress

During the process of invasion, proteins stored within the rhoptry bulb (ROPs) are also discharged into the host cell. While the functions of many ROPs are unknown, some are responsible for modulating host cell immunity during the initial stages of infection (Boothroyd & Dubremetz, 2008). Although these activities are important for parasite growth, many of the ROPs are individually dispensable *in vitro*, suggesting either redundancy from paralogs or importance in *in vivo* contexts (Sidik et al., 2016). An example of this are the rhoptry kinases (ROPKs), of which there are at least 44 known members, and are defined by a conserved C-terminal protein kinase-like domain (El Hajj et al., 2006; Peixoto et al., 2010). This family can be split into two clades, the first containing the majority of putatively active kinases with an intact lysine-aspartate-aspartate catalytic triad motif. The best understood of these kinases, ROP16, induces phosphorylation and activation of host transcription factors STAT3 and STAT6, thereby limiting IL-12 production and subverting a Th1 pro-inflammatory response (Robben et al., 2004; Saeij et al., 2007). Interestingly, a single amino acid polymorphism of ROP16 in type II parasites severely reduces this protective activity and partially explains their reduced virulence (Yamamoto et al., 2009).

The other ROPK clade consists of the inactive pseudokinases ROP2/4/5/7/8 (with incomplete catalytic triads) and a sole kinase ROP18. The function of ROP5 and ROP18 have been scrutinized as the main determinants of parasite virulence for murine models. In mice, immunity against intracellular pathogens is mediated by IFN-γ-inducible p47 immunity related GTPases (IRGs) and p65 guanylate-binding proteins (GBPs) (Shenoy et al., 2007). During a *T. gondii* infection, IRGs Irgb6 and Irgb10 are the first to load (in a matter of minutes) onto the cytoplasmic face of the parasitophorous vacuolar membrane (PVM), and they proceed to recruit other IRGs and multimerize in a GTP-dependent manner (Khaminets et al., 2010). They function to kill the parasite by vesiculation of the *T. gondii* PVM, disruption of the parasite plasma membrane, and eventual lysosomal degradation (Ling et al., 2006; Taylor et al., 2007). In virulent type I parasites, this loading of IRGs is considerably reduced, increasing parasite survivability against IFN-γ-mediated immunity. This phenotype can be attributed to ROP18, which localizes to the outer PVM surface via arginine-rich amphipathic helices conserved in the ROPK family (Reese & Boothroyd, 2009). ROP18 directly phosphorylates both Irgb6 and Irgb10 *in vitro*, and crystal structures of Irgb6 reveal that this phosphorylation occurs in the switch I loop of the GTP-binding domain, blocking homodimerization, which is necessary to form a functional complex (Fentress et al., 2010; Ghosh et al., 2004; Steinfeldt et al., 2010).

Surprisingly, ROP18 by itself is not sufficient to confer virulence, but instead is highly dependent on the catalytically-inactive psuedokinase ROP5 (Behnke et al., 2012; Fleckenstein et al., 2012). ROP5 is arranged in the genome as a cluster of tandem polymorphic alleles, and deletion of the entire locus in type I RH parasites renders them completely avirulent *in vivo* in mice and severely growth-inhibited *in vitro* in IFN-γ treated mouse embryonic fibroblasts (Behnke et al., 2011; Fleckenstein et al., 2012; Reese et al., 2011). These paralogs are divergent among the three

lineages, and while the type II genome contains more copies (11 vs. 6 in type I and III), these isoforms are relatively ineffective at reducing IRG load despite the parasite expressing functional ROP18 (Niedelman et al., 2012). Investigation of a type I ROP5 allele revealed that it binds to the IRG Irga6, forcing this protein in a GDP-bound inactive state while also blocking the dimer interface (Fleckenstein et al., 2012). During this non-catalytic interaction, ROP18 may then irreversibly phosphorylate the IRG, although the more severe avirulence phenotype seen with ROP5-deficient parasites implies that ROP5 may be sufficient for the majority of IRG immobilization or involved in other immunity pathways (Behnke et al., 2012). Complementation of two different isoforms of ROP5 into RH*Δrop5* parasites leads to a greater recovery of virulence compared to two copies of the same allele, suggesting that polymorphic divergence promotes protection against a broader range of host response proteins (Reese et al., 2011). This assemblage of kinase and psuedokinase pairs serve to efficiently abolish host cell immunity in the murine model.

It is important to note that unlike mice, humans lack IFN-γ-dependent IRGs, and neither ROP5 nor ROP18 play a significant role for survival in IFN-γ-treated human foreskin fibroblasts (HFF) (Niedelman et al., 2012). However, humans do express seven GBPs that are involved in innate immunity against intracellular pathogens (Tripal et al., 2007). The rhoptry kinase ROP54 was the first parasite effector protein shown to limit PVM loading of murine GBP2, although similar activity was not assessed in human cells (Kim et al., 2016). GBPs function to eliminate the pathogen through multiple pathways including ubiquitination of the vacuole, inflammasome activation, and xenophagy (Coers & Haldar, 2015). Unfortunately, it is currently unclear to what extent these GBPs confer an immune response against *T. gondii*, as variability is seen in the method

of parasite destruction, between mouse and human models, and even between different human cell types (Praefcke, 2018).

After successful invasion, constitutive secretion of the dense granules is responsible for the maturation of the newly formed PV to maintain a replication-permissive niche for the parasite. This continued release of these organelles during the span of intracellular growth contrasts with the single burst of rhoptry effector secretion coinciding with the start of invasion. The dense granules are released to the PV through fusion with the plasma membrane, although how they bypass the underlying IMC is unclear (Cesbron-Delauw, 1994; Dubremetz et al., 1993; Heaslip et al., 2016). Within the PV, dense granule proteins either remain soluble in the lumen, or associate with membranes through hydrophobic or amphipathic alpha-helices or transmembrane domains (Lebrun et al., 2014). A network of membranous nanotubules called the intravacuolar network (IVN) is formed, which is hypothesized to increase host-parasite boundary surface area (Sibley et al., 1995). Biogenesis of the IVN is dependent on a subset of dense granule proteins with tubulating properties, including GRA2 and GRA6. Intriguingly, these GRAs only properly associate with membranes when phosphorylated by the recently described coccidian-specific With-No-Gly-loop (WNG) kinases (Beraki et al., 2019). In addition to being involved in IVN formation, GRA2 and GRA6 have also been linked to sequestration of lipid-containing host Rab vesicles (Mercier et al., 2002; Romano et al., 2017). Similarly, GRA39 appears to be involved in lipid import into the parasite, as disruption causes accumulation of lipid deposits in the PV (Nadipuram et al., 2016). The GRA protein MAF1 induces association of the PVM to host mitochondria, a phenomenon seen with many intracellular pathogens (Pernas et al., 2014). A subset of GRAs (GRA16, GRA24, GRA28, *Tg*IST) are able to traverse the PVM and traffic to the host nucleus, where they alter transcription continuously during the span of intracellular growth (Krishnamurthy & Saeij, 2018).

GRA17 and GRA23 form a nonspecific small molecule (up to ~1.9 kDa) pore complex at the PVM that is necessary for osmoregulation and exchange of both nutrients and waste products (Gold et al., 2015; Schwab et al., 1994). MYR1, MYR2, and MYR3 appear to comprise a cross-PVM protein translocation machinery, but unlike the well-characterized *Plasmodium* translocon of exported proteins (PTEX), more work is needed to confirm the composition of the translocon and how it functions in protein export into the host cell (Ho et al., 2018; Marino et al., 2018).

Once established in the PV, *T. gondii* grows by scavenging host glucose, lipids, and amino acids (Blader & Koshy, 2014). The parasite replicates exponentially by endodyogeny, yielding two progeny per maternal cell every 6 to 8 hours *in vitro* (Black & Boothroyd, 2000). Once the vacuole contains 64 to 128 parasites, they actively egress from the host cell, lethally rupturing it in the process, and begin searching for new hosts by gliding motility. Egress is triggered by multiple factors that reflect the intracellular environment. Abscisic acid, a small molecule hormone responsible for calcium release in plants, is constantly produced by intracellular *T. gondii* and induces egress when sufficient levels are accumulated (Nagamune et al., 2008). Acidification of the PV lumen late in infection is also linked to egress, as artificially lowering the vacuolar pH can prematurely start this process (Roiko et al., 2014). Recent work suggests that residual bodies, which are composed of material that was not taken up by the daughter cells after endodyogeny, contains accumulated acidocalcisome organelles that eventually release into the PV to both lower pH and increase calcium concentration (Attias et al., 2019). In response to these signals, Ca^{2+}-dependent microneme secretion releases perforin-like protein 1 (PLP1) (Kafsack et al., 2009). In low pH environments, PLP1 assembles into pore-forming complexes that permeabilize and weaken the PV and host membrane, similar to perforins used by cytotoxic lymphocytes and cytolysins used by pathogenic bacteria (Kafsack et al., 2009; Roiko et al., 2014).

1.3 – The inner membrane complex

1.3.1 – Morphology of the *T. gondii* IMC

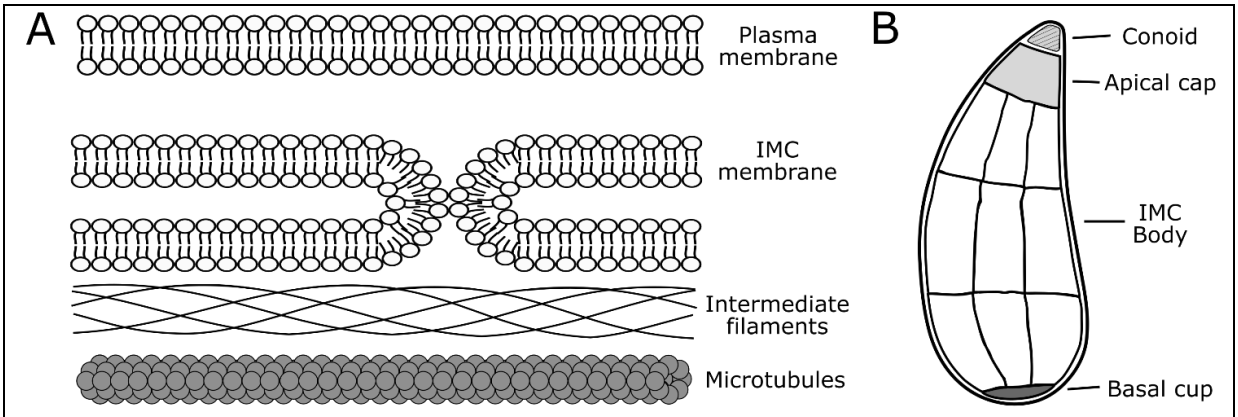

Figure 1-4. The IMC is composed of a membrane and cytoskeletal layer. (A) The IMC is peripherally located under the parasite plasma membrane. It consists of flattened membrane vesicles called alveoli and a supporting intermediate filament network. This cytoskeletal network provides tensile strength to the cell in conjunction with the subpellicular microtubules. The IMC serves as a scaffold for the unique process of endodyogeny as well as hosting the glideosome complex needed for motility. (B) The IMC is longitudinally separated into an apical cap, a body that is composed of an array of rectangular alveolar membranes, and a posterior basal cup.

The *T. gondii* IMC is situated underneath the plasma membrane and is composed of an array of membranous vesicles supported by a rigid cytoskeletal network (Fig 1-4A). The IMC is delineated longitudinally into an anterior apical cap, central body region, and the posterior basal complex (Hu et al., 2006). While a single large cone-shaped membrane vesicle composes the apical cap, the membrane organization in the IMC body, which makes up the majority of the organelle, can be strikingly seen as a series of rectangular plates in freeze-fracture electron micrographs (Figure 1-4B, Porchet & Torpier, 1977). A combined microtubule and intermediate filament-based IMC cytoskeleton tightly associates with the membrane layer through protein-protein interactions and fatty acylations to govern morphology and tensile strength (Chen et al., 2015; Tremp et al., 2017, 2013). A classic method to determine IMC residency is treatment of parasites with *Clostridium septicum* alpha-toxin, which causes osmotic distention that separates the plasma

membrane from the IMC and can be easily visualized by immunofluorescence assay (IFA) (Beck et al., 2010; Wichroski et al., 2002). This process does not disrupt co-localization of the cytoskeletal and membrane portions of the IMC.

The alveolar vesicles contain several membrane-associated proteins that are anchored by either transmembrane domains or lipid post-translational modifications. The transmembrane gliding-associated proteins GAP40 and GAP50 are embedded in the layer facing the plasma membrane and are indispensable components of the glideosome, as well as playing an important role in daughter formation (Frénal et al., 2010; Gaskins et al., 2004; Harding et al., 2016). Another family of transmembrane IMC proteins, the glideosome-associated proteins with multiple-membrane spans (GAPMs), localize to the cytoplasmic face of the alveoli (Bullen et al., 2009). These proteins co-immunoprecipitate (co-IP) components of the IMC cytoskeleton and depletion of some members causes loss of IMC integrity, suggesting a role in linking the membrane and cytoskeletal layers together (Bullen et al., 2009; Harding et al., 2016, 2019).

Proteins lacking hydrophobic domains also associate with the IMC membrane through N-myristoyl and S-palmitoyl lipid modifications. Along with one general N-myristoyltransferase, *T. gondii* has 18 protein S-acyltransferases (called TgDHHCs for the conserved catalytic motif) of which two, TgDHHC2 and TgDHHC14, localize to the IMC membranes (Frénal et al., 2013). Attempts to knockout these two genes were unsuccessful, indicating that palmitoylation is essential for proper IMC function (Frénal et al., 2013). One myristoylated and palmitoylated protein, IMC sub-compartment protein 2 (ISP2), results in multiple daughter formation and aberrant growth when disrupted (Beck et al., 2010). However, this effect does not explain the lethal phenotype seen with the TgDHHC proteins, indicating that other acylated targets play more central roles in IMC functions.

The cytoskeletal network underlying the membrane alveoli are composed of 8-10 nm interlaced filaments (Mann & Beckers, 2001). This network is composed of 14 proteins called alveolins (IMC1 and IMC3-15), which are not particular conserved except for a loosely defined proline and valine-rich alveolin repeat domain. These alveolins have differing localizations in *T. gondii*, both between subcompartments (i.e. apical cap, body, and basal complex) and between maternal and daughter IMC during replication, but the exact organization of these proteins is unknown (Dubey et al., 2017; Gould et al., 2008). The alveolin domain of IMC3 and IMC8 alone appears to be mostly sufficient for correctly targeting to the IMC, suggesting that this low complexity region can assemble into insoluble macromolecular structures with other alveolin proteins (Anderson-White et al., 2011). However, partial mislocalization to the cytoplasm does occur for these two protein mutants and is resolved by restoring the N-terminal and C-terminal flanking regions, implying that these domains are also important for proper trafficking or other functions. Interestingly, 5 of the 14 alveolins are also strongly predicted to be N-terminally palmitoylated, indicating that elements other than the alveolin domain are needed for faithful targeting and that there is a direct link between the IMC membrane and cytoskeleton (Ren et al., 2008).

The IMC is further supported by 22 subpellicular microtubules extending roughly two-thirds of the length of the parasite from the apical end (Leung et al., 2017). The polymer structure is stabilized and made detergent-insoluble through a coating of accessory proteins like SPM1 (Tran et al., 2012). Additionally, thioredoxin-like proteins TrxL1 and TrxL2 bind to SPM1, and although their purpose is not known, this opens up the possibility of a catalytic function in the IMC cytoskeletal milieu (Liu et al., 2013). These microtubules extend from a unique microtubule-organizing center (MTOC) called the apical polar ring (APR), which is positioned at the edge of

the IMC apical cap (Russell & Burns, 1984). Within the APR center is the conoid, made up of 14 tubulin polymers, two additional intraconoid microtubules, and two preconoidal ring MTOCs from which these tubulin structures originate (Leung et al., 2017; Nichols & Chiappino, 1987). In extracellular parasites, the position of the conoid is dynamic, transitioning between a retracted state surrounded by the subpellicular microtubules below the APR and an extended state past the APR, and this activity is suspected to be associated with invasion (Carey et al., 2004). The protein RNG2 spans the APR and conoid, and interestingly, movement of the conoid can be visualized as a flip in the orientation of the RNG2 N- and C-termini. Disruption of RNG2 does not affect conoid extrusion but does limit microneme secretion, and there is likely a close relationship between the two phenomena, as both are Ca^{2+}-dependent and important for host invasion (González Del Carmen et al., 2009; Katris et al., 2014; Mondragon & Frixione, 1996).

1.3.2 – The glideosome

At its core, the glideosome complex that drives gliding motility is an actomyosin motor situated in the cortical space between the IMC and plasma membranes. This activity is driven by myosin A (MyoA), an atypical myosin (class XIVa) with a short neck and tail domain, degenerate IQ motifs, and lack of several highly conserved residues (Foth et al., 2006; Heaslip et al., 2010b; Heintzelman & Schwartzman, 1997; Herm-Götz et al., 2002). Even without these features, this motor protein functions *in vitro* as efficiently as fast skeletal muscle myosins (Herm-Götz et al., 2002). MyoA directly binds to the EF-hand domain-containing myosin light chain 1 (MLC1) and two essential light chains (ELC1/2), despite missing the canonical IQ motifs that govern calmodulin interaction in conventional myosins (Bähler & Rhoads, 2002; Herm-Götz et al., 2002; Nebl et al., 2011; Williams et al., 2015). MyoA is attached to the IMC membrane through

interactions with the gliding-associated proteins GAP40, GAP45, and GAP50. GAP40 and GAP50 are embedded in the outer IMC membrane layer by 9 and 1 transmembrane domain(s), respectively (Frénal et al., 2010; Gaskins et al., 2004). GAP45 is a unique protein that spans the distance between the IMC and plasma membrane (Frénal et al., 2010; Gaskins et al., 2004). Its N-terminus is anchored into the plasma membrane by myristoylation and palmitoylation while its C-terminus is associated with the IMC membrane, likely by directly binding to GAP40 and/or GAP50. GAP45 is responsible for recruiting the normally soluble MyoA to the cell periphery through a shared interaction with MLC1 (Frénal et al., 2010). Lacking the tail that dictates trafficking in conventional myosins, MyoA instead binds to the C-terminal EF-hand domains of MLC1 with its degenerate IQ motifs in a Ca^{2+}-independent manner (Frénal et al., 2017). The N-terminal region of MLC1 binds to the GAP45 C-terminus, although strongly predicted palmitoylation sites also suggest MLC1 may associate with the IMC membrane directly through these lipid modifications (Frénal et al., 2010; Ren et al., 2008). These five proteins compose the main glideosome complex, but the question of how they remain static to impart a motive force remains unanswered. One reasonable hypothesis would be some anchor to the underlying cytoskeleton that is situated on the other side of the IMC membrane. Although the composition of the alveolar lumen is not well understood, the N-terminus of GAP50, which makes up the majority of the protein (350 aa, 91.8% total), is located within this space and may be interacting with cytoplasmic-facing IMC resident proteins such as the GAPMs (Gaskins et al., 2004; Harding & Meissner, 2014). An alternative theory suggests that the glideosome is immobilized in regions of high cholesterol-containing detergent-resistant membranes (Johnson et al., 2007).

Like most other myosin motors, MyoA hydrolyzes ATP to process along an actin filament towards the barbed (+) end to generate motion (Herm-Götz et al., 2002; Sellers, 2000). However,

in *T. gondii* and other apicomplexans, actin is also quite unusual. Unlike in most other eukaryotic cells where it is found as extensive filaments on the order of microns in length, parasite actin is intrinsically unstable and only form short strands of ~100 nm (Boucher & Bosch, 2015; Skillman et al., 2011). To complete the connection for gliding propulsion, the actomyosin motor must be associated with the transmembrane adhesins that attach to external surfaces. This is mediated by the glideosome-associated connector (GAC), which is a cytosolic protein that rapidly relocalizes to the periphery upon ionophore-induced microneme secretion (Jacot et al., 2016). Its N-terminal armadillo-repeat domain forms a large superhelical structure that wraps around multiple actin protomers, while the C-terminus binds to the short cytoplasmic tail of MIC2. However, attachment to other adhesins such as AMA1 has not been assessed. A C-terminal pleckstrin-homology domain also binds to phosphatidic acid, which is a phospholipid required for microneme release and also may help orient this protein towards the plasma membrane (Bullen et al., 2016; Jacot et al., 2016). Apicomplexans lack the classical Arp2/3 actin nucleation complex, and in *T. gondii*, polymerization only occurs at the apical tip of the parasite by the formin FRM1 (Daher et al., 2010; Jacot et al., 2016). This localized activity guarantees that movement initiates near the apical complex, where the MJ machinery is secreted and assembled. Attached to adhesins through GAC, the actin filaments are moved posteriorly by passing from one MyoA assembly to another, consequently propelling the parasite forward (Skillman et al., 2011). The short polymer length of actin likely limits the number of motor proteins on a single filament and facilitates faster turnover, which is advantageous in other highly motile cells (Skillman et al., 2011). Treatment with the actin stabilizer jasplakinolide or disruption of *T. gondii* actin depolymerization factor (ADF) causes increased actin filamentation, faster but erratic motility, and defective invasion and egress (Mehta & Sibley, 2011; Wetzel et al., 2003).

Although the MyoA complex is the only glideosome motor in *Plasmodium* and is the major driver in *T. gondii*, separate glideosome assemblies in the latter have been characterized and warrant discussion (Baum et al., 2006). One is found at the extreme tip near the conoid and is driven by MyoH (class XIVc), which has a unique α-tubulin suppressor 1 (ATS1) domain in the tail region (Foth et al., 2006; Graindorge et al., 2016). Using this domain, MyoH is able to bind directly to the conoid microtubules, establishing the static positioning needed for gliding (Graindorge et al., 2016). At the apical tip, where micronemal attachment and actin filamentation also occur, MyoH initiates movement as it translocates the adhesion complexes down to the beginning of the IMC membrane. There, MyoA continues the process along the entire body of the parasite. At the apical cap portion of the IMC, the coccidian-specific homolog GAP70 substitutes for GAP45 (Frénal et al., 2010). The acylated N-terminus and IMC-binding C-terminus are conserved in GAP70, but a longer central region results in a greater separation of the plasma and IMC membranes at the apical cap for an unknown reason. Yet another glideosome complex is found at the basal complex and composed of GAP80 (another GAP45 homolog), MyoC (class XIVb), and IMC-associated protein 1 (IAP1), which recruits both components to the posterior region (Frénal et al., 2014b). As the adhesin complexes travel to the basal end of the parasite, rhomboid proteases cleave the transmembrane domain to release the connection between parasite and surface and prevent buildup of these proteins (Brossier et al., 2005). Interestingly, AMA1, which forms the tight ring-shaped MJ around the parasite, may be temporarily protected from this cleavage by changing conformation after binding to RON2 (Krishnamurthy et al., 2016).

Ultimately, functional characterization of the individual IMC body and basal complex glideosomes is confounded due to redundancies between the two complexes (Frénal et al., 2014b). MyoA and MyoC are able to relocalize and compensate for each other, although parasites are not

able to tolerate disruption of both proteins. Similarly, GAP70 and GAP80 are dispensable, presumably due to compensation by the more abundant GAP45 (Frénal et al., 2014b; Frénal et al., 2010). Indeed, even depletion of GAP45 can be overcome by overexpression GAP80 (Frénal et al., 2014b). However, MyoH is special with its direct conoid microtubule-binding ability, and is essential for motility as the initiating motor (Graindorge et al., 2016).

1.3.3 – The role of the IMC in endodyogeny

The asexual forms of *T. gondii* divide by endodyogeny, where two daughters form internally within a maternal cell (Figure 1-3). The nascent daughter IMC serves as a scaffold for organelle biogenesis and sequestration from the maternal cell. Elongation and division of the Golgi apparatus marks the earliest step of mitosis (Nishi et al., 2008). Concurrently, the centrioles, which have an unusual parallel 9+1 structure, migrate posterior to the nucleus and duplicate (Francia & Striepen, 2014; Nishi et al., 2008). Next, the 2 daughter IMCs are constructed from the anterior end and encapsulate the Golgi and centrosome (Nishi et al., 2008). As these IMC scaffolds elongate, the divided apicoplast, nucleus, endoplasmic reticulum, and mitochondrion are sequentially incorporated. The secretory organelles (micronemes, rhoptries, dense granules) are formed *de novo* through vesicular transport mediated by the dynamin-related proteins DrpB and DrpC and targeted in part by Rab GTPases (Breinich et al., 2009; Heredero-Bermejo et al., 2019; Kremer et al., 2013). To complete division, the maternal IMC is disassembled by both ubiquitin-mediated degradation and recycling, and the two new daughters adopt the maternal plasma membrane (Hu et al., 2006; Ouologuem & Roos, 2014; Silmon de Monerri et al., 2015).

The involvement of the IMC in replication begins with the alveolin IMC15, which initially co-localizes with the newly replicated centrosomes (Anderson-White et al., 2011). Rab11B is also

seen as early as IMC15 and mediates vesicular trafficking to the nascent IMC membrane, indicating that biogenesis of the cytoskeletal and membrane layers are coordinated from the beginning of endodyogeny (Agop-Nersesian et al., 2010). The microtubule components of the apical complex (e.g. APR and conoid) are also formed at this stage. They are connected to the centrosome by a striated fiber assemblin (SFA) complex (resembling an ancestral flagellar basal body rootlet) that may serve as the structure from which the apical MTOCs are derived (Francia et al., 2012). The next stage of early daughter bud formation is marked by MORN1, which assembles into ring structures that label the immature apical and basal complexes (Gubbels et al., 2006; Heaslip et al., 2010a). The basal ring migrates posteriorly as the IMC and subpellicular microtubules elongate, and the separate longitudinal regions of the IMC can now be differentiated with the membrane-associated IMC subcompartment proteins (ISPs) (Beck et al., 2010; Hu et al., 2006). The cytoskeletal alveolins IMC1/3/4/6/10 assemble into the filamentous network of the daughter IMC body, while GAP40 and GAP50 target to the membrane as the first members of the glideosome (Anderson-White et al., 2012; Dubey et al., 2017). As growth of the daughter buds reaches the midpoint, IMC5/8/9/13, which initially localized to the growing scaffold, migrate to the MORN1-labeled basal complex (Anderson-White et al., 2011). The calcium binding protein Centrin2 is recruited to the posterior end of the MORN1 ring and is believed to be responsible for basal complex constriction that leads to the tapered shape of mature progeny (Hu, 2008). As the two new IMC organelles replace the maternal one, GAP45 and GAP70 establish the tight association between IMC and plasma membrane (Frénal et al., 2010). Finally, the alveolins IMC7/12/14 are expressed after replication is completed and are somehow incorporated into the maternal IMC, possibly to distinguish it from the new daughters in the next division cycle (Anderson-White et al., 2012). This process of endodyogeny results in a posterior residual body,

which is composed of unincorporated membrane and cytoplasmic material. Interestingly, this residual body persistently connects parasites after multiple rounds of intracellular divisions and only disassociates from the cells during egress (Caldas et al., 2010). While originally regarded as a depository for degraded cytoskeletal material, a newly characterized residual body-specific actin network also implicates this organelle in other important roles such as facilitating communication (e.g. synchronization of replication) and resource sharing between cells (Morrissette & Sibley, 2002b; Tosetti et al., 2019; Tran et al., 2010).

1.4 – Unnatural amino acids

1.4.1 – History of expanding the genetic code

The genetic code is a fundamental paradigm of life on Earth: 61 three-base codons map to the 20 standard proteinogenic amino acids and 3 nonsense codons act as terminators during ribosomal translation (Koonin & Novozhilov, 2017; Nirenberg, 2004). Despite saturation of all possible codons, it would be desirable to produce proteins containing unnatural amino acids (UAAs) that are engineered to have special chemical properties using conventional translation. Fortunately, while the genetic code may seem immutable, exceptions already exist in nature. For example, the usage of the other 2 special proteinogenic amino acids, selenocysteine and pyrrolysine, occurs in select organisms at opal (TGA) and amber (TAG) stop codons, respectively (Berry et al., 1993; Srinivasan et al., 2002). Similarly, mitochondria in many eukaryotes, including yeast and humans, encode tryptophan at the UGA stop codon, among other differences (Macino et al., 1979; Richter et al., 2010). As the ribosomal process of peptide elongation does not discriminate against a non-cognate tRNA with a correct anticodon, the hurdle for efficient UAA incorporation is dependent on the faithful formation of charged UAA-tRNAs by an aminacyl-

tRNA synthetase (aaRS) (Ibba & Söll, 1999). One approach for overcoming the amino acid specificity of synthetases is to use UAAs of close size, as with photo-leucine and photo-methionine, which contain a photocrosslinking diazirine group (Suchanek et al., 2005). More feasibly, mutation of the amino acid binding pocket of an aminoacyl-tRNA synthetase allows for optimal UAA specificity, as well as reducing unintentional charging by the original amino acid. A mutant *Escherichia coli* methionyl-tRNA synthetase specific for the structural analog UAA azidonorleucine for subsequent copper-catalyzed click chemistry was recently applied to *T. gondii* (Tanrikulu et al., 2009; Wier et al., 2015). The disadvantage of these two methods is the lack of specificity towards a particular protein of interest, as they affect all proteins in the cell.

Expansion of the genetic code by site-specific UAA incorporation at precise locations of a protein was accomplished by exploiting differences in aaRS/tRNA pairs between the three domains of life (Figure 1-5). This was first discovered when a eukaryotic *Saccharomyces cerevisiae* glutamine tRNA was found to be compatible with the prokaryotic *E. coli* ribosome but unable to be charged by any *E. coli* aaRS, while the cognate *S. cerevisiae* glutaminyl-tRNA synthetase was also did not exhibit nonspecific charging of *E. coli* tRNA (Liu & Schultz, 1999). Consequently, the *S. cerevisiae* aaRS/tRNA pair could be expressed in *E. coli* with complete functionality for translation but no tRNA charging cross-reactivity. Mutation of the anticodon to 5'-CUA-3' results in an amber suppressor tRNA, enabling incorporation of an amino acid site-specifically within a protein of interest engineered with an in-frame amber stop codon, thereby establishing a new sense codon. Mutagenesis of the aaRS for specificity towards UAAs with different side chains was achieved with a resistance marker that could only be fully translated with a correctly charged amber suppressor tRNA. Subsequent UAA systems using a similar amber suppression approach soon followed, establishing improvements in range of allowable UAAs (e.g.

tyrosyl-tRNA synthetase template for bulkier functional groups) and increased specificity and efficiency (e.g. an orthogonal pair from the archaea *Methanococcus jannaschii*) (L. Wang et al., 2000; L. Wang & Schultz, 2001). Using prokaryotic aaRS/tRNA pairs, genetically encoded UAAs have been adapted to a broad range of eukaryotic systems, including multicellular organisms, but, to date, has not been previously demonstrated in a protozoan (L. Wang, 2017b). While the amber stop codon was initially chosen for this purpose in *E. coli* due to the significantly lower frequency compared to the two other nonsense codons (only ~7% of all genes), UAA incorporation by amber suppression is well tolerated by other organisms that have a greater ratio of amber codons, and have been used for sensitive applications such as live cell imaging (Aloush et al., 2018; Hoffmann et al., 2015; Young & Schultz, 2010). Concerns about potential toxicity through nonspecific incorporation of the UAA can also be mitigated using a conditionally expressed aaRS system (Sakamoto et al., 2002).

UAAs enable proteins of interest to exhibit new and beneficial properties while simultaneously limiting perturbation of the protein in its natural cellular environment. Fluorescent moieties are useful for sensitive microscopy techniques such as single-molecule imaging and fluorescence resonance energy transfer (Lemke, 2011; Pantoja et al., 2009). Phosphomimetic, glycosylated, and acetylated UAAs can be used for studying effects of post-translational modifications on native protein function (Q. Wang et al., 2009). Heavy atom-containing UAAs such as *p*-iodophenylalanine have aided in crystallographic structure determination using anomalous diffraction without the need for crystal soaking (Xie et al., 2004). Isotopic and fluoridated UAAs have been used in assignment strategies for nuclear magnetic resonance spectroscopy (Jones et al., 2009). Photoreactive UAAs provide an efficient method for inducing

several desirable chemical changes, such as selective activation of photocaged residues, autocleavage of the protein backbone, and photoactivated crosslinking (Young & Schultz, 2010).

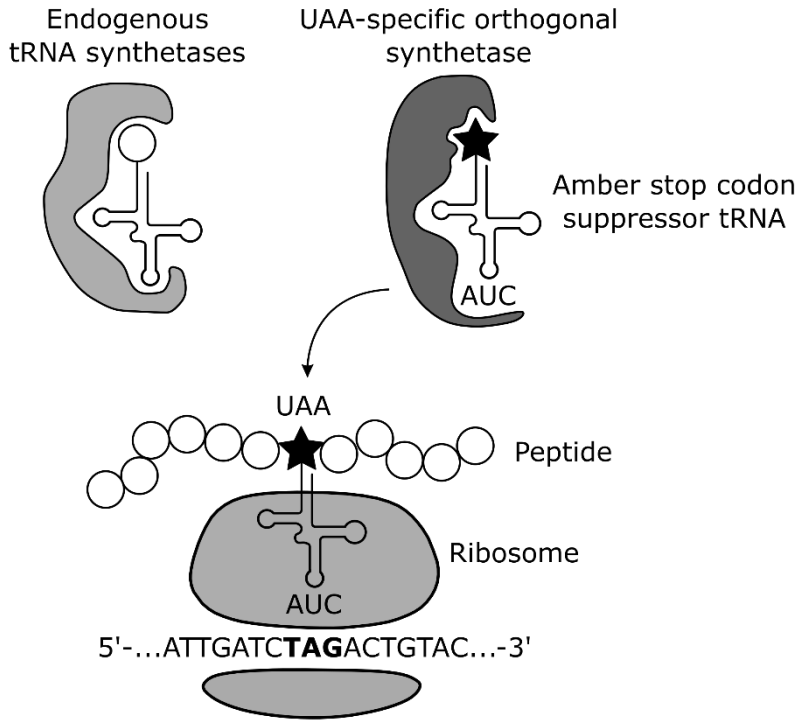

Figure 1-5. Site-specific unnatural amino acid incorporation by amber stop codon suppression. Unnatural amino acids can be incorporated into a protein of interest by expressing an orthogonal mutant aminoacyl-tRNA synthetase and cognate anti-amber tRNA pair. The newly introduced synthetase should not aminoacylate endogenous tRNAs, and the amber suppressor tRNA should not be aminoacylated by endogenous synthetases. However, the tRNA must be compatible with the endogenous ribosome. By expressing a gene with an engineered in-frame amber stop codon (TAG), the desired unnatural amino acid will be added to the primary sequence of the full-length protein.

1.4.2 – The photoactivated crosslinker *p*-azidophenylalanine

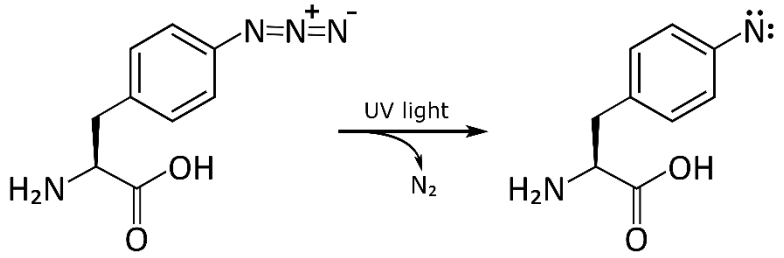

Figure 1-6. *P*-azidophenylalanine is a photoactivated crosslinker. *P*-azidophenylalanine (shown left) is an aromatic unnatural amino acid with an azide moiety. This amino acid can be incorporated into a protein of interest using amber stop codon suppression. Upon exposure to ultraviolet light, diatomic nitrogen is released and a reactive nitrene intermediate is generated and subsequently forms covalent crosslinks with proximal residues.

The UAA *p*-azidophenylalanine (Azi) belongs to a class of photoreactive crosslinkers called aryl azides, which have been employed in biological contexts since 1969 (Fleet et al., 1969). Upon activation of the aryl azide by ultraviolet light, diatomic nitrogen is liberated and an unstable nitrene intermediate is formed (Figure 1-6) (Hermanson, 2013). The nitrene quickly reacts with neighboring peptides, either directly through carbon-hydrogen and nitrogen-hydrogen insertions, or by nucleophilic substitution of amines by a ring expanded dehydroazepine intermediate. The short activation period (~0.1-1 ms) is beneficial for selectively trapping strong interactions, but these intermediates are also able to react with solvent water if no protein is sufficiently close for crosslinking (Staros, 1980). In addition, unlike commonly used chemical crosslinkers that employ extended spacer arms (e.g. primary amine-reactive N-hydroxysuccinimide esters), the reactive moiety of Azi is spatially limited. Therefore, proper placement of Azi within the binding interface between two proteins is necessary for efficient crosslinking. While peak excitation of the aryl azide occurs with UV-C (254 nm), successful activation has been demonstrated using lower energy UV-A (365 nm), significantly reducing nonspecific protein damage (Takimoto et al., 2009).

The Azi-specific amber suppression system implemented in *T. gondii* for this thesis was derived from the pIre-Azi3 construct designed for mammalian cells (Coin et al., 2013). This was

accomplished using a hybrid *E. coli* mutant tyrosyl-tRNA synthetase and *Bacillus stearothermophilus* amber suppressor tRNA pair. Specificity of the tyrosyl-tRNA synthetase towards Azi was obtained by successive mutagenesis (Y37L, D182S, F183M, L186A, D265R) selecting for efficient Azi incorporation to reporter proteins (Chen et al., 2007; W. Liu et al., 2007; Takimoto et al., 2009). The *B. stearothermophilus* $tRNA^{Tyr}$, which can be aminoacylated by the *E. coli* synthetase despite sequence differences, initially had to be used instead of the corresponding *E. coli* tRNA as the latter lacks intragenic control regions necessary for type 2 RNA polymerase III transcription in eukaryotes (Bedouelle, 1990; Sakamoto et al., 2002). The *B. stearothermophilus* tRNA was kept even after tRNA expression was transitioned to the U6 RNA polymerase III promoter, which has well-defined upstream initiator and downstream poly-thymine terminator elements, although any amber suppressor tRNA could now theoretically be expressed (W. Wang et al., 2007). Multiple copies of the tRNA cassette are built into the expression construct to maximize UAA incorporation, and yields up to ~30% of wild-type (the upper efficiency limit of stop codon suppression) have been obtained in a wide range of organisms including human cells, *E. coli*, and *Drosophila melanogaster* (Coin et al., 2011; Mukai et al., 2010; Ryu & Schultz, 2006; Sakamoto et al., 2002).

1.5 – Objectives

Toxoplasma gondii is a highly successful opportunistic pathogen that poses risk for severe and potentially fatal neurological issues during immunocompromised states and primary congenital infections. *T. gondii* also serves as a model organism for studying other members of the parasitic phylum Apicomplexa, including *Plasmodium*, the etiologic agent of malaria. The IMC is a hallmark of apicomplexans, and is innately involved in parasite motility, invasion, and replication. Study of this organelle is challenging using traditional methods, such as co-immunoprecipitations, due to its dual cytoskeletal and membrane composition. Here, I document the adaptation of a photoactivatable crosslinking unnatural amino acid system in *T. gondii* that enables covalent capture of protein-protein interactions within the normal intracellular environment, providing information about the spatial orientation of these associations and allowing identification of binding partners through either a candidate or *de novo* approach. Chapter 2 discusses the controls necessary to demonstrate functionality in the parasite system, and application of the UAA system towards the essential IMC protein ILP1. This is the first time that interactions between two components of the IMC cytoskeleton have been elucidated. Chapter 3 expands the work done on ILP1 to the N-terminal EF-hand domain to confirm yet another direct IMC binding partner. Chapter 4 explores application towards ARO, an essential protein responsible for tethering of the rhoptries. The objective of this work is to establish a new technology that is broadly practical for studying the mechanisms for invasion and growth of this unique pathogen.

CHAPTER 2:

A photoactivatable crosslinking system in *Toxoplasma gondii* reveals organization of the parasite inner membrane complex

2.1 - Abstract

The *Toxoplasma gondii* inner membrane complex (IMC) is an important organelle involved in parasite motility and replication. The IMC resides beneath the parasite's plasma membrane and is composed of both membrane and cytoskeletal components. Although the protein composition of the IMC is becoming better understood, the protein-protein associations that enable proper functioning of the organelle remain largely unknown. Determining protein interactions in the IMC cytoskeletal network is particularly challenging, as disrupting the cytoskeleton requires conditions that disrupt protein complexes. To circumvent this problem, we demonstrate the application of a photoreactive unnatural amino acid (UAA) crosslinking system to capture protein interactions in the native intracellular environment. In addition to identifying binding partners, the UAA approach maps the binding interface of the bait protein used for crosslinking, providing structural information of the interacting proteins. We apply this technology to the essential IMC protein ILP1 and demonstrate that distinct regions of its C-terminal coiled-coil domain crosslink to the alveolins IMC3 and IMC6, as well as IMC27. We also show that the IMC3 C-terminal domain and the IMC6 N-terminal domain are necessary for binding to ILP1, further mapping interactions between ILP1 and the cytoskeleton. Together, this study develops a new approach to study protein-protein interactions in *Toxoplasma* and provides the first insight into the architecture of the cytoskeletal network of the apicomplexan IMC.

2.2 - Introduction

The phylum Apicomplexa consists of some of the most successful eukaryotic intracellular parasites in the world. Apicomplexans that cause disease in humans include *Toxoplasma gondii*, which causes toxoplasmosis in immunocompromised patients and congenitally infected neonates, *Plasmodium spp.*, which cause malaria, and *Cryptosporidium spp*., which are major causes of diarrheal disease in children (Hill et al., 2005; Mackintosh et al., 2004; Sow et al., 2016). Other members of the phylum such as *Eimeria, Theileria, Babesia,* and *Neospora* are veterinary pathogens and result in billions of dollars in losses per year worldwide in the poultry and cattle industries (Dubey, 2003; Kivaria, 2006; Sharman et al., 2010). *T. gondii* serves as a model organism for the study of apicomplexan biology due to its relative ease of continuous culture, high rate of transformation, and a robust set of tools for genetic manipulation and functional analyses.

Apicomplexans exhibit a number of specialized organelles that enable them to occupy their intracellular niche. One of these is the inner membrane complex (IMC), a unique structure that underlies the plasma membrane of the parasite and consists of flattened membrane vesicles supported by a cytoskeletal filament network (Harding & Meissner, 2014). The membrane and cytoskeletal components of the IMC work in concert to perform critical roles in the lytic cycle of the parasite. First, the IMC houses the glideosome, the actomyosin motor complex that enables gliding motility and host cell invasion (Boucher & Bosch, 2015). Second, it serves as the scaffold for the apicomplexan replication process of internal budding, in which daughter cells are formed within the maternal cytoplasm, ultimately adopting the maternal plasma membrane and yielding progeny (Blader et al., 2015). The asexual stages of *Toxoplasma* undergo endodyogeny, where two daughter cells are produced per maternal parasite with each replication cycle. Other apicomplexans often replicate using variations of this internal budding process called schizogony

or endopolygeny, in which multiple rounds of nuclear replication and karyokinesis result in the generation of up to 64 daughters at once (Morrissette & Sibley, 2002a).

In *Toxoplasma*, the IMC is partitioned into a cone-shaped apical cap (a coccidian-specific structure), a central body portion characterized by an array of rectangular membrane plates, and a basal complex, which is responsible for closure of the daughter buds to complete division (Frénal et al., 2010; Heaslip et al., 2010a). Interestingly, recent studies using *in vivo* proximity-dependent biotin labeling (BioID) and other approaches have revealed that most IMC proteins localize to only one of these subregions (Chen et al., 2015, 2017). Similarly, detergent solubilization studies have shown that the apical cap and body contain separate groups of membrane-associated and cytoskeleton-associated proteins, supporting the idea that each section is composed of specialized cargo that serves varying purposes. While the membrane and cytoskeletal layers are distinct, they are closely associated with each other through protein-protein interactions and fatty acylations that can tether cytoskeletal proteins to the membrane vesicles of the organelle.

Despite an increased understanding of the protein constituents that make up the IMC, the precise roles of most of these proteins and how they are organized remain largely unknown. The filamentous network of the IMC is believed to be formed by the alveolins, a family of fourteen proteins that are characterized by a poorly conserved proline and valine-rich alveolin repeat domain (Anderson-White et al., 2011; Gould et al., 2008). The alveolins have different localizations within the three IMC subregions and likely serve roles in providing structural support for each of these compartments. However, the identification of many non-alveolin detergent-insoluble IMC proteins suggests that the IMC cytoskeleton is a complex structure whose organization remains enigmatic. One such protein is IMC localizing protein 1 (ILP1), which is an IMC body protein that is enriched in forming daughter buds, similar to a subgroup of alveolins

(IMC3/6/10) (Lorestani et al., 2012). We have demonstrated that conditional knockout of ILP1 causes a collapse of IMC integrity and inability to properly replicate, a lethal phenotype for the parasite (Chen et al., 2015). Interestingly, the *Plasmodium* ortholog of ILP1 (*Pf*G2) is not essential, but its disruption results in significant morphological changes in ookinetes and sporozoites, reduced motility, and a loss of sporozoite infectivity (Tremp et al., 2013). How ILP1 imparts structural stability to the parasite would be best understood by determining its binding partners, but studying protein-protein interactions in the IMC cytoskeleton is typically challenging due to its detergent-insoluble nature.

One approach to overcome this difficulty is the use of inducible crosslinking unnatural amino acids (UAA). The UAA technology involves the expansion of the genetic code using an orthogonal aminoacyl-tRNA synthetase and amber stop codon (TAG) suppressor tRNA pair (L. Wang, 2017a; L. Wang et al., 2006). The tRNA is charged with the desired synthetic UAA and can be used by the endogenous ribosomal machinery to incorporate the UAA into the primary sequence of a protein of interest at an engineered in-frame amber stop codon. The UAA *p*-azidophenylalanine belongs to a class of photoreactive crosslinkers called aryl azides and forms a highly reactive nitrene moiety upon exposure to relatively non-destructive 365 nm (UV-A) light (Chin et al., 2003; Takimoto et al., 2009). Because Azi is a zero-length crosslinker, it should only form crosslinks when the UAA is positioned within the binding interface of the bait protein and its partner. Successful crosslinking of the bait can be observed as a higher molecular weight species by western blot. The bound partner can then be verified by immunoblot when the crosslinked partner is suspected, or purified and identified by mass spectrometry if unknown.

Here, we report the successful implementation of a photo-activated UAA crosslinking system in *T. gondii* and the application towards uncovering protein interactions within the intricate

multiprotein IMC cytoskeleton complex. We first demonstrate that this system functions efficiently in the parasite in terms of both Azi incorporation and photocrosslinking. We then use this technology to show that ILP1 directly interacts with multiple components of the cytoskeleton of the IMC, revealing the first organization of this organellar compartment and identifying the precise binding regions through which ILP1 associates with IMC network. This photoactivatable UAA system provides a unique tool to dissect additional protein-protein interactions that will help to unravel aspects of *T. gondii* cell biology that may have historically been difficult to study.

2.3 - Results

Adaptation of the photoreactive unnatural amino acid crosslinking system in *Toxoplasma gondii*

In an amber suppression system, UAAs such as Azi are incorporated into an engineered amber stop codon (sequence TAG) within the protein sequence in lieu of premature termination (Fig 2-1A, B). To adapt this system to *T. gondii*, we generated a construct containing the Azi-specific enhanced *E. coli* aminoacyl-tRNA synthetase (E2AziRS) (Coin et al., 2013) with a C-terminal Ty epitope tag driven by the *GRA1* promoter (Fig 2-1C). We also engineered an amber suppressor tRNA expression cassette driven by the *Toxoplasma* U6 promoter, which was recently characterized for use in the CRISPR/Cas9 system (Sidik et al., 2014). To maximize expression of the tRNA, we assembled three tandem copies of the cassette, a strategy that improves expression in mammalian systems (Coin et al., 2013). Transfection of this construct into RHΔ*hxgprt* strain parasites showed that E2AziRS-Ty localizes to the cytoplasm, as expected (Fig 2-1D). We were able to generate stable lines expressing E2AziRS-Ty, demonstrating that *T. gondii* tolerates constitutive expression of the aminoacyl-tRNA synthetase/tRNA cassettes.

To demonstrate that this system can be used to incorporate Azi into an endogenously translated protein, we explored the use of surface antigen 1 (SAG1), a highly abundant yet dispensable GPI-anchored cell surface protein (Burg et al., 1988; K. Kim & Boothroyd, 1995). We built a SAG1 expression construct in which the second codon is mutated to the amber stop codon (SAG1 $F2_{TAG}$, Fig 2-1E). We disrupted endogenous SAG1 using CRISPR/Cas9 and used this strain for expression of the aminoacyl-tRNA synthetase/tRNA cassettes and the SAG1 nonsense mutant (Sidik et al., 2014). In the absence of Azi, these parasites express E2AziRS-Ty but not SAG1 as observed by immunofluorescence assay (IFA, Fig 2-1F). However, upon overnight incubation in growth medium supplemented with Azi, robust expression of SAG1 is observed at the cell periphery. Quantification by western blot intensity shows ~35% SAG1 expression compared to wild-type parasites, which is on par with the best efficiency observed in mammalian systems (Fig 2-1G) (Coin et al., 2013; Sakamoto et al., 2002). Therefore, Azi can be imported into the parasite's cytoplasm and efficiently incorporated into a control protein in the context of amber suppression.

Successful photoactivatable crosslinking using the UPRT homodimer

To determine if we could obtain UV-induced crosslinking of Azi in *Toxoplasma*, we employed the protein uracil phosphoribosyltransferase (UPRT), which forms a homodimer as revealed by the crystal structure (PDB: 1BD4, 1JLR) (M. A. Schumacher et al., 1998; Maria A. Schumacher et al., 2002). UPRT was also selected because it is a small cytoplasmic protein that is produced in abundance yet is not essential for parasite survival. The major region for dimer stabilization was reported to be a hydrophobic β-arm between residues 82 to 103. Within this region, we chose leucine 92 and tyrosine 96 for amber substitution (L92 and Y96) based on their

polarity and orientation towards the partner subunit (Fig 2-2A). The L92 and Y96 mutants were engineered in an HA tagged UPRT construct, which localized to the cytoplasm upon addition of Azi to the media, as expected (Fig 2-2B). In addition, to demonstrate that any potential crosslinked products observed by western blot are indeed due to a covalently bound homodimer, we also expressed a Myc-tagged wild type copy of UPRT, which should not be crosslinked unless bound to an activated Azi-containing UPRT-HA monomer (Fig 2-2C). To assess crosslinking, extracellular parasites were irradiated with 365 nm UV light, lysed in sample buffer for SDS-PAGE, and probed with anti-HA and anti-Myc antibodies. We observed upshifted signals corresponding to crosslinked species in both UPRT-HA Azi mutants, whereas the wild type UPRT-HA control does not form appreciable signal other than nonspecific background (Fig 2-2D). The same upshifts are observed in the anti-Myc blot indicating the products are *bona fide* crosslinked homodimers (Fig 2-2E). The discrepancy in migration between L92 and Y96 is likely to be a consequence of crosslinking to distinct regions of the partner subunit. The upshifts also do not correspond to a direct addition of constituent monomer masses, but instead tend to reflect a larger mass, again likely due to the aberrant SDS-PAGE migration of the nonlinearly crosslinked peptides.

Characterization of potential posttranslational modifications of ILP1

Prior to applying this crosslinking technology to ILP1, we first aligned the protein sequence from model apicomplexans and identified regions of interest that may be responsible for its trafficking and function (S1 Fig). The *Plasmodium* ortholog of ILP1 is named *Pf*G2 due to a conserved glycine at position 2 that is likely myristoylated and is essential for proper trafficking of the protein (Tremp et al., 2013). To assess whether this residue is similarly important in *T.*

gondii, we mutated the second position glycine to alanine (G2A) and expressed it as a second copy in the parasite. ILP1 also contains two cysteine-cysteine motifs that are weakly predicted to be palmitoylated by CSS-PALM (Ren et al., 2008), thus a quadruple C95S, C96S, C273S, C274S mutant (4Cys) was also generated. Surprisingly, both the G2 and 4Cys mutants appeared to correctly traffic to the IMC (S2B Fig). To determine if these sites were important for function, the endogenous copy of ILP1 was disrupted by CRISPR/Cas9 and the knockout was verified by IFA and PCR (S2A Fig). Quantification of plaque assays showed the 4Cys mutation did not have any significant effect on plaque formation, but the G2A mutant resulted in significantly smaller plaques, suggesting that myristoylation does play at least some role in ILP1 function (S2C Fig). *Pf*G2 expressed in *Toxoplasma* unexpectedly localized to the cytoplasm and attempts to knockout the endogenous ILP1 in this background were not successful, indicating that the *Plasmodium* ortholog cannot complement *Toxoplasma* ILP1 (S2B Fig).

Application of the UAA system to ILP1 and preliminary identification of its partners

As the posttranslational modification sites were not critical for ILP1, we suspected that interaction with other components of the IMC cytoskeleton played an important role in function. Phyre2 analysis reveals a potential N-terminal EF hand-like domain from residues 25-109 (Fig 2-3A) (Kelley et al., 2015). However, this domain appears to be a degenerate EF hand domain that is unlikely to bind calcium. Intriguingly, COILS analysis indicates a potential coiled-coil domain in the C-terminal region of the protein (residues 129-230) (Fig 2-3B) (Lupas, 1997). Coiled-coil domains are alpha-helical assemblies that are involved in many protein binding-dependent functions such as vesicle transport and structural scaffolding, suggesting this region may be involved in ILP1 function (Lupas & Bassler, 2017). We first attempted co-immunoprecipitation

(co-IP) experiments to determine putative targets of ILP1. Due to the detergent-insoluble nature of ILP1, we employed extensive sonication to disrupt the cytoskeleton and release ILP1 for co-IP (Lorestani et al., 2012). Mass spectrometric analysis of the co-precipitated proteins revealed the IMC network-forming alveolins IMC1/3/4/6/10 as well as the glideosome-associated proteins MLC1 and GAP45 (S3 Fig). However, this approach was insufficient for determining direct partners, suggesting our UAA approach might better reveal direct interactions of ILP1.

To apply the UAA system to ILP1, we focused on the coiled-coil domain of the protein and used secondary structure and residue burial predictions to guide the construction of 14 amber mutants (Fig 2-3C: K130, E140, Q150, T152, Y160, Q168, Q170, T184, T187, I188, R194, A204, E209, K212). Each of the mutants were stably expressed in parasites containing the aminoacyl-tRNA synthetase/tRNA cassettes and the strains were subjected to Azi incorporation and photocrosslinking. Western blot analysis of the irradiated parasites resulted in six appreciable crosslinked upshifts (strains Y160, Q168, T184, T187, I188, and E209) that appeared to represent three distinct migration patterns at ~65kDa, ~200kDa and ~140kDa (Fig 2-3D).

Identification of IMC3 as a binding partner of ILP1

To identify the shifted partners of ILP1, we investigated the possibility of a direct interaction between ILP1 and one of the alveolins, as several of these components of the IMC cytoskeleton were present in our IP data. IMC3, 6, and 10 are enriched in nascent daughter buds during endodyogeny similar to ILP1 (Dubey et al., 2017), and their sizes are consistent with the shifts observed for the two larger crosslinked products. However, IMC1 and IMC4 also represent good candidates even though these proteins are more equally present in daughter buds and maternal parasites. To determine if IMC3 was one of the larger products, we endogenously Myc-

tagged this protein in the T184, T187, I188 and E209 UAA strains (Fig 2-4A). Unfortunately, potential crosslinked products in the western blot of whole cell lysates were not visible above background, preventing us from determining if IMC3 was the shifted partner. We thus used a denaturing IP approach, in which the IMC cytoskeleton was first disrupted by boiling in 1% SDS and then diluted to standard RIPA conditions for IP (Fig 2-4B). We were able to purify both uncrosslinked ILP1 and the shifted products as assessed by anti-HA staining (Fig 2-4C). Probing the eluates with anti-Myc antibodies showed that IMC3 was indeed crosslinked to ILP1 in the T184, T187, and I188 strains, but not the E209 strain. This result demonstrates that ILP1 binds to IMC3 in the IMC cytoskeleton and maps the IMC3 binding interface on ILP1.

The C-terminal region of IMC3 is necessary for ILP1 crosslinking.

We were interested to determine which region of IMC3 binds to ILP1 via residues T184, T187, and I188. The alveolin domain of IMC3 has been shown to be sufficient for targeting to the IMC, enabling this region to be tested as a binding partner using the UAA system (Anderson-White et al., 2011). We thus generated V5 epitope tagged expression constructs of the alveolin domain alone ($IMC3_A$) and the alveolin domain plus the C-terminal region of the protein ($IMC3_{AC}$) to determine if these would crosslink to ILP1 (Fig 2-5A). While the IMC3 alveolin domain alone can direct the protein to the IMC as described, we also noticed some diffuse cytoplasmic staining. Complete trafficking to the IMC appears to be restored when the C-terminal region is included, demonstrating that this portion of the protein also plays a role in proper localization to the IMC. Upon Azi crosslinking in the T187 strain, $IMC3_A$ did not form an additional shifted ILP1 product, indicating that this region is not sufficient for binding to T187 (Fig 2-5B). However, the $IMC3_{AC}$ construct did result in a new smaller crosslinked product at the expected size for this IMC3

truncation. IP of ILP1 again showed the smaller product only in the $IMC3_{AC}$ strain (Fig 2-5C). Probing with V5 revealed that this new shifted product is indeed $IMC3_{AC}$. We additionally pulled down $IMC3_{AC}$ using anti-V5 IP and observed that this co-precipitated crosslinked ILP1 (Fig 2-5D). This result suggests that ILP1 binds to the C-terminal region of IMC3, downstream of the alveolin domain.

ILP1 crosslinks to IMC6 at residue E209

To identify the protein crosslinked at residue E209, we examined the predicted sizes of the other alveolins for likely candidates. IMC4 and IMC6 have a smaller theoretical mass compared to IMC3, which may be reflected in the faster migrating upshift. We therefore tagged IMC4 and IMC6 with 3xMyc tags in the E209 strain and also in the T187 strain as a negative control (as this residue binds IMC3). Interestingly, the ILP1 E209 shifted product migrated slightly slower in the IMC6-3xMyc strain compared to those tagged for IMC3 and IMC4, indicating that IMC6 is likely the crosslinked partner (Fig 2-6A). In the T187 strains, a slight shift can also be detected when IMC3 was tagged, but the relative shift was less apparent due to the overall larger masses. Denaturing co-IPs were then performed to verify that IMC6 is the E209 crosslinked partner (Fig 2-6B). Anti-Myc staining demonstrated that E209 is indeed covalently crosslinked to IMC6, confirming this second interaction of ILP1 with an alveolin in the cytoskeleton.

The N-terminal region of IMC6 is necessary for crosslinking to ILP1

Having shown that ILP1 binds to the C-terminal region of IMC3, we attempted similar domain mapping experiments with IMC6. We again generated V5 tagged constructs of the alveolin domain alone ($IMC6_{A}$) or alveolin plus the C-terminal region ($IMC6_{AC}$, Fig 2-7A). Curiously, the

diffuse localization in the maternal cytoplasm occurred in both the $IMC6_{A}$ and $IMC6_{AC}$ strains. Neither of these truncations resulted in an additional crosslinked product, by western blot of either whole cell lysates or immunoprecipitations (Fig 2-7B-D). Instead, proper staining at the parasite periphery was observed when the N-terminal portion of IMC6 was added to the alveolin domain ($IMC6_{NA}$, 2-Fig 7E). ILP1 E209 Azi incorporation and photocrosslinking in this background resulted in a new upshifted product of the anticipated size for $IMC6_{NA}$ (Fig 2-7F). This interaction was confirmed by denaturing IP as performed above. Together, this data indicates that the ILP1 binding site resides within the N-terminal region of IMC6.

IMC27 is the third ILP1 binding partner

None of the alveolins were candidates for the lower molecular weight product identified by Y160 and Q168, thus we performed a large scale crosslinking and IP experiment to identify the partner at these residues. As Y160 showed more robust crosslinking, this strain was expanded for a large scale denaturing IP and the eluted proteins were separated by SDS-PAGE and viewed by Coomassie staining (Fig 2-8A). Proteins within the gel slice corresponding to the upshifted species were identified by LC-MS/MS (S4 Table). As expected, ILP1 was the top hit in the spectrum, and the second most abundant protein identified was IMC27, a protein we previously identified using *in vivo* biotinylation in the IMC (Chen et al., 2017). Detergent fractionation revealed that IMC27 is a component of the IMC cytoskeleton similar to ILP1 (Fig 2-8B), and the protein migrates at ~26 kDa (including a ~5 kDa epitope tag), potentially agreeing with the observed crosslink size. To confirm this interaction, IMC27 was endogenously 3xMyc tagged and this strain was transfected with the synthetase/tRNA and either ILP1 Y160 or Q168 constructs. IMC12 was also 3xMyc tagged in the Y160 strain as a negative control. Western blot analysis showed a distinct

difference in migration between IMC27 tagged and untagged lines, indicating that IMC27 is the partner at these residues (Fig 2-8C). Denaturing IPs demonstrated that the shifted product stains with both HA (ILP1) and Myc (IMC27) antibodies, confirming that IMC27 is the crosslinked partner (Fig 2-8D). Intriguingly, while ILP1 and its partners IMC3 and IMC6 are all enriched in daughter buds, IMC27 is completely restricted to the maternal IMC (Fig 2-8E). Thus, the interaction between ILP1 and IMC27 is likely to only occur in maternal parasites following the completion of replication.

2.4 - Discussion

The implementation of a photoactivatable UAA crosslinking system in *T. gondii* enables a new tool for studying protein-protein interactions that govern parasite-specific biology. Mutant proteins containing the photoreactive UAA Azi are produced *in vivo*, ensuring proper folding and localization of target complexes in their native cellular environment. This avoids the disadvantages encountered in exogenous protein interaction techniques such as recombinant expression and yeast two-hybrid screens, where artificial experimental conditions may disrupt legitimate associations or form false positives. Unlike more traditional chemical crosslinkers that employ a spacer arm, Azi is considered a zero-length crosslinker and therefore requires proper positioning of amber stop codon substitution near a binding interface to obtain crosslinking. While amber stop codon positioning can be challenging, successful crosslinking not only identifies the interacting partner but also maps the precise interaction domain on the bait protein, thereby providing more structural information of a complex compared to alternative protein-protein interaction approaches.

A common concern for expanding the genetic code for UAAs is the appropriation of a stop codon. When initially developed in *E. coli*, the system was designed to use the amber stop codon

as it is the least frequent (~7%) of the three nonsense codons (Wals & Ovaa, 2014). While *T. gondii* exhibits a more uniform stop codon distribution (Nakamura et al., 2000), we were able to obtain robust incorporation and reproducible crosslinking patterns with our proteins of interest, indicating that apprehensions regarding nonspecific incorporation or crosslinking are unwarranted. This is likely because Azi located at the C-terminus of the majority of proteins would rarely reside in a binding interface required for the zero-length crosslinker. In addition, background derived from undesired Azi incorporation and photocrosslinking of endogenous proteins would not be observed by western blot unless these proteins were to somehow nonspecifically crosslink to our bait protein. A related concern is that Azi incorporation into endogenous proteins terminating with amber codons could result in the C-terminal extension of polypeptides during translation and disruption of proper termination. In our experience, prolonged exposure to Azi during growth does result in slower growth and ultimately cellular arrest similar to prior observations using an alternative UAA (Wier et al., 2015), but this is not a significant issue as the parasites are collected and processed within 24 hours of induction. Of the four proteins discussed (ILP1, IMC3, IMC6, and IMC27), the endogenous IMC3 gene terminates in an amber stop codon, but the effect of nonspecific Azi incorporation was not considered as this amber codon was changed to an ochre stop codon (TAA) in the process of C-terminal endogenous epitope tagging.

Our SAG1 and UPRT controls demonstrate efficient incorporation and crosslinking of Azi in target proteins of *T. gondii*. We initially chose an aromatic amino acid replacement in SAG1 (F2 to Azi) to limit any potential loss-of-function. However, our later experiments revealed that proteins generally appear to tolerate the single amino acid changes well, regardless of the properties of the residue being substituted. The risk of disrupting more critical residues is also mitigated by testing multiple mutants within a candidate interaction domain. To assess

crosslinking, we utilized UPRT due to the available crystal structure and an understanding of its homodimer formation dynamics, guiding us toward the placement of amber codons at L92 and Y96. Both mutants generated SDS-PAGE upshifted products upon exposure to UV light, which were verified as homodimers using an alternatively tagged copy of UPRT. We observed that the migration of upshifted products is consistently slower than the combined mass of the partners and may vary depending on crosslinking site. Similar aberrations in migration in Azi crosslinked samples have been observed in other systems (Coin et al., 2013; Mehnert et al., 2014; Takimoto et al., 2009).

The challenges of studying protein-protein interactions in the IMC are reflected in our initial ILP1 co-IP, where we identified several IMC proteins but were not able to determine meaningful interactions. The UAA system overcomes these challenges and enables determination of precise interactions within the rigid cytoskeletal meshwork of the IMC. The small size and distinct coiled-coil region of ILP1 provided a reasonable area to test for interactions via Azi crosslinking. None of the point mutations appeared to affect IMC trafficking, but differences in the efficiency of Azi incorporation among the different mutants were observed by western blot, suggesting that some substitutions are better tolerated than others (Fig 2-3). As the alveolins are believed to compose the cytoskeletal foundation through formation of intermediate filament-like polymers, those that shared similar localization patterns to ILP1 (IMC 3/6/10) were top candidates for binding partners. We demonstrated direct crosslinking of ILP1 to both IMC3 and IMC6, providing the first insight into the organization of the alveolar network. When verifying these interactions, we found that the denaturing co-IP procedure was particularly useful for reducing nonspecific background and also dramatically reducing undesirable amounts of uncrosslinked prey that otherwise confounded our western blot results. Like UPRT, the ILP1 upshifts consistently

migrated slower than anticipated, but unlike the control, the crosslink clusters seemed to migrate similarly, possibly due to the linear nature of the coiled-coil domain. The binding sites on ILP1 are relatively close to each other and whether one ILP1 molecule can simultaneously bind to both partners remains unclear. We constructed a T187/E209 double Azi mutant in an attempt to determine if a trimeric complex was possible, but lower UAA incorporation in this mutant and the large expected mass made the results inconclusive.

Our IMC3 and IMC6 deletion analyses also demonstrated that the C-terminal region of IMC3 downstream of the alveolin domain and the N-terminal region of IMC6 upstream of the alveolin domain are necessary for binding to ILP1. The improved localization to the IMC upon inclusion of these regions suggests that interaction with ILP1 enhances its association within the network. While these results strongly suggest that ILP1 binds to these domains of IMC3/6, we cannot exclude the possibility that our deletions alter how the proteins interact. Additional truncations of IMC3/6 are likely to isolate a sufficiently small region that would enable precise determination of the corresponding binding regions on IMC3 and IMC6 using the UAA system.

IMC27 was identified as the binding partner at residues Y160/Q168 of ILP1 using a large scale IP and LC-MS/MS peptide identification approach. Our success demonstrates that even though the abundance of crosslinked material is a fraction of the total amount of the purified bait protein, we can obtain yields that are adequate for mass spectrometric analysis. We explored the use of software such as Crossfinder, a tool for finding crosslinked peptides in a LC-MS/MS spectrum, to attempt to map the binding location of the prey, but this was unsuccessful (Mueller-Planitz, 2015). This may be due to a particularly large region of IMC27 (residues 96-141, 28% of the total length) that lacks tryptic cleavage sites. Intriguingly, IMC27 localizes solely to the maternal IMC, indicating that there is a transition where ILP1 forms new interactions following

the maturation of the budding daughter IMC. Because our experiments were carried out using extracellular parasites, the binding of IMC3 and IMC6 are also likely occurring in the maternal IMC. However, the precise colocalization of ILP1, IMC3 and IMC6 throughout the cell cycle suggests that these associations are likely to occur in both the maternal and daughter IMC. Future experiments comparing intracellular and extracellular parasites will help distinguish events that occur in the daughter and maternal IMC.

The interactions of ILP1 and its binding partners also begin to unravel how each are differently utilized in the *Toxoplasma* and *Plasmodium* IMC. In *Toxoplasma*, ILP1 is essential and its alveolin partners IMC3 and IMC6 are predicted by genome-wide CRISPR studies to be very important or essential as well (Sidik et al., 2016). In contrast, both *Pf*G2 and *Pf*IMC1h (*Toxoplasma* IMC3) can be disrupted, resulting in similar morphological changes in ookinetes and sporozoites that suggest these partners play important, but not essential, roles in organizing the IMC cytoskeleton (Tremp et al., 2013; Volkmann et al., 2012). Unlike IMC3, IMC6 (*Pf*IMC1k) and IMC10 (*Pf*IMC1j) appear to be essential or important for growth in both apicomplexans (Zhang et al., 2018), indicating a more conserved role in maintaining IMC integrity. Interestingly, *Toxoplasma* IMC27 is predicted to be dispensable while its Plasmodial ortholog PF3D7_0518900 is considered to be either essential or important for growth, suggesting that there is additional functional divergence in the IMC between these apicomplexans. Overall, these comparisons indicate that *Toxoplasma* relies on ILP1 and its binding partners for structural support of the IMC to a greater degree compared to *Plasmodium*.

To our knowledge, this is the first use of photoreactive crosslinkers by expansion of the genetic code in any protozoan. We have demonstrated that site-specific crosslinking using Azi can be used to decipher the interactions of ILP1 within the IMC, and we anticipate successful

application towards other IMC proteins such as the alveolins to further determine the organization of this organelle. Intriguingly, a recent proteomic analysis of the microtubule-based conoid has revealed that many of its constituent proteins have coiled-coil domains, making this compartment another good candidate for our system. Alternative regions of ILP1, such as the N-terminal EF-hand domain, are also open for investigation. Assuming the UAA system is applicable to other protozoans, photoreactive crosslinkers also would be excellent tools for probing other unique structures such as the flagellar pocket of trypanosomes, the axostyle of trichomonads, or the ventral disc of *Giardia* (Benchimol, 2004; Brown et al., 2016; Nosala et al., 2018; Perdomo et al., 2016; Vaughan & Gull, 2016).

2.5 - Materials and Methods

Toxoplasma gondii and host cell culture

Parental *T. gondii* RHΔ*hxgprt* and subsequent strains were grown on confluent monolayers of human foreskin fibroblasts (HFF) at 37°C and 5% CO_2 in Dulbecco's Modified Eagle Medium (DMEM) supplemented with 5% fetal bovine serum (Gibco), 5% Cosmic calf serum (Hyclone), and 1X penicillin-streptomycin-L-glutamine (Gibco). Constructs containing selectable markers were selected using 1 µM pyrimethamine (DHFR-TS), 50 µg/mL mycophenolic acid-xanthine (HXGPRT), or 40 µM chloramphenicol (CAT) (Donald et al., 1996; Donald & Roos, 1993; K. Kim et al., 1993). Homologous recombination to the UPRT locus was negatively selected using 5 µM 5-fluorodeoxyuridine (FUDR) (Donald & Roos, 1995).

Plasmid construction and mutagenesis

Sequences for E2AziRS and cognate amber suppressor tRNA (*Bst*-Yam) were obtained from pIre-Azi3 (Coin et al., 2013; Takimoto et al., 2009). Primers P1/P2 were used to amplify E2AziRS with NsiI/PacI overhangs and a C-terminal Ty1 epitope tag. This product was ligated into pGRA-HA-HPT (Saeij et al., 2006) to drive constitutive expression from the *GRA1* promoter and enable stable integration with HXGPRT (pGra-E2AziTy.HPT). The tRNA cassette was generated by synthesizing a gBlock gene fragment (IDT) consisting of the 82 bp *Bst*-Yam tRNA sequence flanked by a portion of the *T. gondii* U6 promoter and poly-thymine RNA polymerase III terminator as described (Sidik et al., 2014), with AvrII/XbaI restriction sites (S6 Text). This insert was ligated into AvrII/XbaI-digested pU6-Universal to restore the complete U6 cassette, replacing the CRISPR/Cas9 gRNA scaffold with *Bst*-Yam. The cassette (TgU6-$tRNA_{CUA}$) was amplified with P3/P4 to incorporate 5' Acc65I-XhoI and 3' SalI-BglII-XbaI restriction sites and subcloned into the pJET1.2/blunt vector (ThermoFisher). Triple tandem cassettes were constructed as previously described (Coin et al., 2013). Briefly, a XhoI/SalI-flanked TgU6-$tRNA_{CUA}$ insert was ligated into a SalI-linearized TgU6-$tRNA_{CUA}$ pJET vector using complementary ends. This was iterated to double and triple tandem copies of the tRNA cassette, confirming orientation of each cassette by diagnostic digests. The triple cassette was excised with Acc65I/BglII and ligated into pGra-E2AziTy.HPT to obtain the final construct pGra-E2AziTy.HPT.tRNAx3.

The following plasmids were all generated in a similar fashion by ligating a gene of interest using NsiI/PacI overhangs into a modified pGRA-HA-HPT backbone (Saeij et al., 2006). First, HXGPRT was replaced with a DHFR cassette amplified from p3xHA.LIC-DHFR (Huynh & Carruthers, 2009; Konrad et al., 2011) using primers P5/P6 and cloning via HindIII/NgoMIV. *SAG1* (TgGT1_233460) was amplified from RH genomic DNA using primers P7/P8, which

flanked the gene with NsiI/PacI sites and mutated the second codon TTT to the amber stop codon TAG, which appears as the third codon due to the NsiI site (the correct start of the gene begins with the sequence MFPKAV...). The *UPRT* coding sequence was amplified from RH cDNA either with an N-terminal c-Myc tag (P9/P10) or a C-terminal HA tag (P11/P12) and ligated to obtain pGRA-Myc-UPRT_wt.DHFR and pGRA-UPRT-HA_wt.DHFR. Amber mutations L92* and Y96* were generated in pGRA-UPRT-HA_wt.DHFR using the Q5 Site Directed Mutagenesis kit (New England Biolabs) using primers P13/P14 and P15/P16. The mutant UPRT-HA cassettes were amplified with NotI/PciI flanks (P17/P18) and ligated into pJET1.2/blunt. The cassette was excised with NotI and ligated into NotI-linearized pGRA-Myc-UPRT_wt.DHFR to obtain the final double Myc-UPRT/UPRT-HA expression vectors.

An ILP1 expression construct was assembled with the endogenous promoter driving *ILP1* with a C-terminal 3xHA epitope tag and a DHFR marker (pILP1-3xHA_wt.DHFR). ILP1 amber mutants were generated using this parent vector using the Q5 Mutagenesis kit using primers P19-46. For IMC3 and IMC6 truncations, a UPRT locus knockout plasmid template with an ILP1 promoter and V5 C-terminal epitope was used for Gibson assembly. This vector was amplified with Q5 Hot Start polymerase (NEB) using primers P47/48. Coding sequences of the IMC3 and IMC6 truncations were amplified with Q5 polymerase using the online NEBuilder (https://nebuilder.neb.com) tool to append compatible Gibson overhangs. P49/P50 were used for amplifying IMC3 alveolin only, P49/P51 for IMC3 alveolin and C-terminus, P52/P53 for IMC6 alveolin only, P52/P54 for IMC6 alveolin and C-terminus, and P53/P55 for IMC6 N-terminus and alveolin domains. Purified amplicons were used to generate the final constructs using the NEBuilder HiFi DNA Assembly kit (NEB). The plasmids were linearized using DraIII or XmnI

(NEB), transfected into endogenously tagged IMC3-3xMyc or IMC6-3xMyc RHΔ*hxgprt* parasites, and selected for recombination at the UPRT locus using FUDR.

Antibodies

The hemagglutinin (HA) epitope was detected with mouse monoclonal (mAb) HA.11 (BioLegend) or rabbit polyclonal (pAb) anti-HA (Thermo Fisher). The Ty1 epitope was detected with mouse mAb BB2 (Bastin et al., 1996). The c-Myc epitope was detected with mouse mAb 9E10 (Evan et al., 1985) or rabbit pAb anti-Myc (Thermo Fisher). The V5 epitope was detected with mouse mAb anti-V5 (Thermo Fisher). *Toxoplasma*-specific antibodies include rabbit pAb anti-SAG1 (Dunn et al., 2008), mouse mAb anti-IMC1 (Wichroski et al., 2002), mouse pAb anti-ISP3 (Beck et al., 2010), and mouse mAb anti-ROP7 (Rome et al., 2008). Production of rat pAb anti-ILP1 and rabbit pAb anti-IMC6 is described below.

Immunofluorescence assay and western blot

HFF were grown to confluence on glass coverslips and infected with *T. gondii*. After 18-36 hours, the coverslips were fixed with either 3.7% formaldehyde in PBS or 100% methanol and processed for immunofluorescence as described (Bradley et al., 2005). Primary antibodies were detected by species-specific secondary antibodies conjugated to Alexa Fluor 488/594 (Thermo Fisher). Coverslips were mounted in Vectashield (Vector Labs) and viewed with an Axio Imager.Z1 fluorescent microscope (Zeiss).

For western blot, parasites were lysed in 1x Laemmli sample buffer with 100 mM DTT and boiled at 100°C for 10 minutes. Lysates were resolved by SDS-PAGE, transferred to nitrocellulose membranes, and proteins detected with the appropriate primary antibody and

corresponding secondary antibody conjugated to horse radish peroxidase. Chemiluminescence was induced using the SuperSignal West Pico substrate (Pierce) and imaged on a ChemiDoc XRS+ (Bio-Rad). Quantification of western blot signal was performed with Image Lab software.

Detergent extraction assay

Detergent solubility of IMC27 was assessed as previously described (Chen et al., 2015). Briefly, IMC27-3xHA tagged parasites were collected and lysed in a 1% Triton X-100, 50 mM Tris-HCl pH 7.4, 150 mM NaCl buffer supplemented with Complete Protease Inhibitor Cocktail (Roche) and incubated on ice for 30 minutes. Lysates were centrifuged, and equivalent loads of the total, supernatant, and pellet samples were run on SDS-PAGE and immunoblotted, using IMC1 as the insoluble control and ISP3 as the soluble control.

Endogenous epitope tagging of genes of interest.

For C-terminal endogenous tagging, a pU6-Universal plasmid containing a protospacer against the 3'UTR of the gene of interest ~100 bp downstream of the stop codon was generated as previously described (Sidik et al., 2014). A homology directed repair (HDR) template was PCR-amplified using the *Δku80*-dependent LIC vectors (e.g. p3xHA.LIC-DHFR, p3xMyc.LIC-CAT) which includes the epitope tag, 3'UTR, and selection cassette. The 60bp primers include 40 bp of homology immediately upstream of the stop codon or 40 bp of homology within the 3'UTR downstream of the CRISPR/Cas9 cut site. This template was amplified in a total of 400 µL, purified by phenol-chloroform extraction, precipitated in ethanol, and electroporated into RH*Δhxgprt* parasites along with 100 µg of the sequence-verified pU6-Universal plasmid. Transfected cells were allowed to invade a confluent monolayer of HFF and appropriate selection

was applied the following day. Successful tagging was monitored by IFA and clonal lines of properly tagged parasites were obtained through limiting dilution. IMC3 was C-terminally tagged with this process using gRNA and HDR primers P56-59, IMC4 using P60-63, IMC6 using P64-P67, IMC12 using P68-71, and IMC27 using P72-75.

In vivo photocrosslinking of protein complexes

Parasites expressing the synthetase/tRNA cassette and mutant protein of interest constructs were allowed to infect HFFs overnight at a multiplicity of infection of ~3 and the growth medium was replaced with fresh medium supplemented with 1 mM Azi (Bachem). Following a 24-hour incubation period and lysis of the host cells, extracellular parasites were collected by centrifugation and resuspended in an adequate volume of PBS for UV irradiation (~10^7 parasites per mL of PBS, in tissue culture plates). The plates containing resuspended parasites were floated on an iced water bath and placed without lids in a Spectrolinker XL-1000 UV crosslinker (Spectroline) equipped with 365 nm (UV-A) bulbs. Parasites were irradiated for 20 minutes with periodic mixing using a micropipette. The cells were then collected by centrifugation and lysed for either co-immunoprecipitation or directly in sample buffer for SDS-PAGE.

Co-immunoprecipitation (co-IP)

Traditional co-IP was carried out as previously described (Beck et al., 2010). For denaturing co-IP of crosslinked proteins, irradiated parasites were lysed in a 1% SDS/50 mM Tris pH 8.0/150 mM NaCl buffer and boiled at 100°C for 10 minutes to completely denature protein complexes. The lysate was centrifuged, and the supernatant was diluted ten-fold to RIPA conditions prior to IP. Precipitated proteins are either eluted in sample buffer or by high pH with

a 100 mM triethylamine solution and dried using a vacuum concentrator. Colloidal Coomassie staining was accomplished using GelCode Blue Stain (ThermoScientific). Gel slices were excised and processed for mass spectrometry. Immunoprecipitations were performed using rat anti-HA (Roche) or mouse anti-V5 (Sigma) agarose beads.

Characterization of ILP1 acylation mutants and *Pf*G2 complementation

ILP1 acylation mutants were generated using pILP1-3xHA_wt.DHFR as a template. For the G2A mutant, the ILP1 promoter and N-terminal region was amplified using primers P76/P77, incorporating the desired mutation. This fragment was ligated using HpaI/HindIII to the vector digested with EcoRV/HindIII. For the C95S, C96S, C273S, C274S (4Cys) mutation, the C95S, C96S mutant was made using the Q5 Site-Directed Mutagenesis kit with primers P78/P79. The 4Cys mutant was then constructed by amplifying the C95S, C96S template with primers P80/P81, which incorporates the C-terminal C273S and C274 mutations, and cloned using HpaI/NotI. The codon optimized *Pf*G2 coding sequence gBlock (S6 Text) was synthesized and incorporated into an ILP1 promoter expression construct.

The HA epitope tag in pUPRTKO-HA plasmid (Reese et al., 2011) was replaced with a V5 tag by digesting the vector with NotI/PacI and ligating NotI-V5-PacI annealed oligos P82/P83. This vector was then digested with NheI/NotI, and the ILP1 promoter along with the wild-type, G2A, and 4Cys ILP1 mutants or *Pf*G2 gene were ligated with the same sites. The final pUPRTKO-V5 constructs were linearized with DraIII and transfected into ILP1-3xHA DHFR RH*Δhxgprtku80* parasites, and expression of the mutants was confirmed by IFA. Clonal lines were then transfected with a NcLiv *GRA7* driven HXGPRT HDR knockout template with flanking homology to the endogenous ILP1 locus (Chen et al., 2017), and the pU6-Universal plasmid

against a protospacer within the first intron of the genomic sequence (P84-87). After selection, loss of endogenous ILP1-3xHA expression was confirmed by IFA. Genomic DNA was extracted using the PureLink Genomic DNA kit (Invitrogen) and successful knockouts were confirmed by PCR using P88/P89 spanning two introns, and P90/P91 spanning the ILP1 promoter/NcGra7 promoter interface.

Plaque assay of the ILP1 complementation mutants was performed as previously described (Nadipuram et al., 2016). 6-well plates were seeded with HFF and allowed to reach confluency. 100-600 parasites were added per well and allowed to grow for 7 days. The monolayers were fixed with 100% methanol for 3 minutes, washed with PBS, and stained for visualization. The areas of 50 plaques per condition were quantified with the ZEN 2 software (Zeiss). Significance levels were calculated by unpaired *t*-test.

Antibody production

The complete coding sequences for ILP1 and IMC6 were cloned into the pET His6 TEV LIC bacterial expression vector (a gift from Scott Gradia, Addgene plasmid #29653), using primers P92-95. The constructs were transformed into BL21(DE3) *E. coli*, and proteins were induced with 1 mM IPTG and purified using Ni-NTA agarose under denaturing conditions as described (Bradley et al., 2005). The samples were then dialyzed into PBS to remove the urea and rat or rabbit antisera were produced by Cocalico Biologicals.

Tandem mass spectrometry

The protein mixtures were reduced, alkylated, and digested by the sequential addition of trypsin and Lys-C proteases. Samples were then desalted using Pierce C18 tips, eluted in 40%

acetonitrile, and dried and resuspended in 5% formic acid. Desalted samples were separated on C18 reversed phase (1.9 μM, 100A pores, Dr. Maisch GmbH) columns, packed with 25 cm of resin in a 75 μM inner diameter fused silica capillary. Digested peptides were fractionated online using a 140-minute water-acetonitrile gradient with 3% DMSO ionized using electrospray ionization by application of a distal 2.2 kV.

Upon electrospray ionization at 2.2 kV, ionized peptides were interrogated via tandem mass spectrometry (MS/MS) in a Thermo Orbitrap Fusion Lumos. For discovery acquisitions, Data-Dependent Acquisition (DDA) was utilized with an MS1 scan resolution of 120,000 and MS2 resolution of 15,000 and a cycle time of 3 seconds. Data analysis was performed using the Integrated Proteomics Pipeline 2 (Integrated Proteomics Applications, San Diego, CA). MS/MS spectra were searched using the ProLuCID algorithm and peptide-to-spectrum matches (PSMs) were organized and filtered based on decoy database-estimated false discovery rate of <1% using the DTASelect algorithm. Database searching was performed using a FASTA protein database containing *T. gondii* GT1 translated ORFs downloaded from ToxoDB on 2-23-2016. Label free intensity-based quantitation (LFQ) of the LC-MS/MS data was carried out by MS1 feature detection using chromatographic peak areas for peptide abundance through MaxQuant software package *v*.1.6.3.3 (Cox & Mann, 2008).

2.6 - Acknowledgements

We thank Dr. Lei Wang at UCSF for the plasmid pIre-Azi3 and for Dr. Ken Bradley for advice in adapting the UAA system to *Toxoplasma gondii*. We thank Dr. Gary Ward at UVA for the mouse anti-IMC1 monoclonal antibody and Dr. John Boothroyd for the rabbit anti-SAG1 antibody. We also acknowledge Dr. Pascal Egea for helpful comments on the manuscript.

2.7 – Figure and Table Legends

Fig 2-1. **Engineering the UAA system and demonstrating efficient incorporation of Azi in *T. gondii*.**

(A) Diagram showing the use of amber stop codon suppression to incorporate UAAs into a nascent peptide strand using the endogenous translation machinery. (B) Chemical structure of the photoreactive UAA *p*-azidophenylalanine (Azi). Exposure of Azi to UV-A (365 nm) ultraviolet light causes the azide group to irreversibly form a reactive nitrene intermediate, which forms covalent crosslinks with proximal proteins. (C) Construct showing the Ty1-tagged aminoacyl-tRNA synthetase (E2AziRS) driven by the constitutively active *GRA1* promoter and three tandem cassettes of the cognate amber suppressor tRNA driven by the RNA polymerase III-specific U6 promoter. (D) IFA showing that stably expressed E2AziRS localizes to the parasite cytoplasm as expected. Green: mouse anti-Ty1. (E) Construct showing the *SAG1* gene driven by the *GRA1* promoter, in which the second amino acid F2 has been mutated to an amber codon. (F) IFA showing RH*Δhxgprt*Δ*sag1* parasites stably transfected with the synthetase/tRNA and SAG1 constructs. E2AziRS expression is confirmed by anti-Ty1 staining. Without Azi in the growth medium, SAG1 is not detected due to the in-frame stop codon. Upon addition of Azi, robust expression of SAG1 is observed trafficking properly to the cell periphery. Red: rabbit anti-SAG1 antibody, green: mouse anti-Ty1 antibody. (G) Western blot of whole cell lysates shows SAG1 only when Azi is added to the medium. Quantification of the chemiluminescence intensity indicates that ~35% expression of the mutant SAG1 by amber suppression can be obtained compared to endogenous SAG1.

Fig 2-2. Site-specific crosslinking of UPRT in *T. gondii*.

(A) The UPRT homodimer is stabilized by a β-arm (darker pink, structure adapted from PDB entry 1BD4). L92 and Y96 were chosen for Azi substitution based on orientation towards the other subunit in the crystal structure. (B) IFA showing cytoplasmic localization for parasites expressing the Y96 mutant UPRT-HA upon addition of Azi. Red: mouse anti-HA. (C) Schematic for UPRT dimer formation using a second copy of UPRT with a Myc tag. UPRT proteins will assemble as either HA/HA or Myc/Myc homodimers, or a HA/Myc heterodimer. As the Myc-tagged monomers lack Azi, they should be crosslinked only when bound to an Azi-containing UPRT-HA partner. (D) Anti-HA western blot of UPRT crosslinking using strains expressing the synthetase/tRNA and either WT, L92, or Y96 UPRT-HA. Uncrosslinked UPRT migrates at 27 kDa (blue arrow). A small amount of UPRT is observed without Azi, indicating nonspecific incorporation of other amino acids can occur, but this material is low abundance and lacks crosslinking ability. In the +Azi/+UV conditions, shifted products can be observed for both L92 and Y96 lines (red arrowheads), indicating successful crosslinking of a UPRT dimer. (E) Immunoblot of the UPRT crosslink samples with anti-Myc antibody verifies that the shifted products are covalently crosslinked UPRT homodimers. The Myc blot shows a lower relative efficiency of crosslinked to uncrosslinked material, presumably because the Myc-tagged monomers can only crosslink as the heterodimer, while the HA-tagged UPRT can crosslink as both the heterodimer and an HA/HA homodimer.

Fig 2-3. Site-specific crosslinking of ILP1 reveals multiple potential binding partners.

(A) Diagram of ILP1 showing an N-terminal putative EF-hand domain (grey) followed by a coiled coil domain (yellow). Also shown is the JPred secondary structure prediction of ILP1 revealing

alpha-helices (black bars) and beta-strands (white arrows) as well as buried residue prediction used for choosing likely exposed residues for amber substitution (Drozdetskiy et al., 2015). Also noted are the potentially myristoylated glycine at position two (teal) and tandem cysteine prenylation/palmitoylation motifs internally and at the extreme C-terminus (purple). Fourteen residues in ILP1 were chosen for amber mutagenesis to test for Azi-mediated crosslinking (green). (B) COILS prediction of ILP1, the window size refers to the number of residues used in the analysis. (C) Representative IFA of the Q168 ILP1 mutant containing Azi, which localizes properly to the parasite periphery. Red: rabbit anti-HA antibody, green: mouse anti-Ty1 antibody. (D) Western blot of the ILP1 Azi mutants after UV irradiation reveals three major crosslinked species (red arrowheads). A smaller upshift (~65 kDa) is observed for residues Y160 and Q168, with weak similar products for T152 and Q170. Residues T184, T187, and I188 exhibit a major band at approximately 200 kDa. E209 and K212 form a third upshift at approximately 140 kDa. Uncrosslinked ILP1 is denoted by the blue arrows (~35 kDa).

Fig 2-4. **IMC3 is a direct binding partner of ILP1**.

(A) ILP1-3xHA amber mutants yielding the two large upshifted bands (T184, T187, I188, and E209) were expressed in an endogenously tagged IMC3-3xMyc background that also contains the synthetase/tRNA pair. Following Azi addition and UV irradiation, the crosslinked species (black asterisks) can be reproduced in this strain. When probing for IMC3-3xMyc, a persistent high molecular weight background prevents confirmation of any potential upshift of IMC3. (B) Strategy for denaturing IP. Boiling in SDS disrupts the parasite's cytoskeleton and protein-protein interactions of its components. The lysate is diluted to RIPA conditions for IP and only the target protein (red) and covalently attached partners (green) are purified. (C) Western blot analysis of

ILP1 denaturing IP. This eliminates the majority of the Myc background as well as most of the uncrosslinked IMC3 (blue arrow). Probing with anti-Myc shows reactivity with the crosslinked band for residues T184, T187, and I188, demonstrating that IMC3 is indeed the partner at these residues. In contrast, no Myc reactivity is seen for E209, indicating that this residue does not bind to IMC3.

Fig 2-5. **The C-terminal region of IMC3 is required for binding to ILP1 at T187**.

(A) Diagram and IFA of IMC3 truncations expressed in *Toxoplasma* to determine which region of IMC3 binds to ILP1 T187. In endogenously tagged IMC3-3xMyc parasites, regions corresponding to alveolin only (112-279, $IMC3_A$) and alveolin plus C-terminus (112-538, $IMC3_{AC}$) were tagged with V5 and localized. $IMC3_A$ partially mislocalizes to the maternal cytoplasm, suggesting that although the alveolin domain plays a role in IMC targeting, the inclusion of the C-terminal region of the protein improves IMC targeting similar to wild-type IMC3. Red: mouse anti-V5 antibody, green: rabbit anti-Myc antibody. (B) Western blot showing the high molecular weight product corresponding to a crosslinked full length IMC3 in parasites expressing either $IMC3_A$ or $IMC3_{AC}$ (top band). However, another smaller band (red arrowhead) is seen in the $IMC3_{AC}$ lysate, likely representing an ILP1/$IMC3_{AC}$ crosslinked product. (C) ILP1-3xHA T187 denaturing IP shows the same ILP1 shifted products seen in whole cell lysates (first panel), but an anti-V5 blot now clearly labels a band migrating at the same position as the new smaller anti-HA upshifted product (second panel, red arrowhead), demonstrating that this species corresponds to ILP1 T187 crosslinked to the $IMC3_{AC}$. The light chain signal seen at 25 kDa obscures detection of residual uncrosslinked $IMC3_A$. However, detecting the original ILP1 T187/IMC3 full length species in the anti-Myc blot (third panel) shows that IP in both $IMC3_A$ and $IMC3_{AC}$ conditions was successful. (D) Western

blot analysis of anti-V5 denaturing IP performed with the same strains. Both $IMC3_A$ and $IMC3_{AC}$ are robustly enriched, but crosslinked ILP1 is only obtained in the $IMC3_{AC}$ condition (first panel, red arrowhead). Some uncrosslinked IMC3-3xMyc is seen in the IP, likely reflecting interactions of this abundant alveolin in the lysate (third panel).

Fig 2-6. IMC6 is another direct binding partner of ILP1.

(A) Crosslinking of T187 and E209 in strains endogenously 3xMyc-tagged for IMC3, IMC4 or IMC6. Tagging of IMC6 results in slower migration for the E209 Azi crosslinked product compared to the IMC3/4-3xMyc lines, which can be attributed to the addition of the epitope tag. A subtle shift can also be seen in the T187/ IMC3-3xMyc strain (black asterisk), as IMC3 is the partner at this residue. (B) Denaturing ILP1 co-IP to verify the E209/IMC6 interaction using IMC6 tagged parasites (T187, which binds IMC3, is used as a control). The anti-HA blot shows the expected crosslinked products in the tagged lines, but only the E209 product is detected with anti-Myc, confirming the interaction with IMC6 (red arrowhead). Uncrosslinked IMC6, which was mostly removed by denaturation, is also present in both conditions (blue arrow).

Fig 2-7. The N-terminal region of IMC6 is required for binding to ILP1 at E209.

The experimental design mimics the one reported for IMC3 in Fig 2-6. (A) Alveolin only (128-290, $IMC6_A$) and alveolin plus C-terminus (128-444, $IMC6_{AC}$) truncations tagged with a V5 epitope were visualized. Both truncations localize to the growing daughter IMC, but also exhibit partial mislocalization in the maternal cytoplasm, which does not appear to be rescued with the addition of the C-terminal region. Red: mouse anti-V5 antibody, green: rabbit anti-Myc antibody. (B) Western blot of whole cell lysate showing uncrosslinked ILP1 and the original upshifted

species but no visible lower molecular weight band that would indicate crosslinking to the smaller size truncations. (C) ILP1-3xHA E209 denaturing IP enriches for ILP1 (first panel), but no upshift is observed in the anti-V5 blot (second panel), indicating that neither $IMC6_{A}$ nor $IMC6_{AC}$ is sufficient to crosslink to ILP1 at residue E209. The $IMC6_{A}$ band is obscured by antibody light chain cross-reactivity. The anti-Myc blot (third panel) confirms successful IP, as seen by the original ILP1 E209/IMC6 full length upshift. (D) Anti-V5 denaturing IP enriching for the IMC6 truncations correspondingly lacks any ILP1-3xHA signal (first panel). (E) An N-terminus plus alveolin domain truncation of IMC6 (1-290, $IMC6_{NA}$) appears to rescue localization like wild-type IMC6. Red: mouse anti-V5 antibody, green: rabbit anti-Myc antibody. (F) Anti-HA immunoblot of both whole cell lysate (first panel, red arrowhead) and after anti-HA denaturing IP (second panel, red arrowhead) reveals a smaller upshifted species (~90 kDa) for the $IMC6_{NA}$ strain, suggesting that ILP1 E209 is crosslinking to this mutant. Anti-V5 blot confirms that $IMC6_{NA}$ is detected at this molecular weight size (third panel, red arrowhead), demonstrating the identity of a ILP1 E209/$IMC6_{NA}$ crosslink. Anti-Myc blot confirms successful co-IP of the original IMC6 upshift (fourth panel).

Fig 2-8. Mass spectrometric identification of crosslinked proteins reveals IMC27 as an ILP1 binding partner.

(A) Western blot and Coomassie gel analyses of large scale denaturing IP of Y160. The region of gel containing the crosslinked ILP1 species (red arrowhead) was excised and processed for LC-MS/MS peptide identification. (B) Detergent fractionation showing that IMC27 is firmly associated with the IMC cytoskeleton, like ILP1 (Lorestani et al., 2012). IMC1 is a control for the insoluble fraction whereas membrane-associated ISP3 is readily solubilizes upon detergent

extraction. (C) Photocrosslinking of Y160 and Q168 in strains endogenously 3xMyc tagged for IMC27 (or IMC12 as a control). Tagging of IMC27 results in slower migration of the crosslinked product compared to that of the IMC12 tagged strain, indicating IMC27 is the partner. The shifted products are also detected in the anti-Myc blot. (D) Denaturing IP shows the same pattern of shifted products for ILP1. Probing the samples with anti-Myc (for IMC29 or IMC12) confirms the higher migrating shifted product are IMC27 (red arrowhead), while uncrosslinked IMC27 is largely removed (blue arrow). IMC12-3xMyc is completely eliminated by denaturation. (E) IFA of IMC27-3xMyc parasites reveals that it localizes solely to the maternal IMC, indicating that interaction with ILP1 via Y160 and Q168 occurs within this subcompartment rather than the forming daughters. Red: mouse anti-Myc antibody, green: rat anti-ILP1 antibody.

Fig 2-1. Engineering the UAA system and demonstrating efficient incorporation of Azi in *T. gondii*.

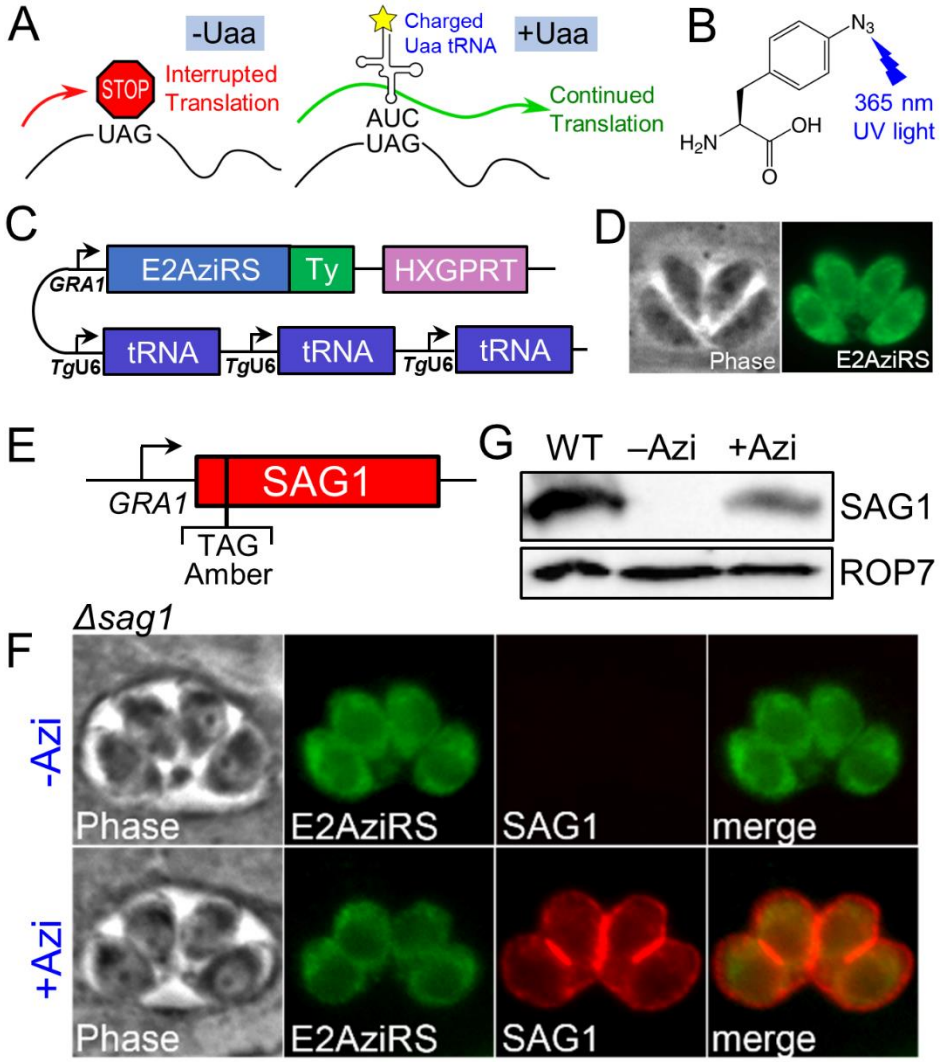

Fig 2-2. Site-specific crosslinking of UPRT in *T. gondii*.

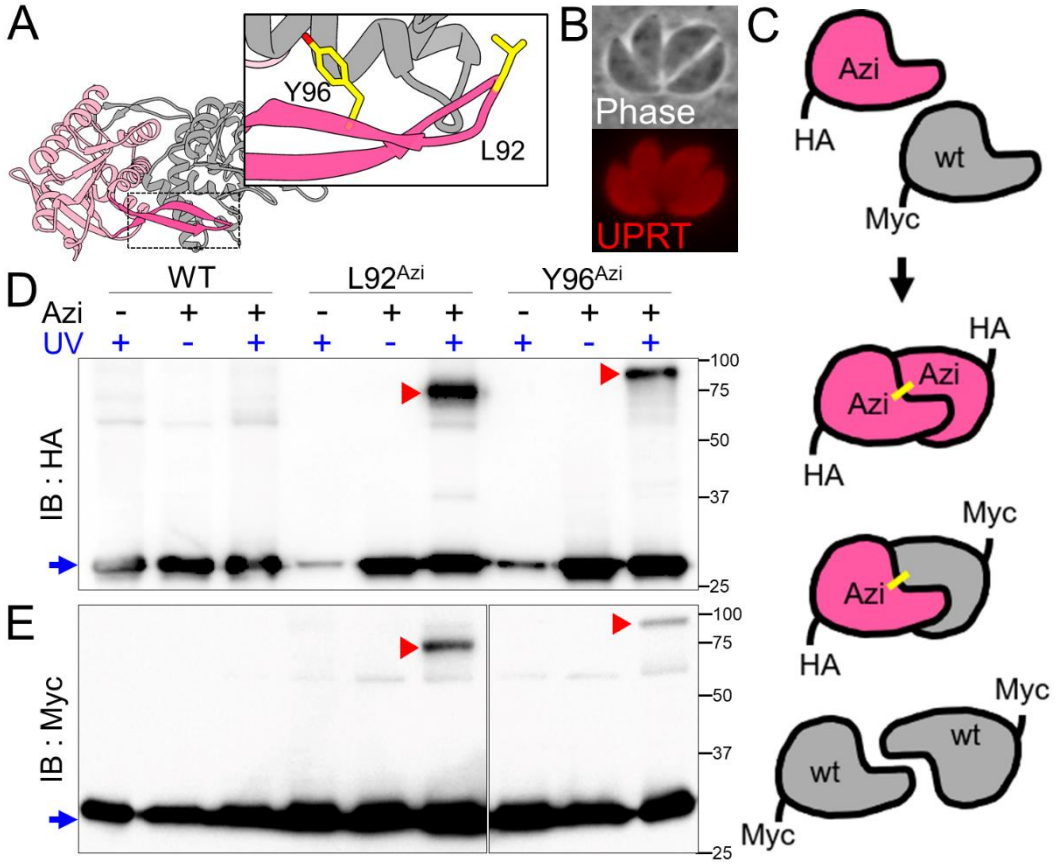

Fig 2-3. Site-specific crosslinking of ILP1 reveals multiple potential binding partners.

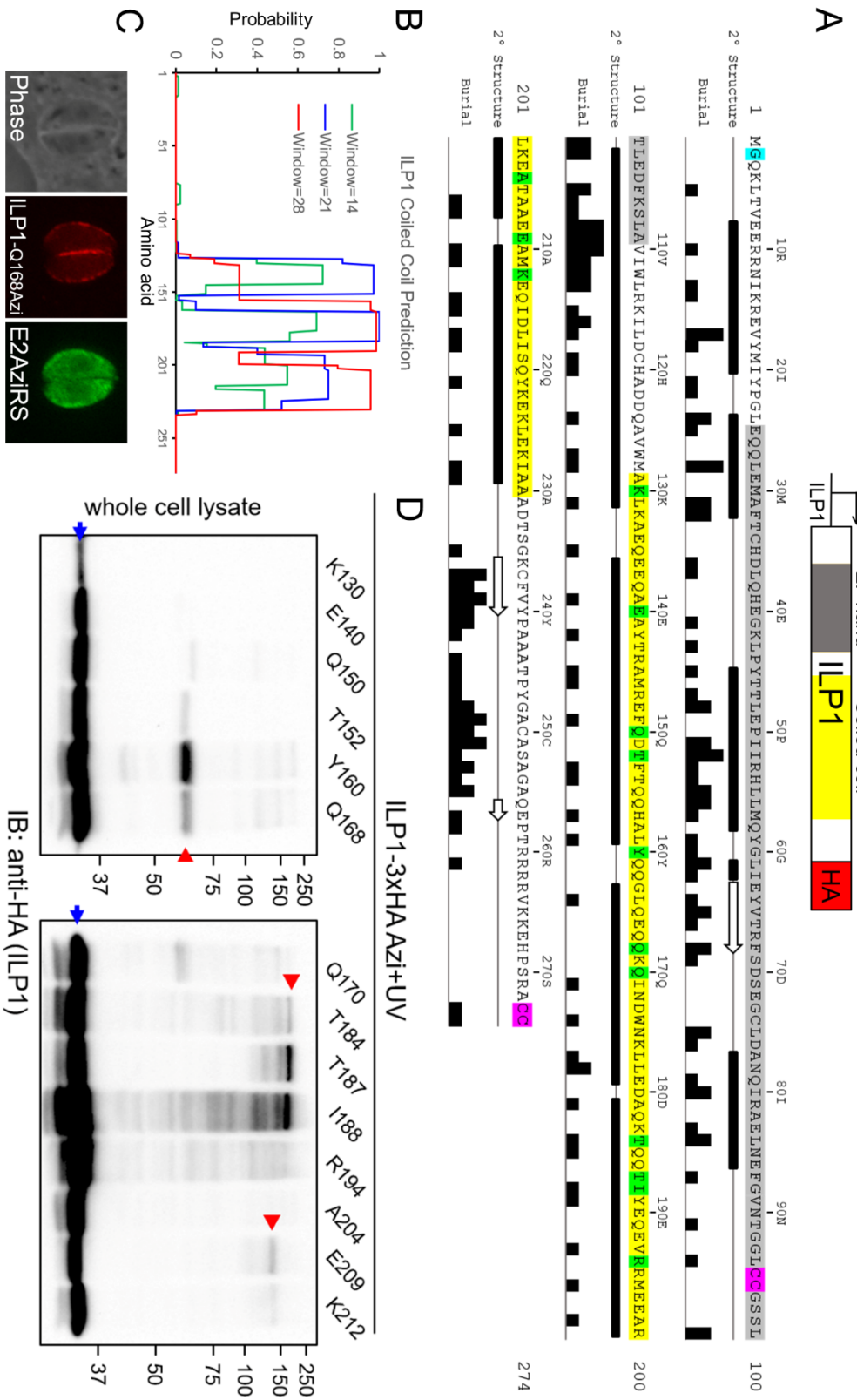

Fig 2-4. IMC3 is a direct binding partner of ILP1.

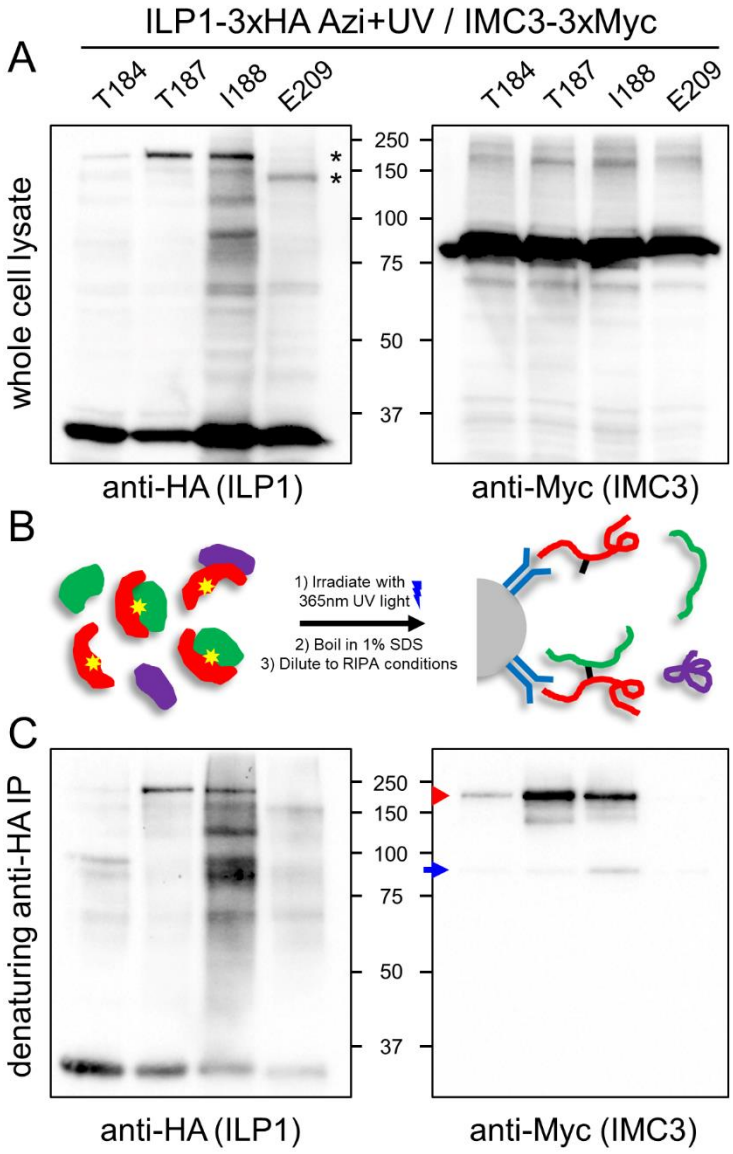

Fig 2-5. The C-terminal region of IMC3 is required for binding to ILP1 at T187.

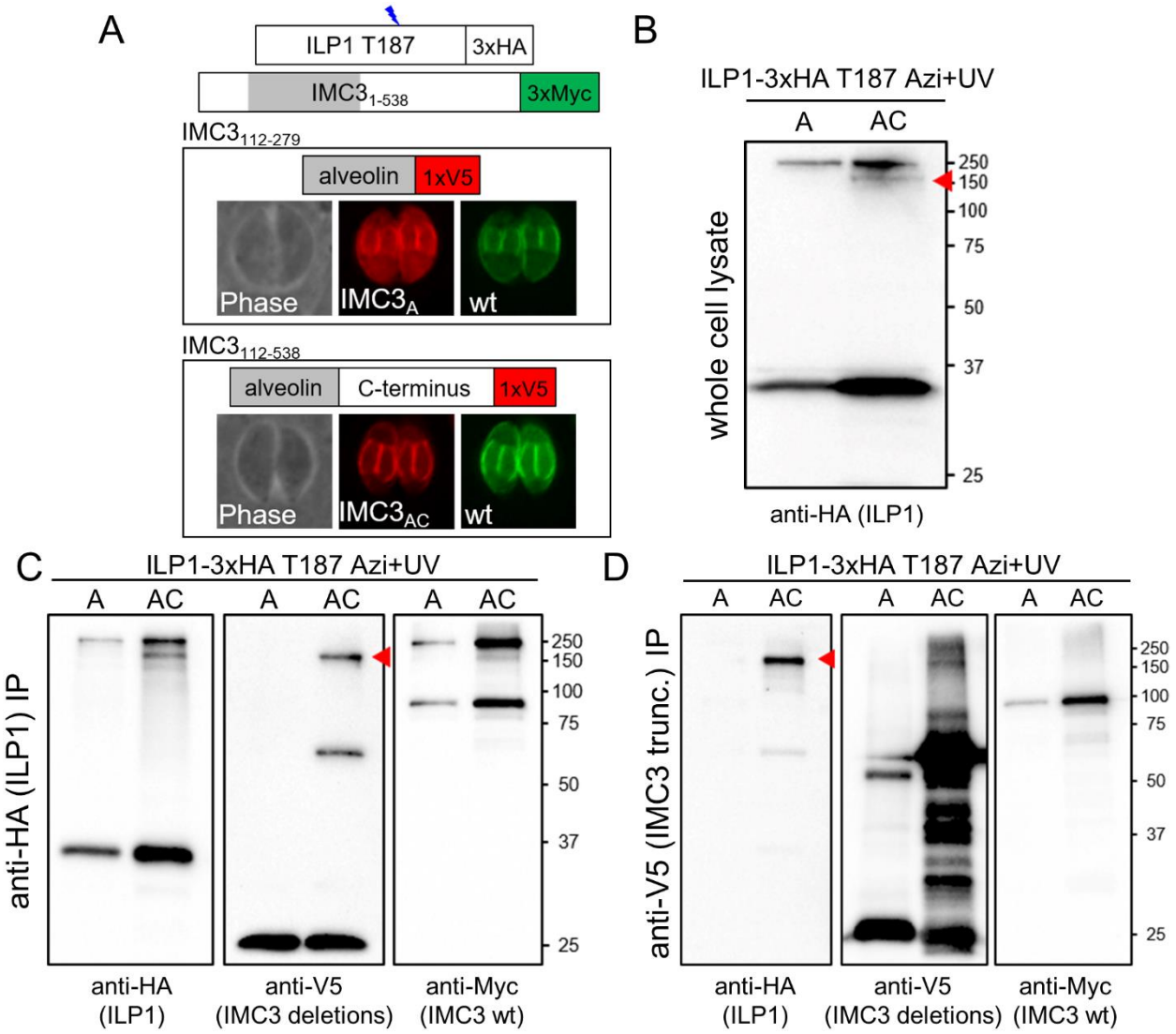

Fig 2-6. IMC6 is another direct binding partner of ILP1.

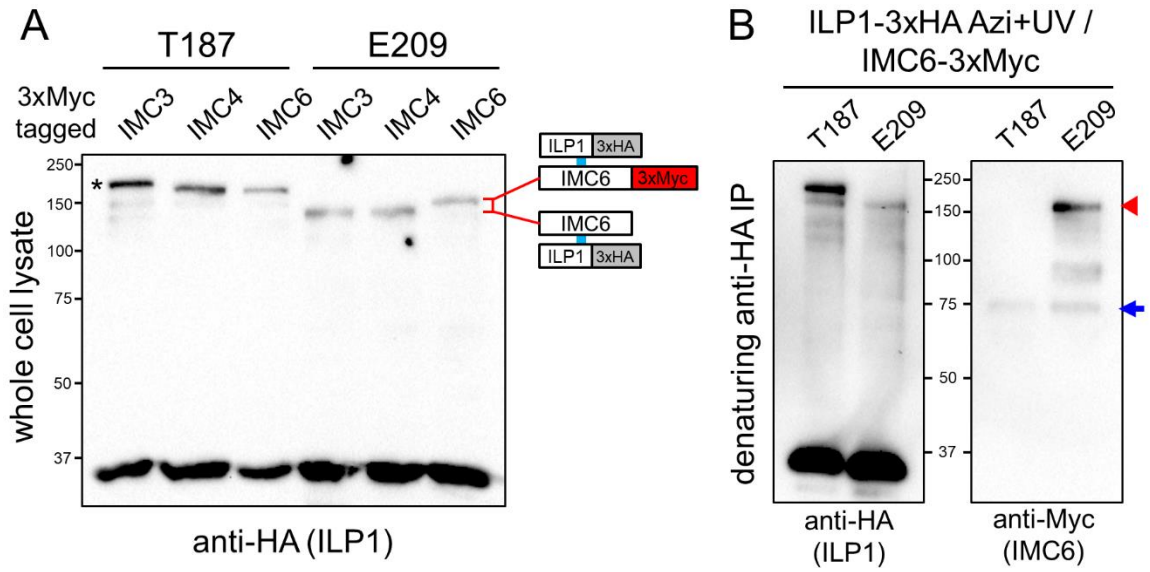

Fig 2-7. The N-terminal region of IMC6 is required for binding to ILP1 at E209.

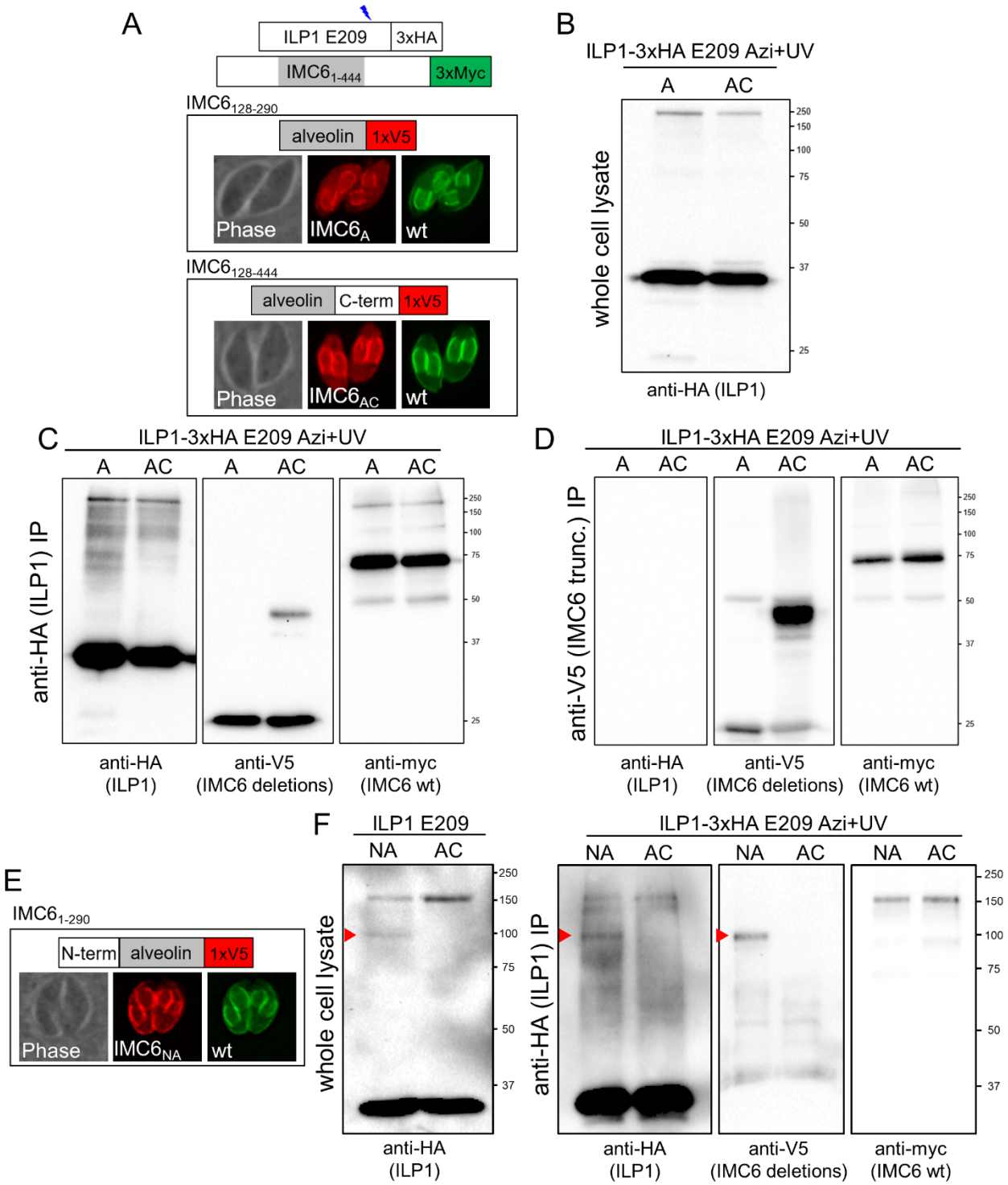

Fig 2-8. Mass spectrometric identification of crosslinked proteins reveals IMC27 as an ILP1 binding partner.

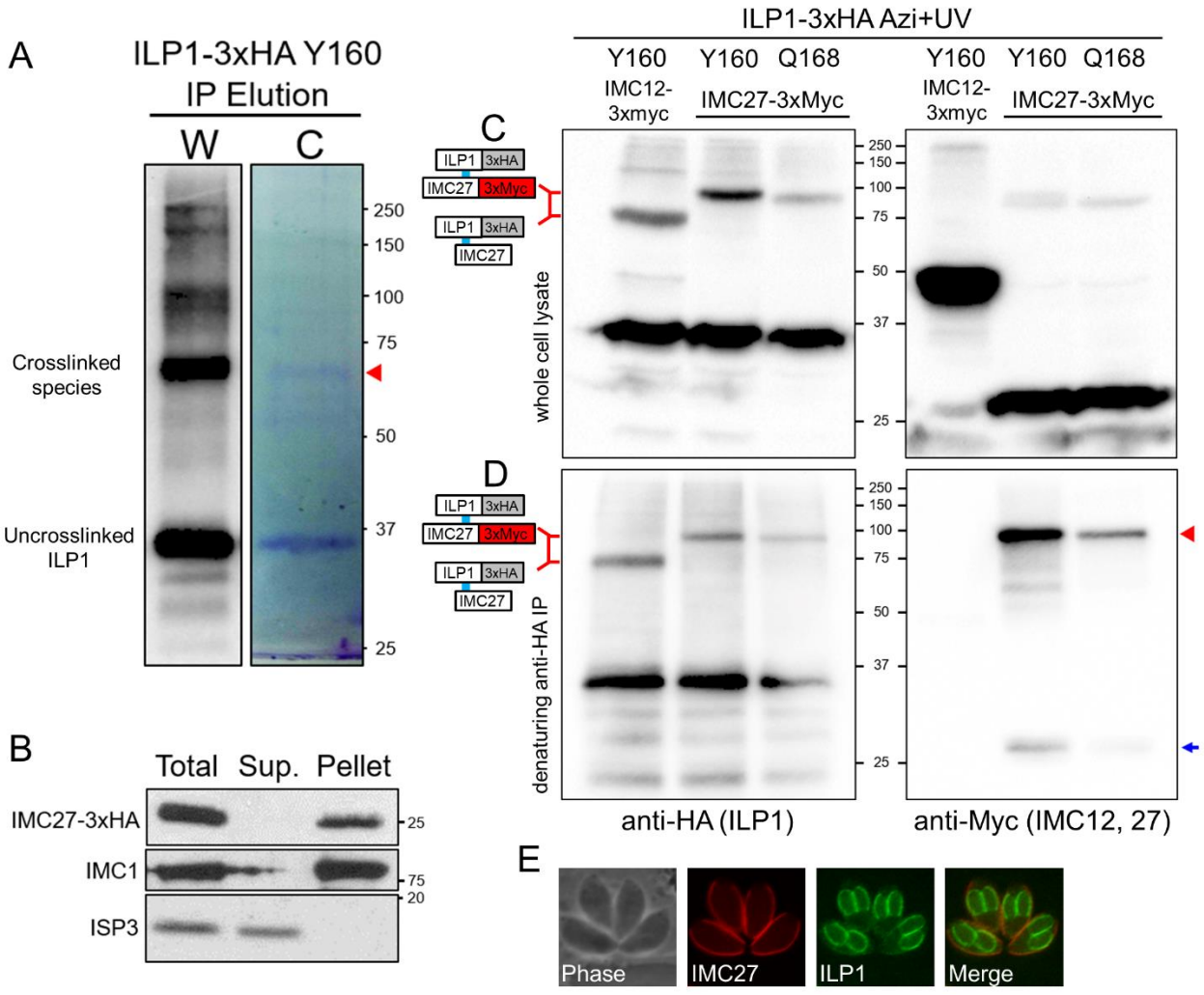

2.8 - Supporting Information Legends

Fig 2-S1. Alignment of ILP1 in representative apicomplexans.

ILP1 is well conserved in coccidians, while the *Plasmodium falciparum* ortholog is more divergent. The likely myristoylated glycine at position 2 is conserved. Two putatively palmitoylated cysteine pairs are present in the *Toxoplasma* sequence at residues C95, C96 and C273, C274. The internal pair is present in *Plasmodium*, although missing in *Eimeria*, while the C-terminal pair is conserved in coccidians but only present as a single cysteine in *Plasmodium*.

Fig 2-S2. Mutation of ILP1 putative post-translational modifications and Plasmodium G2 localization.

Loss of function mutations of the putative myristoylation (G2A) and palmitoylation (4Cys, C95S, C96S, C273S, C274S) sites were assessed by knocking in mutant copies to the UPRT locus and disrupting the endogenous ILP1 locus using CRISPR/Cas9. (A) Strategy and PCR analysis of endogenous ILP1 disruption. Knockouts were assessed by absence of amplification using intronic primers and positive amplification of the sequence between the ILP1 promoter and NcGra7 promoter following HDR. (B) IFA showing that exogenous ILP1 WT, G2A, and 4Cys copies all localize normally to the parasite periphery. The *Plasmodium* G2 ortholog fails to localize properly and could not compensate for the endogenous ILP1 knockout. Red: mouse anti-V5 antibody, green: rabbit anti-IMC6 antibody. (C) Plaque assays of the ILP1 mutants following knockout of endogenous ILP1. The ILP1 G2A mutant has a slight but significant growth defect when compared to the ILP1 WT strain (~50% reduction). The 4Cys mutant does not have any growth disadvantage compared to control.

Fig 2-S3. Co-immunoprecipitation of ILP1 yields several known IMC proteins.

(A) Representative silver stain of an anti-HA IP of ILP1-3xHA parasites performed after fractionation in 1% Triton-X 100 and extensive sonication of the pellet to solubilize the IMC cytoskeleton. RH parasites were used as a control. A gel slice containing a unique band (blue arrow) was excised and proteins were identified by mass spectrometry. Identified proteins included the alveolins and components of the glideosome.

Table 2-S4. MaxQuant intensities of upshifted ILP1-Y160 band.

Top 30 protein intensities calculated by MaxQuant of the excised band following ILP1-Y160 crosslinking and large scale anti-HA IP. ILP1 and IMC27 are the top two proteins that are identified.

Table 2-S5. List of primers used in chapter 2.

Table 2-S6. List of synthesized gene fragments used in chapter 2.

Fig 2-S1. Alignment of ILP1 in representative apicomplexans.

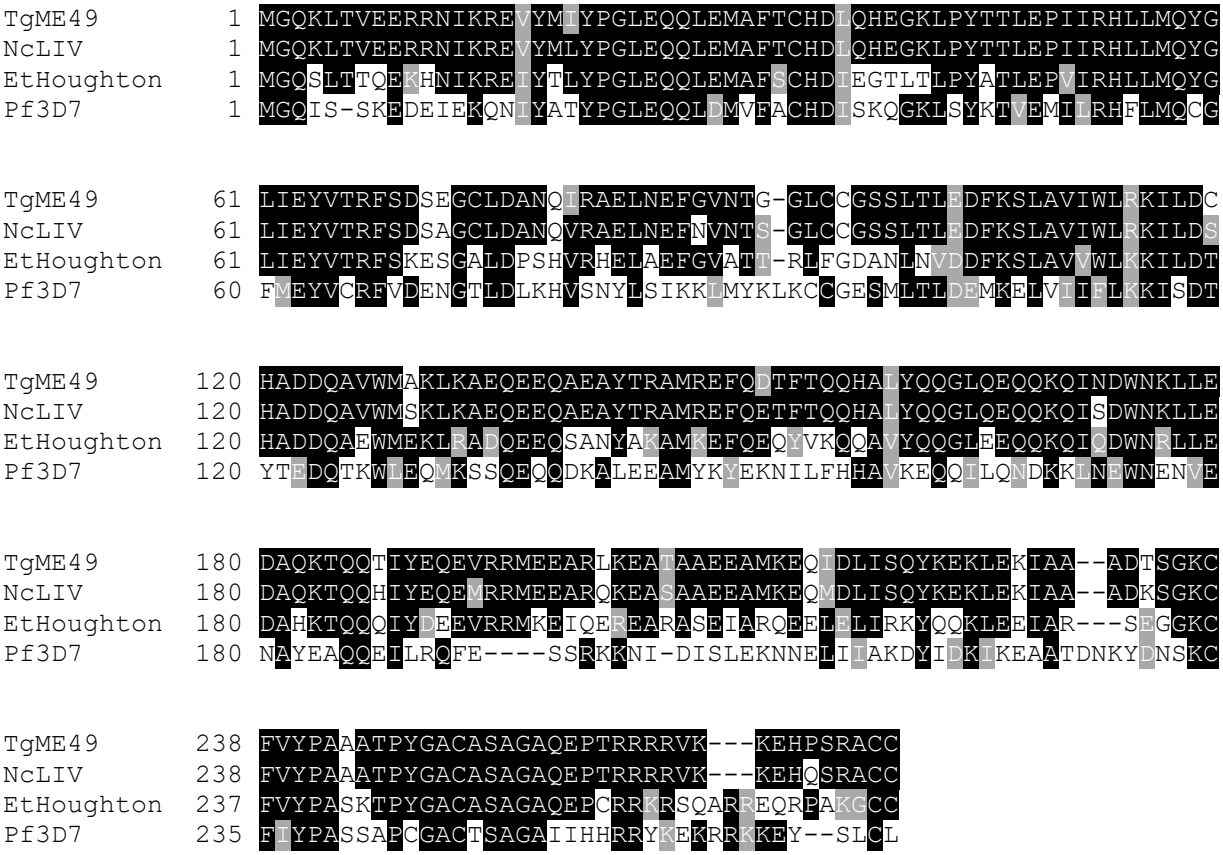

Fig 2-S2. Mutation of ILP1 putative post-translational modifications and Plasmodium G2 localization.

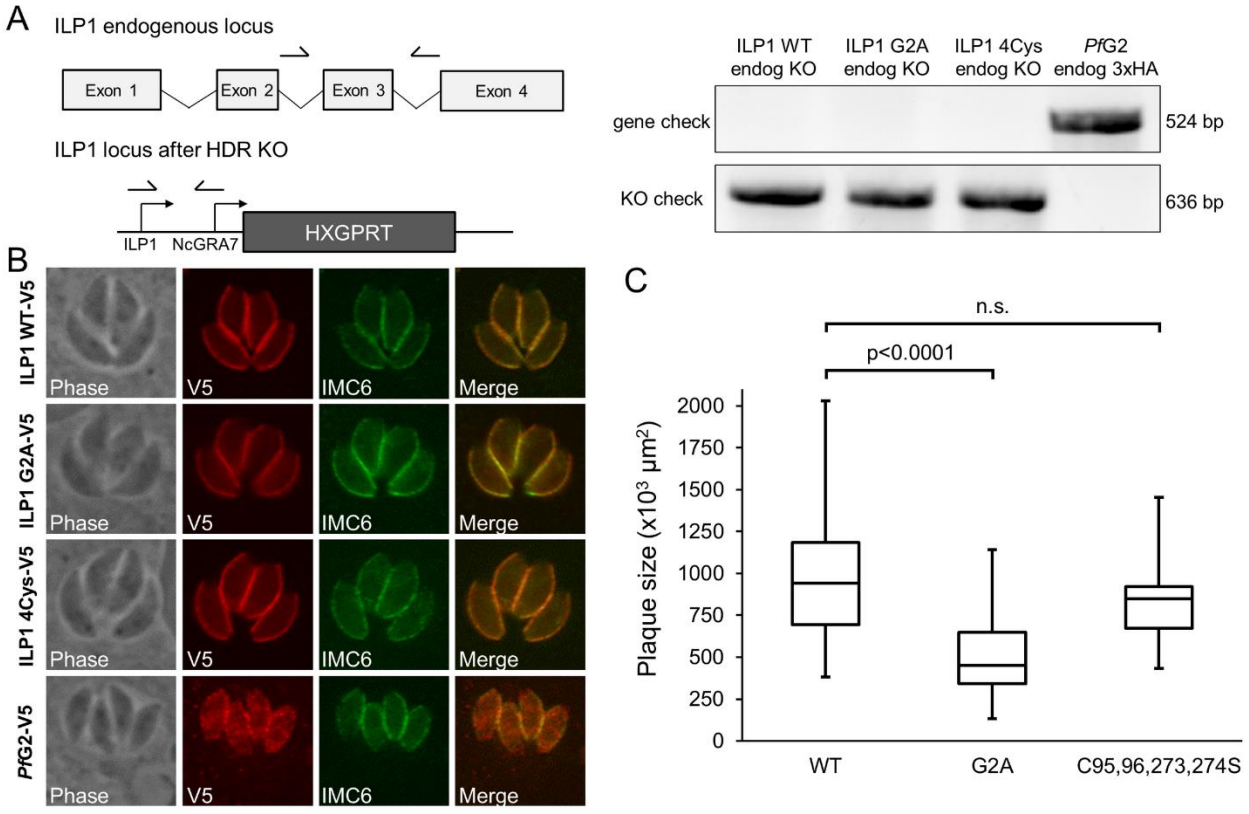

Fig 2-S3. Co-immunoprecipitation of ILP1 yields several known IMC proteins.

A

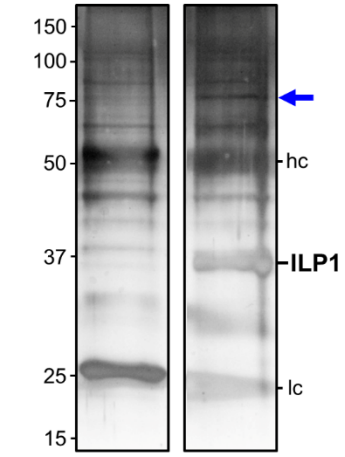

B

		Unique Peptides		
Protein	**Gene ID**	**Replicate 1**	**Replicate 2**	**Control**
ILP1	TgGT1_313380	12	12	3
IMC1	TgGT1_231640	9	15	5
IMC3	TgGT1_216000	5	8	2
IMC4	TgGT1_231630	5	6	0
IMC6	TgGT1_220270	4	3	0
IMC10	TgGT1_230210	9	5	0
IMC28	TgGT1_239400	0	2	0
MORN2	TgGT1_292120	8	2	0
-	TgGT1_248740	4	4	0
MLC1	TgGT1_257680	3	0	0
GAP45	TgGT1_223940	2	0	0

Table 2-S4. MaxQuant intensities of upshifted ILP1-Y160 band.

Protein IDs	Intensity	MS/MS count	Comments
TGGT1_313380	4691700000	47	ILP1
TGGT1_259630	2572700000	32	IMC27
TGGT1_300200;TGGT1_261250	864130000	10	Histones H2AZ, H2A1
TGGT1_261240;TGGT1_218260	386590000	3	Histones H3, H3.3
TGGT1_411760	375850000	176	Unassigned actin (Human origin?)
TGGT1_308090;TGGT1_411430	256160000	22	ROP5
TGGT1_289140	104590000	3	putative ribosomal protein l22/l43
TGGT1_231630	100920000	14	IMC4
TGGT1_270510	60540000	18	asparaginyl-tRNA synthetase
TGGT1_294800A;TGGT1_286420A	56037000	7	elongation factor 1-alpha
TGGT1_316400B	40527000	6	TUBA1
TGGT1_273760	38475000	11	HSP70
TGGT1_247550	26420000	11	HSP60
TGGT1_209030	21023000	8	ACT1
TGGT1_248340	18760000	2	GTP-binding nuclear protein ran/tc4
TGGT1_227360	16940000	3	ribosomal protein RPL3
TGGT1_291890	16773000	7	MIC1
TGGT1_239260	16588000	5	histone H4
TGGT1_304880	15341000	3	hypothetical protein
TGGT1_233460	13895000	7	SAG-related sequence SRS29B
TGGT1_204400	13741000	7	putative ATPase synthase subunit alpha
TGGT1_310700	11998000	4	serine/threonine phosophatase PP1
TGGT1_232250	11695000	4	catalase
TGGT1_312640	11188000	1	hypothetical protein
TGGT1_311720	10231000	9	chaperonin protein BiP
TGGT1_221470	10181000	6	hypothetical protein
TGGT1_231640	8165700	3	IMC1
TGGT1_221620;TGGT1_266960;TGGT1_212240	7551600	7	beta-tubulin
TGGT1_210330	7192200	1	SAG-related sequence SRS37B
TGGT1_261010	6857800	2	putative tat-binding family protein

Table 2-S5. List of primers used in chapter 2.

Name	Description	Sequence 5'-3'
E2AziRS cloning		
P1	NsiI-E2AziRS fwd	ATGCATGCAAGCAGTAACTTGATTAAAC
P2	E2AziRS-Ty-stop-PacI rev	TTAATTAATTAGTCAAGTGGATCTTGGTTAGTATGGACCTCTTTCCAGCAAATCAGACAGTAATTCTTTTTACC
P3	Acc65i-XhoI-U6 fwd	ggtaccctcgagGATGAGACAAAGTGCGCGAG
P4	U6term-SalI-BglII-XbaI rev	tctagaagatctgtcgacGAAAAAGAAAAAAAAATGGAGGGGG
SAG1 cloning/mutagenesis		
P5	HindIII-DHFR_cassette fwd	actgacAAGCTTcagcacgaaaccttgcattca
P6	DHFR_cassette-NgoMIV rev	actgacGCCGGCtcctgcaagtgcatagaagga
P7	NsiI-SAG1_F2* fwd	agctaatgcatTAGCCGAAGGCAGTGAGACGC
P8	SAG1-PacI rev	agctattaattaaTCACGCGACACAAGCTGCG
UPRT cloning/mutagenesis		
P9	NsiI-myc-UPRT_CDS fwd	atgcatGAACAAAAGTTGATTTCTGAAGAAGATTTGGCGCAGGTCCCAGCGAGC
P10	UPRT_CDS-PacI rev	ttaattaatcaCATGGTTCCAAAGTACCGGTCAC
P11	NsiI-UPRT_CDS fwd	atgcatGCGCAGGTCCCAGCGAGC
P12	UPRT_CDS-HA-PacI rev	ttaattaatcaAGCGTAGTCCGGGACGTCGTACGGGTACATGGTTCCAAAGTACCGGTCAC
P13	UPRT-L92* mut fwd	atgtgtcataccaTGGAGTTTCCTTTTATTCCAAG
P14	UPRT-L92* mut rev	cctaaggggttgtcACTTCCTTCTTTTCGAACG
P15	UPRT-Y96* mut fwd	atgtgtcatagcaTGGAGTTTCCTTTTATTCCAAG

P16	UPRT-Y96* mut rev	ccagaggggttgtcACTTCCTTCTTTTCGAACG
P17	NotI-Gra1_pro fwd	gcggccgccgaaggctgtagtactggtgc
P18	Gra2_3'utr-PciI rev	acatgtctggcgaaatcaacgcacacc
ILP1 cloning/mutagenesis		
P19	ILP1-K130* mut fwd	GTGGATGGCCtagCTGAAGGCGG
P20	ILP1-K130* mut rev	ACAGCCTGGTCATCTGCG
P21	ILP1-E140* mut fwd	AGAGCAGGCGtagGCCTACACGC
P22	ILP1-E140* mut rev	TCCTGTTCCGCCTTCAGC
P23	ILP1-Q150* mut fwd	GCGTGAATTTtagGATACATTCACCCAGCAGCATG
P24	ILP1-Q150* mut rev	ATGGCGCGCGTGTAGGCT
P25	ILP1-T152* mut fwd	ATTTCAAGATtagTTCACCCAGCAGCATGCCCTGTACCAGC
P26	ILP1-T152* mut rev	TCACGCATGGCGCGCGTG
P27	ILP1-Y160* mut fwd	GCATGCCCTGtagCAGCAAGGCT
P28	ILP1-Y160* mut rev	TGCTGGGTGAATGTATCTTGAAATTCACG
P29	ILP1-Q168* mut fwd	GCAGGAACAGtagAAGCAGATCAA
P30	ILP1-Q168* mut rev	AAGCCTTGCTGGTACAGG
P31	ILP1-Q170* mut fwd	ACAGCAGAAGtagATCAACGACTG
P32	ILP1-Q170* mut rev	TCCTGCAAGCCTTGCTGG
P33	ILP1-T184* mut fwd	CGCCCAGAAGtagCAACAGACCATC
P34	ILP1-T184* mut rev	TCCTCAAGCAACTTGTTC
P35	ILP1-T187* mut fwd	GACCCAACAGtagATCTATGAACAGGAAGTGC
P36	ILP1-T187* mut rev	TTCTGGGCGTCCTCAAGC
P37	ILP1-I188* mut fwd	CCAACAGACCtagTATGAACAGGAAGTGCGAC
P38	ILP1-I188* mut rev	GTCTTCTGGGCGTCCTCA
P39	ILP1-R194* mut fwd	ACAGGAAGTGtagCGCATGGAGG

P40	ILP1-R194* mut rev	TCATAGATGGTCTGTTGG
P41	ILP1-A204* mut fwd	ACTGAAGGAAtagACTGCCGCGGAGGAG
P42	ILP1-A204* mut rev	CGAGCCTCCTCCATGCGT
P43	ILP1-E209* mut fwd	TGCCGCGGAGtagGCAATGAAGG
P44	ILP1-E209* mut rev	GTTGCTTCCTTCAGTCGAGCC
P45	ILP1-K212* mut fwd	GGAGGCAATGtagGAACAGATTGACCTC
P46	ILP1-K212* mut rev	TCCGCGGCAGTTGCTTCC
IMC3 and IMC6 truncations		
P47	pUPRT-ILP1pro_V5 gibson fwd	GGCAAGCCCATCCCTAATC
P48	pUPRT-ILP1pro_V5 gibson rev	catCTTGTTGCGAAGGAAAAG
P49	IMC3-alv gibson fwd	tccttttccttcgcaacaagatgCCTCCAGAGGTCCGACAGAAG
P50	IMC3-alv gibson rev	ggattagggatgggcttgccTGGCGGCTGGTACGGGAT
P51	IMC3-Cterm gibson rev	ggattagggatgggcttgccCTGCTCGTAGACGACTTCG
P52	IMC6-alv gibson fwd	tccttttccttcgcaacaagatgCCCGTCGTCCCCGTCCCC
P53	IMC6-alv gibson rev	ggattagggatgggcttgccCACATCGAAGACAGGGACGAAGCGTTC
P54	IMC6-Cterm gibson rev	ggattagggatgggcttgccGTGCACCTCGCCTTCGGAGTTG
P55	IMC6-Nterm gibson fwd	tccttttccttcgcaacaagatgGCTCAGACAGCCCCGAAC
Epitope tagging of other genes		
P56	IMC3_3'utr gRNA fwd	AAGTTgacggcgcgagatgctttggG
P57	IMC3_3'utr gRNA rev	AAAACccaaagcatctcgcgccgtcA
P58	IMC3-3xmyc_cat HDRki fwd	GAGCCCAGCTGTGCAGGAGCGCGAAGTCGTCTACGAGCAGcgggaattcCCTAGGGAACA

P59	IMC3-3xmyc_cat HDRki rev	gccgctctttctacgccacctccaccacagaagtcctgtgATAGGGCGAATTGGAGCTCC
P60	IMC4_3'utr gRNA fwd	AAGTTgagccgtgcgcatgtggaaagG
P61	IMC4_3'utr gRNA rev	AAAACctttccacatgcgcacggctcA
P62	IMC4-3xmyc_cat HDRki fwd	CCCTCTTGCTCCGGGACAACAGACCCAAGTCAATATCAACcgggaattcCCTAGGGAACA
P63	IMC4-3xmyc_cat HDRki rev	ctcccaacagtgcacaataagaaaaaacagcgccagggtcATAGGGCGAATTGGAGCTCC
P64	IMC6_3'utr gRNA fwd	AAGTTgaggctgagggacaattcaaG
P65	IMC6_3'utr gRNA rev	AAAACttgaattgtccctcagcctcA
P66	IMC6-3xmyc_cat HDRki fwd	TAGCAGAGGCAGCTCTTTCAACTCCGAAGGCGAGGTGCACcgggaattcCCTAGGGAACA
P67	IMC6-3xmyc_cat HDRki rev	ctctgcacggtatcctttcagattcccctgaagactgcgaATAGGGCGAATTGGAGCTCC
P68	IMC12_3'utr gRNA fwd	AAGTTgacttcccctctacggaaaagG
P69	IMC12_3'utr gRNA rev	AAAACcttttccgtagaggggaagtcA
P70	IMC12-3xmyc_cat HDRki fwd	CGCGTCGGAGCGTGCCGAGTCCGTCGACTCCATGCCCCAGcgggaattcCCTAGGGAACA
P71	IMC12-3xmyc_cat HDRki rev	ctactcgttccggctgaactgacaggctgtgtgtctctgcATAGGGCGAATTGGAGCTCC
P72	IMC27_3'utr gRNA fwd	AAGTTgcttctatcgactgccaacccG
P73	IMC27_3'utr gRNA rev	AAAACgggttggcagtcgatagaagcA
P74	IMC27-3xmyc_cat HDRki fwd	TTATTCCAAGCAGTTGAGACAGCTTGCAGAAAAGAGTGCAcgggaattcCCTAGGGAACA
P75	IMC27-3xmyc_cat HDRki rev	tcggcagccccgcagaccatgcttgggtctgcacgggagcATAGGGCGAATTGGAGCTCC
ILP1 acylation mutants and *Pf*G2		
P76	ILP1-G2A fwd	GTTAACCCGGGGACCTTACTGTAAGC
P77	ILP1-G2A rev	AAGCTTCTGCGCCATCTTGTTGCGAAGGAAAAGG

P78	ILP1-C95S_C96S fwd	AGGCGGCCTGtcttcgGGCTCATCGC
P79	ILP1-C95S_C96S rev	GTGTTAACACCGAATTCGTTC
P80	ILP1-C273S_C274S fwd	GTTAACACAGGCGGCCTGtc
P81	ILP1-C273S_C274S rev	gcggccgccgaagaCGCTCGACTTGGGTGTTCCT
P82	NotI-V5-PacI ssDNA to anneal fwd	ggccgccGGCAAGCCCATCCCTAATCCTCTGTTGGGCCTGGATTCGACAtaattaat
P83	NotI-V5-PacI ssDNA to anneal rev	taattaTGTCGAATCCAGGCCCAACAGAGGATTAGGGATGGGCTTGCCggc
P84	ILP1_intron gRNA fwd	AAGTTggattgttcattcatgagctG
P85	ILP1_intron gRNA rev	AAAACagctcatgaatgaacaatccA
P86	ILP1 NcGra7 HDRko fwd	GGGTCGCCAGGTTCCTCTTTCCTTTTCCTTCGCAACAAGCCACTCCATGGAACCTGACTG
P87	ILP1 NcGra7 HDRko rev	TACGCCAGCGAGGCCGTCATTGTCAGGCCCTGTATGCTACctgcaaGtgcatagaaggaa
P88	ILP1 gene KO check fwd	tctcgtatgcagttcgcgtatg
P89	ILP1 gene KO check rev	gcgtcaaaacagagactccatc
P90	ILP1 5utr KO check fwd	gagaggtgacatgttgagctag
P91	ILP1 5utr KO check rev	CCTAGTCAATATGCAACCTGCG
Antibody production		
P92	ILP1 pET-LIC fwd	tacttccaatccaatgcaGGGCAGAAGCTTACCGTCGA
P93	ILP1 pET-LIC rev	TTATCCACTTCCAATGTTATTAGCAGCACGCTCGACTTGGG
P94	IMC6 pET-LIC fwd	tacttccaatccaatgcaGCTCAGACAGCCCCGAACC
P95	IMC6 pET-LIC rev	TTATCCACTTCCAATGTTATTAGTGCACCTCGCCTTCGGAG

Table 2-S6. List of synthesized gene fragments used in chapter 2.

Partial Toxoplasma U6 promoter, BstYam tRNA cassette (AvrII, XbaI flanks)

CCTAGGCCTGACGCGCCTCCTGCAGAACGCGAGACACTGGGATATGTAGAGCCAAGGGGGAAAC
CTTCGAACTCTCGAATGTCTTCTCTGACAAGAATCATATTTCCATCAGTTCTGTCAGATTTTCA
AATGGCGACCTGCAGAGGCCTGCTTCCTCCCTGTGCGCTCTTCGAAGGGGCTTTCTGTCGCGCA
GGGTCACCTCGTCCCCGAAGGGGGTGTTTGCCTTCTGGTAAATGGGGATGTCAAGTTGGAGGGG
TAGCGAAGTGGCTAAACGCGGCGGACTCTAAATCCGCTCCCTTTGGGTTCGGCGGTTCGAATCC
GTCCCCCTCCATTTTTTTTTCTTTTTCtctaga

Plasmodium G2 coding sequence codon optimized for *Toxoplasma*

ATGGGCCAGATCAGTTCCAAGGAAGATGAGATTGAAAAGCAAAATATCTATGCGACTTACCCTG
GACTGGAACAGCAGCTTGATATGGTGTTCGCGTGCCATGACATTTCTAAACAAGGAAAGTTGTC
GTACAAGACAGTTGAAATGATCCTGAGGCACTTTTTGATGCAATGCGGGTTTATGGAGTACGTG
TGCAGATTTGTCGACGAGAACGGAACCTTGGATTTGAAGCACGTGTCCAATTATCTTTCTATCA
AGAAATTGATGTACAAATTGAAATGCTGCGGGGAAAGTATGCTCACGCTGGACGAAATGAAAGA
GTTGGTTATTATCTTCCTCAAGAAAATTTCCGACACCTATACCGAGGATCAGACCAAATGGCTG
GAGCAAATGAAGTCGTCGCAAGAGCAACAAGATAAGGCTCTCGAAGAGGCTATGTATAAATACG
AAAAGAACATTCTGTTTCATCATGCGGTGAAGGAACAGCAAATTCTTCAGAATGATAAAAAACT
GAATGAGTGGAATGAGAACGTGGAGAATGCGTATGAGGCACAACAAGAAATTTTGCGGCAATTC
GAATCCTCCAGGAAGAAAAATATTGATATTTCTCTGGAGAAAAACAACGAACTGATTATCGCAA
AAGACTATATTGACAAGATCAAGGAAGCTGCTACGGATAACAAGTATGATAATTCCAAATGTTT
CATCTATCCAGCGTCTTCTGCGCCTTGCGGCGCATGTACGAGCGCTGGCGCCATCATCCACCAT
AGGCGATACAAGGAAAAACGTAGGAAGAAAGAGTATAGCTTGTGCTTA

CHAPTER 3:

Application of the UAA crosslinking system to the ILP1 EF-hand domain

3.1 - Introduction

Although the C-terminal coiled-coil domain of ILP1 was the initial target for Azi site-specific crosslinking, we were also interested in determining whether other parts of the protein were involved in interactions that played a role in its function. In particular, the N-terminal putative EF-hand region was also enticing, as EF-hand domains confer calcium-sensing activity by interacting with target proteins in either holo or apo conformations (Chazin, 2011). As *T. gondii* relies heavily on calcium signaling for its lytic cycle in addition to conserved eukaryotic functions, it has over sixty proteins that contain EF-hand domains (Chang et al., 2019). One recently characterized member of this group is calmodulin, which localizes to the apical and basal ends of the tachyzoite and recruits cytoplasmic calcineurin to these subcompartments only when the parasite is extracellular, a process that is important for host cell attachment (Paul et al., 2015). Other members include a series of three centrins that localize to the centrosome and spindle pole bodies to serve essential functions in nuclear division and replication. Centrin2 is also believed to be responsible for constricting the basal end of the parasite at the completion of endodyogeny (Hartmann et al., 2006; Hu, 2008; Hu et al., 2006). Perhaps the best-studied members are the apicomplexan-specific calcium-dependent protein kinases CDPK1, CDPK3, and CDPK7, which have EF-hands fused to a serine/threonine kinase domain. These proteins have been shown to play critical roles in signaling for egress, microneme secretion, motility, and replication (Hui et al., 2015; J.-L. Wang et al., 2016). These CDPKs have been investigated as potential therapeutic targets, as they are not found in mammalian hosts (Lourido et al., 2012).

Although the calcium-sensing activity of EF-hand domains play important roles, there are also degenerate EF-hands that have lost the ability to coordinate Ca^{2+} ions due to the lack of necessary negatively charged amino acids. These degenerate motifs can retain protein-binding

capabilities or, if part of an enzyme, may make the catalytic domain fixed in an active or inactive state (Bender et al., 2018). For example, the CDPK-related protein kinase family in plants are constitutively active and insensitive towards calcium levels, and at least one of the *T. gondii* noncanonical CDPK has EF-hands that are all degenerate (Furumoto et al., 1996; Long et al., 2016). The *T. gondii* myosin light chains that bind to the neck domains of myosins all contain 4 degenerate EF-hands, but while they do not directly bind calcium, they are subject to calcium-dependent phosphorylation (Nebl et al., 2011; Polonais et al., 2011). Similarly, the recently characterized degenerate calmodulin-like protein CaM3 localizes to the conoid and is detergent-insoluble, suggesting that it binds to some cytoskeletal component such as MyoH, the essential glideosome motor that uniquely binds directly to the conoidal microtubules (Graindorge et al., 2016; Long et al., 2017b). The EF-hand domain proteins in *T. gondii* that have yet to be studied are good potential targets for Azi crosslinking, particularly if they are insoluble like CaM3 and thus are refractory to other analyses for determining protein-protein interactions.

3.2 - Results

Azi crosslinking of the putative degenerate ILP1 EF-hand yields a major product

Although the N-terminal EF-hand domain of ILP1 is not reported on ToxoDB, Phyre2 reports up to 92.4% confidence of this region when compared to several calmodulin-like EF-hand templates (Gajria et al., 2008; Kelley et al., 2015). These predictions indicate that there are two EF-hands with their classical helix-loop-helix secondary structure, but upon inspection, the loop regions of the ILP1 sequence lack the conserved DxDxDG motif that binds to calcium in canonical EF-hand domains (Chazin, 2011; Denessiouk et al., 2014). Interestingly, the top model (Fig. 3-1B) is based off an NMR structure of the *Tetrahymena thermophila* calcium-binding protein 2

(Tcb2) C-terminus (PDB: 2NCP, Kilpatrick et al., 2016). Tcb2, which is largely composed of four EF-hands, is a component of the ciliate cortical cytoskeleton that is orthologous to the apicomplexan IMC. This *in silico* model was analyzed using the ligand binding prediction server COACH, and as suspected, Ca^{2+} binding activity was not highly predicted (Yang et al., 2013a, 2013b). Instead, possible peptide binding was reported based on two templates, the more confident one being an NMR structure of human centrin 2 in complex with a repeat domain of suppressor of fermentation-induced loss of stress resistance protein 1 (Sfi1), an interaction important for centrosome division (PDB: 2K2I, Martinez-Sanz et al., 2010).

Using this prediction, we mutated 11 residues that are in the putative binding interface into amber stop codons for site-specific Azi substitution and crosslinking (Fig. 3-3A: H35, I51, L55, Y64, E83, L102, E103, D104, F105, L108, W112). Intriguingly, the H35 mutant resulted in a robust crosslinked species at approximately 225 kDa. Another consistent upshift at ~130 kDa is observed for residues I51, L55, L102, and E103 at varying intensities, but this was not pursued due to the lower efficiency of crosslinking.

Residue H35 of ILP1 crosslinks to the alveolin IMC1

To identify the crosslinked partner of ILP1 at residue H35, we performed a large-scale crosslinking and denaturing co-IP of the ILP1-3xHA H35 mutant. A distinct band corresponding to the unknown product was observed by Coomassie staining (Fig. 3-2B). The gel slice was excised and analyzed by mass spectrometry, yielding ILP1 and IMC1 as the most abundant proteins (Table 3-4). To confirm this interaction, we sought to epitope tag IMC1 as we have previously done for the ILP1 interactors in Chapter 2. Due to proteolytic processing of the IMC1 C-terminus and potential palmitoylation at the N-terminus, we endogenously inserted a 3xMyc tag internally

between residues 52 and 53, which did not appear to impact trafficking or function of the protein (Fig. 3-2A). Photocrosslinking and denaturing co-IP in the IMC1-3xMyc background verified that the EF-hand domain of ILP1 does indeed bind to IMC1 at residue H35 (Fig 3-2B).

3.3 - Discussion

Based on the results reported here and in Chapter 2, we can construct a model for how ILP1 binds to other elements in the IMC cytoskeleton (Figure 3-3). ILP1 is likely myristoylated at glycine-2, and this fatty acylation is important for growth as quantified by plaque formation. Two cysteine pair motifs are weakly predicted to be palmitoylated by CSS-PALM, but mutating those residues does not lead to an overall growth defect (Ren et al., 2008). A dual myristoylation and palmitoylation mutant should be assessed in the future. Different regions of the C-terminal coiled-coil region of ILP1 bind to IMC3, IMC6, and IMC27, although whether these proteins can bind simultaneously to one ILP1 molecule has not been established. Through further truncation experiments, we determined that although the alveolin domains of IMC3 and IMC6 were mostly sufficient for targeting to the IMC cytoskeleton, the addition of either the IMC3 C-terminus or IMC6 N-terminus greatly improved trafficking. Concurrently, we demonstrated by crosslink formation that ILP1 interacts with the IMC3 C-terminal and IMC6 N-terminal regions, although the precise locations within these proteins have not been determined. This agrees with the prevailing theory that the alveolin domains are mainly involved in forming filamentous structures with other alveolins, but ILP1 appears to improve proper IMC incorporation by interacting with the respective IMC3 and IMC6 regions.

This chapter further explored the N-terminal EF-hand domain of ILP1 and revealed that this region interacts with the alveolin IMC1. This result is exciting, as this suggests that IMC1

behaves differently than other alveolins, despite all of them being categorically lumped together based on their proline and valine-rich repeat domain (Anderson-White et al., 2011). Although our understanding of the other alveolins is not complete, the importance of IMC1 for cytoskeletal integrity has been demonstrated beyond speculation (Anderson-White et al., 2012). Cell cycle expression profiles show that IMC1 is not only produced during endodyogeny, but also during G1 phase and constantly incorporated into the maternal IMC after replication (Hu et al., 2002). Proteolytic cleavage of the IMC1 C-terminus is also coincident with transition from the detergent-soluble nascent daughter IMC scaffold to the rigid, detergent-insoluble maternal cytoskeleton (Tara Mann et al., 2002). IMC1 is also unique that it contains a strongly predicted coiled-coil domain within the alveolin domain (Lupas, 1997). IMC3, IMC10, IMC12, and IMC14 also have predicted coiled-coils, but they are generally low confidence and in other regions of the protein. IMC1 is also the only alveolin that localizes to both the IMC apical cap and body, which are surprisingly segregated in composition, suggesting a more integral role in IMC assembly (Fig. 3-2A) (Beck et al., 2010). It would be interesting to examine whether this interaction between IMC1 and ILP1 somehow differentiates the maternal and daughter IMC. Although we proceeded under the assumption that the ILP1 EF-hands are degenerate due to the lack of negatively charged residues needed to complex Ca^{2+}, we will need to empirically test for this lack of activity using isothermal titration calorimetry or another similar method. Calcium binding activity would have fascinating implications, as activity in the N-terminus may induce conformational changes into the downstream coiled-coil domain, or vice versa.

Azi-mediated crosslinking ability at every residue of ILP1 was not assessed, and therefore it is not possible to make a claim on other potential binding partners of ILP1. However, with the identification of IMC1, IMC3, and IMC6 as definitive interactors, it is tempting to consider how

the other alveolins are organized within the cytoskeletal meshwork. In particular, IMC4 and IMC10 are the remaining two alveolins that colocalize with ILP1 (Dubey et al., 2017). Truncation experiments may reveal how the domains of these proteins behave independently. In addition, although we chose to investigate the prominent band seen in the H35 mutant, we are also interested in the consistent size signal seen in the I51, L55, L102, and E103 mutants, and should be able to rapidly identify this unknown crosslink species using mass spectrometry (Fig. 3-1C). In conclusion, the photoactivated crosslinking amino acid *p*-azidophenylalanine and site-specific UAA incorporation using an amber stop codon suppression technique has proved to be highly useful in determining binding partners of ILP1 and uncovering the first organization of the *T. gondii* IMC cytoskeleton.

3.4 - Materials and Methods

Procedures for ILP1 amber mutagenesis, crosslinking, western blot, immunofluorescence assay, large scale immunoprecipitation, and mass spectrometric analysis are described in Chapter 2. ILP1 EF-hand mutants were generated using primers P1-22 (Table 3-5).

Internal IMC1 3xMyc tagging was performed in the absence of selection using a gene fragment (IDT, Table 3-5) of the 3xMyc tag between residues 52 and 53 with at least 300 bp of IMC1 flanking genomic sequence plus a pU6-universal plasmid targeting a nearby downstream protospacer (P23/24). The gene fragment was first subcloned into pJet1.2 (Thermo Scientific) and amplified using P25/26. A clonal tagged line was obtained through successive rounds of limiting dilution.

3.5 - Figure and Table Legends

Figure 3-1. Crosslinking of the EF-hand domain of ILP1 reveals another major upshift.

(A) Diagram of ILP1 showing an N-terminal putative EF-hand domain (yellow) followed by a coiled-coil domain (grey). 2 degenerate EF-hand loops are labeled. Also shown is the JPred secondary structure prediction of ILP1 revealing alpha-helices (black bars) and beta-strands (white arrows) as well as buried residue prediction used for choosing likely exposed residues for amber substitution (Drozdetskiy et al., 2015). Also noted are the potentially myristoylated glycine at position two and a cysteine prenylation/palmitoylation motif at the C-terminus (teal). Eleven residues in the ILP1 EF-hand domain were chosen for amber mutagenesis and Azi-mediated crosslinking (green). (B) Top Phyre2 *in silico* model of the ILP1 EF-hand domain showing the typical helix-loop-helix structure of EF-hands. (C) Western blot of the ILP1 EF-hand Azi mutants after UV irradiation reveals a new major crosslinked species for residue H35 (~225 kDa, red arrowhead). A fainter band is seen for I51, L55, L102, and E103 (~130 kDa).

Figure 3-2. The ILP1 EF-hand domain binds to IMC1.

(A) IFA of internally tagged endogenous IMC1 showing proper localization to the parasite periphery. Red: mouse anti-Myc antibody, green: rabbit anti-IMC6 antibody. (B) Western blot and Coomassie gel of a large scale anti-HA denaturing IP of the ILP1-3xHA H35 mutant. The ~225 kDa band (red arrowhead) corresponding to the crosslinked product was excised and proteins were identified by mass spectrometry. A separate denaturing anti-HA IP verifies that IMC1 is the H35 partner as the upshifted product is detected with both HA (ILP1) and Myc (IMC1) antibodies.

Figure 3-3. Model of ILP1 interactions determined by Azi crosslinking.

ILP1 is an essential IMC cytoskeletal protein. A likely N-terminal myristoylation associates this protein with the proximal IMC membrane, but interactions with proteins that compose the intermediate filament network render ILP1 insoluble in detergent conditions. ILP1 binds to the alveolin IMC1 at residue H35 of the putatively degenerate N-terminal EF-hand domain, and the alveolins IMC3 (T187) and IMC6 (E209), as well as IMC27 (Y160 & Q168), at different regions of the C-terminal coiled-coil domain. Truncations also reveal that relative to their alveolin domains, the C-terminus of IMC3 and N-terminus of IMC6 are important for binding to ILP1.

Table 3-4. MaxQuant intensities of upshifted ILP1-H35 band.

Top 30 protein intensities calculated by MaxQuant of the excised band following ILP1-3xHA H35 crosslinking and large scale anti-HA IP. ILP1 and IMC1 are the top two proteins that are identified.

Table 3-5. Primers and gene fragments used in chapter 3.

Figure 3-1. Crosslinking of the EF-hand domain of ILP1 reveals other major binding partner.

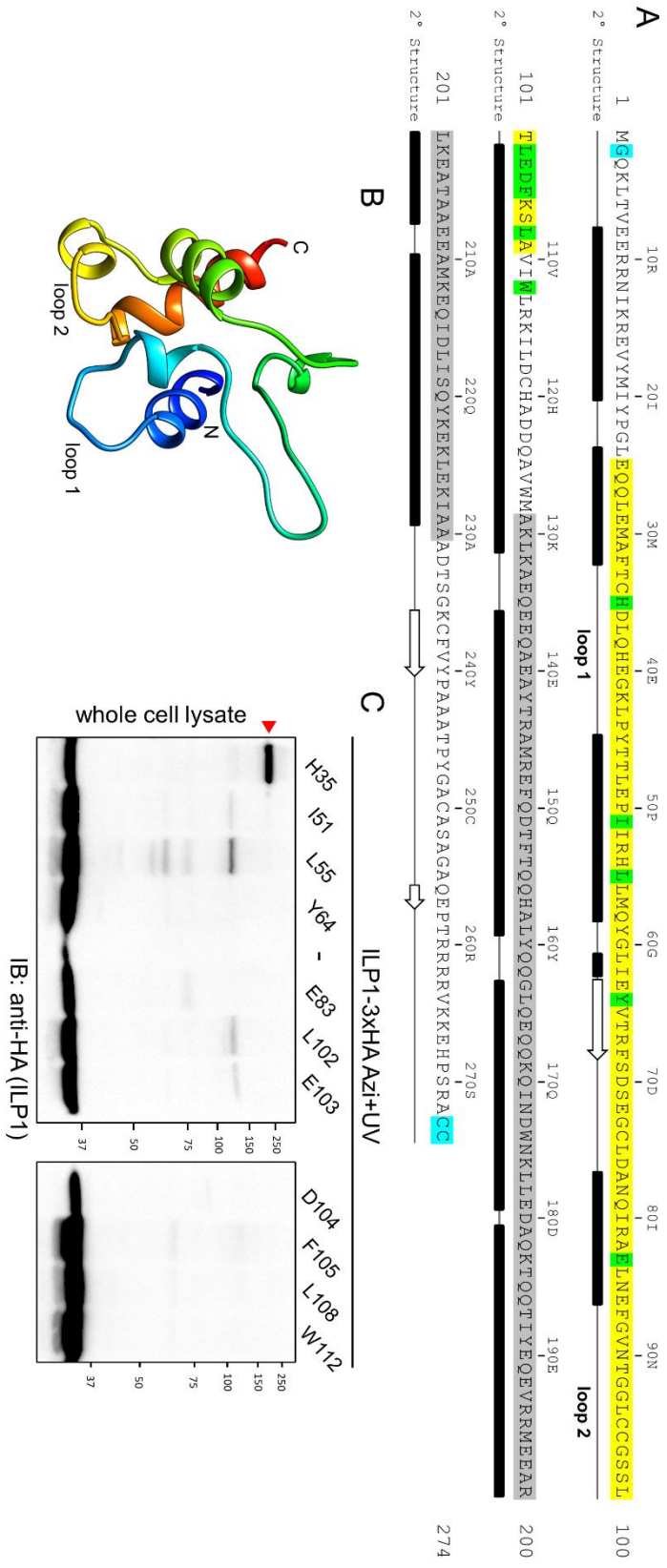

Figure 3-2. The ILP1 EF-hand domain binds to IMC1.

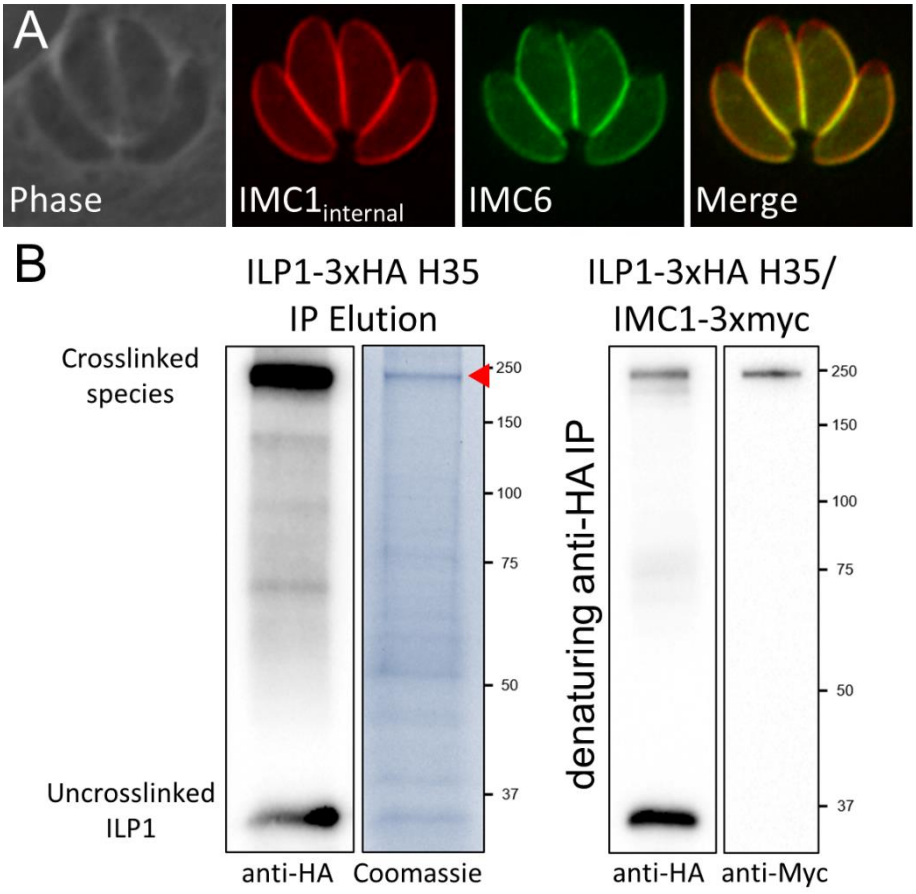

Figure 3-3. Model of ILP1 interactions determined by Azi crosslinking.

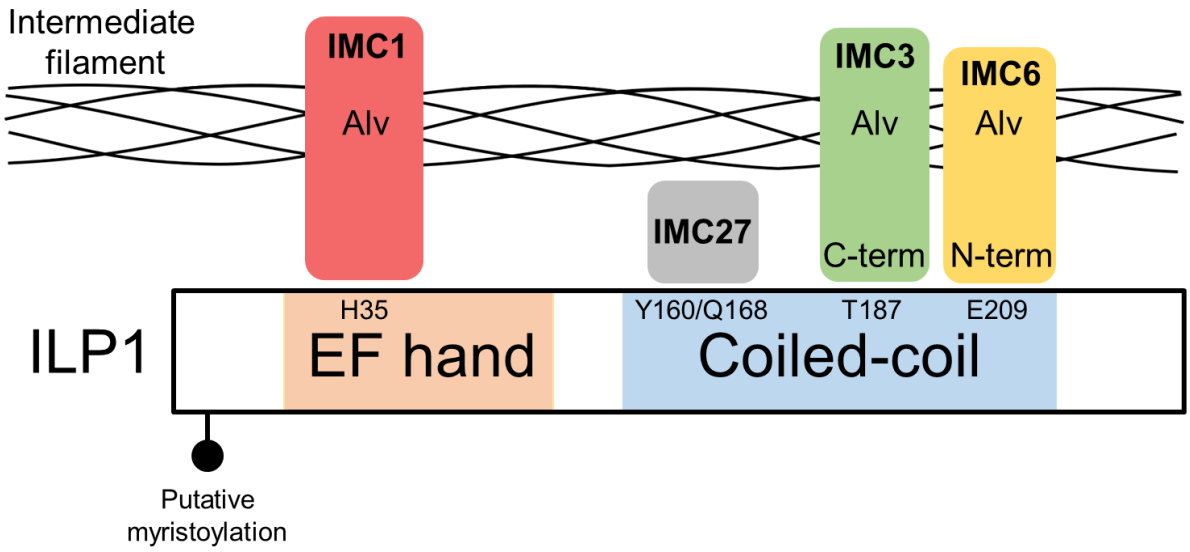

Table 3-4. MaxQuant intensities of upshifted ILP1-H35 band.

Protein IDs	Intensity	MS/MS count	Comments
TGGT1_313380	1939700000	33	ILP1
TGGT1_231640	1727100000	33	IMC1
TGGT1_231630	5705100	5	IMC4
TGGT1_248160	4590900	4	hypothetical protein
TGGT1_230940	4012600	3	hypothetical protein
TGGT1_205470	2901200	2	putative translation elongation factor 2 family protein
TGGT1_291090	2210700	0	SWI2/SNF2-containing protein
TGGT1_226660	1711300	2	hypothetical protein
TGGT1_286420B; TGGT1_259490; TGGT1_294800B; TGGT1_294800A; TGGT1_286420A	1157700	2	putative elongation factor 1-alpha
TGGT1_248740	1036800	3	hypothetical protein
TGGT1_247550	1021000	2	heat shock protein HSP60
TGGT1_290950	929260	1	putative clathrin heavy chain
TGGT1_313360	846060	0	hypothetical protein
TGGT1_244560	802690	2	putative heat shock protein 90
TGGT1_411430; TGGT1_308090	746480	1	ROP5
TGGT1_213900	735110	1	regulator of chromosome condensation RCC1
TGGT1_286580	688520	2	hypothetical protein
TGGT1_273760	660650	4	heat shock protein HSP70
TGGT1_235470	591160	2	myosin A
TGGT1_219260	479670	1	putative cation-transporting ATPase
TGGT1_311720	441720	1	chaperonin protein BiP
TGGT1_311230	419570	1	hypothetical protein
TGGT1_270240	412720	1	MAG1 protein
TGGT1_266960; TGGT1_221620; TGGT1_212240	402310	1	beta-tubulin
TGGT1_216180	387080	0	hypothetical protein
TGGT1_204160	342520	1	GYF domain-containing protein
TGGT1_258870B; TGGT1_258870A	328840	1	hypothetical protein
TGGT1_288650	317090	1	dense granule protein GRA12
TGGT1_278205	315430	0	hypothetical protein
TGGT1_209210	292540	1	hypothetical protein

Table 3-5. Primers and gene fragments used in chapter 3.

P1	ILP1-H35* mut fwd	CTTCACATGCtagGATCTTCAGCATGAGG
P2	ILP1-H35* mut rev	GCCATCTCCAGCTGCTGC
P3	ILP1-I51* mut fwd	GCTGGAGCCTtagATTCGTCACTTG
P4	ILP1-I51* mut rev	GTCGTGTATGGGAGCTTG
P5	ILP1-L55* mut fwd	CATTCGTCACtagCTCATGCAGTAC
P6	ILP1-L55* mut rev	ATAGGCTCCAGCGTCGTG
P7	ILP1-Y64* mut fwd	CCTCATCGAAtagGTTACGAGGTTTT
P8	ILP1-Y64* mut rev	CCGTACTGCATGAGCAAG
P9	ILP1-E83* mut fwd	GATTCGGGCCtagTTGAACGAATTC
P10	ILP1-E83* mut rev	TGGTTGGCATCGAGGCAG
P11	ILP1-L102* mut fwd	ATCGCTCACTtagGAAGACTTCAAGAGCCTTGCCGTC
P12	ILP1-L102* mut rev	GAGCCGCAGCACAGGCCG
P13	ILP1-E103* mut fwd	GCTCACTCTAtagGACTTCAAGAGCCTTGC
P14	ILP1-E103* mut rev	GATGAGCCGCAGCACAGG
P15	ILP1-D104* mut fwd	CACTCTAGAAtagTTCAAGAGCCTTGCCGTC
P16	ILP1-D104* mut rev	AGCGATGAGCCGCAGCAC
P17	ILP1-F105* mut fwd	TCTAGAAGACtagAAGAGCCTTGCCG
P18	ILP1-F105* mut rev	GTGAGCGATGAGCCGCAG
P19	ILP1-L108* mut fwd	CTTCAAGAGCtagGCCGTCATCTG
P20	ILP1-L108* mut rev	TCTTCTAGAGTGAGCGATG
P21	ILP1-W112* mut fwd	TGCCGTCATCtagCTGCGGAAGA
P22	ILP1-W112* mut rev	AGGCTCTTGAAGTCTTCTAGAGTG
P23	IMC1_Nterm gRNA fwd	AAGTTgTGACAGATCGGACAGATTCCG
P24	IMC1_Nterm gRNA rev	AAAACGGAATCTGTCCGATCTGTCAcA
P25	IMC1-3xmyc_fragPCR fwd	ttgttcttgcaaaagttctcgtgg
P26	IMC1-3xmyc_fragPCR rev	cagggctagtacacacatgtca

IMC1 internal 3x-Myc HDR template

3xMyc tag is bold and italicized, protospacer (reverse) is bold, and silent mutation to destroy PAM is underlined

ttgttcttgcaaaagttctcgtggctcgaccgcgggccggactaggggccagcgcgattctgatttgcac
ccggtcgccctctgcgtgtgtgccgagaacctctcggatacttctacctaactccaaagactagtcttcc
tgtttgttgtcagaATGTTTAAGGACTGCGCCGATCCTTGCAGCGATTGCTGCCAGCCTGCTGAACAGCA
GCGCGGCCAGGCCACCCTTCCCTCGCACGTGGTCCTACCTCAGACGTCCGACAGCCCGGCCATCCACGTG
ACTGCCGAAGCTTCTCAGCGACTCAGCTCG***GAACAAAAGTTGATTTCTGAAGAAGATTTGAACGGTGAAC***
AAAAGCTAATCTCCGAGGAAGACTTGAACGGTGCTAGGGCCGAGGAGCAGAAGCTGATCTCCGAGGAGGA
CCTGCCCAGAGCTCTGCAACAGCTCCACGGCACTCA**GGAATCTGTCCGATCTGTCA**CTCTTGAAGAGCGC
GCTGATCGGTCACGAACCGTCCCCATCGGTGAAGAGACTGAGAGACAATGGGtaagagagacgaccacag
gctctaccgctatgttgcggccatgatggaatttggtgctctgcgctcgaattccaacgttttgaggtag
aagccgtggtgacgcgtagattgcaagcagtactgttgcacggtcttcagactggtagttgcgatgcctg
agtctagacagcgtcgggttcgcgaatatgacatgtgtgtactagccctg

CHAPTER 4:

Application of the UAA system

to the ARO rhoptry tethering complex

4.1 - Introduction

As discussed in section 1.2, the rhoptries are apicomplexan-specific secretory organelles that are critical for active invasion and modulation of the initial host cell immune response. These club-shaped organelles are positioned at the apical end of the parasite with their narrow neck regions extending through the middle of the conoid (Paredes-Santos et al., 2012). After attachment to the host through micronemal adhesins, the contents of an individual rhoptry are released into the host cytoplasm through a porosome-like complex at the extreme apical tip of the parasite to form the moving junction complex that mediates invasion of the host cell (Jena, 2009; Paredes-Santos et al., 2012).

During endodyogeny, daughter rhoptries are produced *de novo* through coalescence of acidic vesicles originating from the *trans* Golgi network (Shaw et al., 1998). This process appears to be an adaptation of the endocytic pathway, as many proteins important for rhoptry and microneme biogenesis, such as dynamin-related protein B (DrpB), sortilin-like receptor (SORTLR), Rab proteins, and vacuolar protein sorting 9 (Vps9), are all homologs of members of the yeast Vps system (Breinich et al., 2009; Kremer et al., 2013; Sakura et al., 2016; Sloves et al., 2012). The micronemes are clearly associated with the subpellicular microtubules in electron micrographs, and this is supported by evidence suggesting that dynein light chain 8a (DLC8a) transports these organelles to the apical complex using these microtubules (Dubois & Soldati-Favre, 2019). It may be tempting to speculate that the rhoptries, which are bundled at the conoid, may be similarly recruited by motor proteins on the conoidal or intraconoidal microtubules, but this has not been established (Hu et al., 2006).

The first characterization of the mechanism of rhoptry bundling and tethering to the apical end of the parasite was with the armadillo repeats-only (ARO) protein conserved in *T. gondii* and

Plasmodium spp. (Cabrera et al., 2012). ARO is composed of six armadillo repeat domains, a motif of about 40 amino acids that, while not conserved in sequence, has a characteristic fold of three α-helices. (Mueller et al., 2016; Tewari et al., 2010). These tandem armadillo repeats assemble into a superhelix, forming a large concave face composed solely of α-helices that bind to protein partners (Tewari et al., 2010). These armadillo repeat proteins are diverse in nature and some, such as β-catenin, are known to serve multiple functions through their peptide binding activities (Tewari et al., 2010).

ARO localizes to the cytoplasmic face of the rhoptry membrane through N-terminal myristoylation and palmitoylation, the latter catalyzed by the sole rhoptry-resident protein S-acyltransferase DHHC7 in *T. gondii* (Beck et al., 2013; Mueller et al., 2013). In the kinetic trapping model of fatty acylation, myristoylation of N-terminal glycines first imparts weak affinity of soluble proteins to membranes, whereupon subsequent palmitoylation of cysteine residues solidifies the association (Frénal et al., 2014a). Consequently, individual mutation of either glycine or cysteines of PfARO causes cytoplasmic mislocalization, demonstrating that both modifications are necessary for correct and stable targeting (Cabrera et al., 2012). Conditional knockdown of either ARO or DHHC7 causes a unique lethal phenotype where individual rhoptry organelles are dispersed throughout the parasite cytoplasm, showing that palmitoylated ARO is important for rhoptry tethering to the apex of the parasite (Beck et al., 2013; Mueller et al., 2013).

How ARO mediates this apical tethering through protein interactions remains unknown. However, like other armadillo repeat proteins, this function is likely performed by the concerted effort of the six armadillo repeats. Deletion analysis of individual armadillo repeats resulted in the same rhoptry dispersion phenotype, indicating that the integrity of all six repeats is critical for normal binding activity (Mueller et al., 2016). The sole exception was seen with an ARO mutant

with a deletion of the last repeat (ARO-ΔARM6), which caused an interesting phenotype where the rhoptries were still bundled together but detached from the apical end of the parasite. Although deletion mutations may perturbate normal protein folding, it is tempting to hypothesize that this region of ARO functions separately from the rest of the protein to dock the rhoptries to the conoid or other apical structure. A similar interaction is seen with inhibitor of β-catenin and Tcf (ICAT), which binds to the three most C-terminal (out of 12) repeats of β-catenin (Graham et al., 2002).

Three binding partners of ARO have been identified by co-IP analyses: adenylate cyclase β (ACβ), the class XXII myosin MyoF, and armadillo interacting protein (AIP), which lacks any known domains (Mueller et al., 2013). ACβ binds to ARO through AIP and knockdown of ARO causes mislocalization of both proteins, but neither are essential and have any involvement in rhoptry tethering (Mueller et al., 2016). MyoF is an indispensable motor protein involved in apicoplast inheritance during endodyogeny and depletion does cause accumulation of rhoptry and microneme material in the posterior residual bodies. However, it is possible that the interaction between MyoF and ARO is an artifact of IP or only occurs during replication, as MyoF does not localize to the mature rhoptries (Jacot et al., 2013). Notably, the ARO-ΔARM6 mutant properly recruits ACβ and AIP to the rhoptries and co-IPs MyoF, further suggesting that detachment of the rhoptry bundle from the apical end does not involve any of these three proteins (Mueller et al., 2016).

4.2 - Results

Characterizing two proteins that co-localize with ARO

Our lab previously performed a proximity-dependent biotin labeling (BioID) experiment with ARO (unpublished work, Roux et al., 2012) and identified ACβ (TgGT1_270865) and a

hypothetical protein with pleckstrin homology and cysteine proteinase domains (TgGT1_294630). Both proteins were localized to the rhoptries by C-terminal 3xHA epitope tagging and subsequently disrupted with CRISPR/Cas9 (Fig. 4-1A, B). ACβ was complemented at the uracil phosphoribosyltransferase locus as previously described (Donald & Roos, 1995), and fitness of knockout and complementation strains were assessed by plaque assay (Fig. 4-1A, C). Only slight growth defect is observed in the ACβ knockout strain, which does not reflect the lethal phenotype seen with ARO. The TgGT1_294630 knockout was determined to not have any effect on parasite growth (data not shown).

A novel ARO-associated protein is identified by Azi crosslinking.

To potentially identify novel partners as well as map out the interactome of known partners for ARO, I generated amber mutants for Azi-mediated crosslinking. The protein structure prediction server I-TASSER confirms that ARO folds into a canonical superhelix structure (Fig. 4-2A) (Yang et al., 2015). A solved crystal structure of the homologous *P. falciparum* ARO also gives high confidence for this model (PDB: 5EWP). Three residues (V133, F137, and V182) that are in the major binding groove of the superhelix were initially targeted (Fig. 4-2A). Using the most reactive residue, F137, I performed a large-scale crosslinking experiment and purified ARO-bound targets for mass spectrometric analysis (Fig. 4-2B).

One of the proteins identified was TgGT1_279420, which has a cell cycle expression profile characteristic of *de novo* produced secretory organelle proteins (Fig. 4-3A). C-terminal endogenous epitope tagging of this gene indeed revealed a rhoptry neck localization, concomitant with ARO (Fig. 4-3B). Interestingly, this protein lacks a signal peptide, which is needed for packaging into the rhoptry interior, and any transmembrane domains or fatty acylation motifs,

suggesting that its localization is due to interaction with another resident rhoptry protein (i.e. ARO). Although this protein was a good candidate for being involved in rhoptry tethering based on localization and genome-wide CRISPR/Cas9 score (-1.96 compared to -2.1 for ARO), knockout experiments did not result in any growth defect (data not shown) (Sidik et al., 2016).

A robust crosslinked species is found when targeting armadillo repeat 6 of ARO

We were interested in the unique rhoptry detachment phenotype observed with the ARO-ΔARM6 mutant, as it was possible that the protein interactions mediating bundling were distinct from apical tethering (Mueller et al., 2016). We targeted four initial residues for Azi mutagenesis (Y214, Y221, D263, L267) that were in the fifth and sixth armadillo repeats (Fig. 4-4A). Western blot of the crosslinked mutants revealed a robust ~300 kDa upshift for the L267 strain, suggesting that there was a binding partner in proximity of armadillo repeat 6 of ARO (Fig. 4-4B). We are in the process of determining the identity of this upshifted species.

4.3 - Discussion

Although ARO has three binding partners (ACβ, AIP, MyoF) and two newly identified colocalizing proteins (TgGT1_279630 and TgGT1_279420), none of these proteins share the function of ARO in rhoptry bundling and tethering. MyoF is the only partner that has a severe growth phenotype when knocked down but this is due to an overall defect during replication, not invasion, and a motor protein is unlikely to be involved in the static positioning of the rhoptries in the apical complex (Jacot et al., 2013). It may be possible that ARO is multimerizing to perform a function, as there is evidence of dimerization by human armadillo repeat protein required for cell

differentiation 1 (Rcd1) (Garces et al., 2007). However, this dimerization of Rcd1 occurs at the opposing side of the structure, not within the concave superhelical fold where most ligands fit.

The multiple band pattern observed in the F137 mutant western blot agrees with the possibility of multiple binding partners as observed in other armadillo repeat proteins like β-catenin. However, it is difficult to resolve ambiguous upshifted signals, and other methods of protein identification may be needed to conclusively identify interactors within this fold. We are more interested in definitive crosslink results as seen with the L267 ARO mutant and we foresee no difficulty in elucidating the protein partner seen in this condition.

4.4 - Materials and Methods

Procedures for ARO amber mutagenesis, crosslinking, western blot, immunofluorescence assay, CRISPR/Cas9 knockout, plaque assay, large scale immunoprecipitation, and mass spectrometric analysis are described in chapter 2. ACβ, TgGT1_294630, and TgGT1_279420 were C-terminally epitope tagged using the ligation independent cloning approach as described using P1-6 (Table 4-5) (Huynh & Carruthers, 2009). ACβ and TgGT1_294630 gene loci were disrupted with CRISPR/Cas9 using P7-10.

An ARO expression construct with the endogenous promoter and C-terminal 3xHA epitope tag and DHFR marker was assembled as follows. The vector pNotI-HA-HPT (Beck et al., 2010) was first digested with SacI and self-ligated to excise the HXGPRT marker and swapped for a 3xHA epitope sequence. ARO cDNA flanked with BglII/NotI sites (P11/12), *ARO* promoter flanked with NheI/BglII (P13/14), and a DHFR cassette flanked with BsiWI/NheI (P15/16) were then sequentially ligated into this vector. The BsiWI/NheI flanked cassette was ligated to Acc65I/NheI sites using complementary ends. ARO amber mutants were generated using P17-24.

Additional antibodies used are rabbit anti-ROP13 (Turetzky et al., 2010), rat anti-RON11 (Beck et al., 2013), and rat anti-ARO (unpublished). Polyclonal rat or rabbit antibodies against ARO (P25/26) and TgGT1_279420 (P27/28) were generated as described in chapter 2 using the pET His6 TEV LIC bacterial expression vector (Addgene #29653).

4.5 - Figure and Table Legends

Figure 4-1. Localization of ACβ and TgGT1_294630 and ACβ plaque assay.

(A) IFA showing C-terminally epitope tagged, knockout, and complemented strains for ACβ. Green: mouse anti-HA, red: rabbit anti-ROP13 or rat anti-RON11. (B) IFA showing C-terminally epitope tagged and knockout strains for TgGT1_294630. Green: mouse anti-HA, red: rabbit anti-ROP13 or rat anti-RON11. (C) Plaque assay of ACβ strains.

Figure 4-2. Azi substitution at residue F137 of ARO results in a multiband crosslink pattern.

(A) I-TASSER prediction model of ARO showing the six armadillo repeats. Residues V133, F137, and V182 were used for Azi crosslinking. (B) The ARO F137 mutant localizes properly to the rhoptries. Green: mouse anti-HA (C) Western blot of parasites exposed to UV light show a pattern indicating multiple binding partners to ARO only for the F173 mutant. Gel slices (black asterisks) were excised and protein contents were identified by mass spectrometry.

Figure 4-3. TgGT1_279420 localizes to the rhoptries.

(A) Cell cycle expression profile of TgGT1_279420 resembles rhoptry proteins such as ARO and DHHC7. (B) TgGT1_279420 colocalizes with ARO. Red: mouse anti-HA, green: rat anti-ARO.

Figure 4-4. A robust Azi-crosslinked product is seen with residue L267 of ARO.

(A) Four residues (Y214, Y221, D263, and L267) in armadillo repeats 5 and 6 were mutagenized for Azi substitution. (B) UV crosslinking results in a robust upshift ~300 kDa in the L267 mutant (red arrowhead).

Table 4-5. Primers used in chapter 4.

Figure 4-1. Localization of ACβ and TgGT1_294630 and ACβ plaque assay.

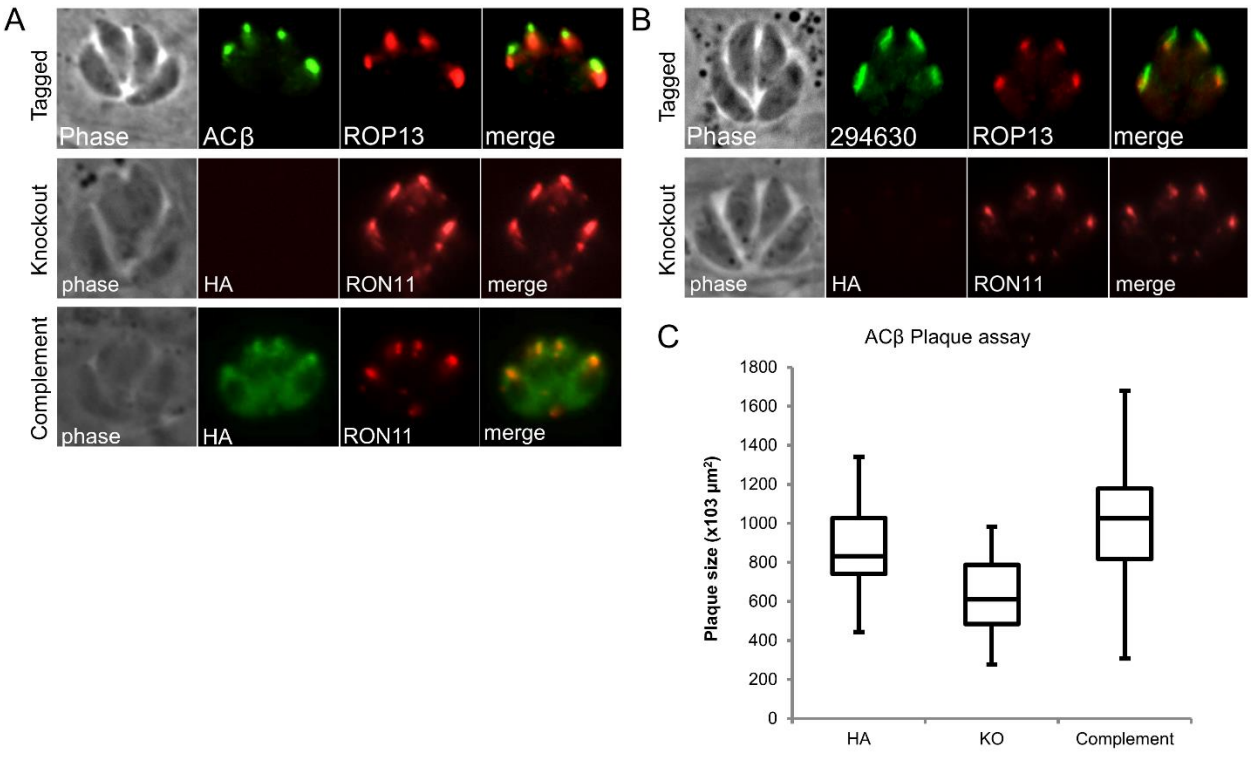

Figure 4-2. Azi substitution at residue F137 of ARO results in a multiband crosslink pattern.

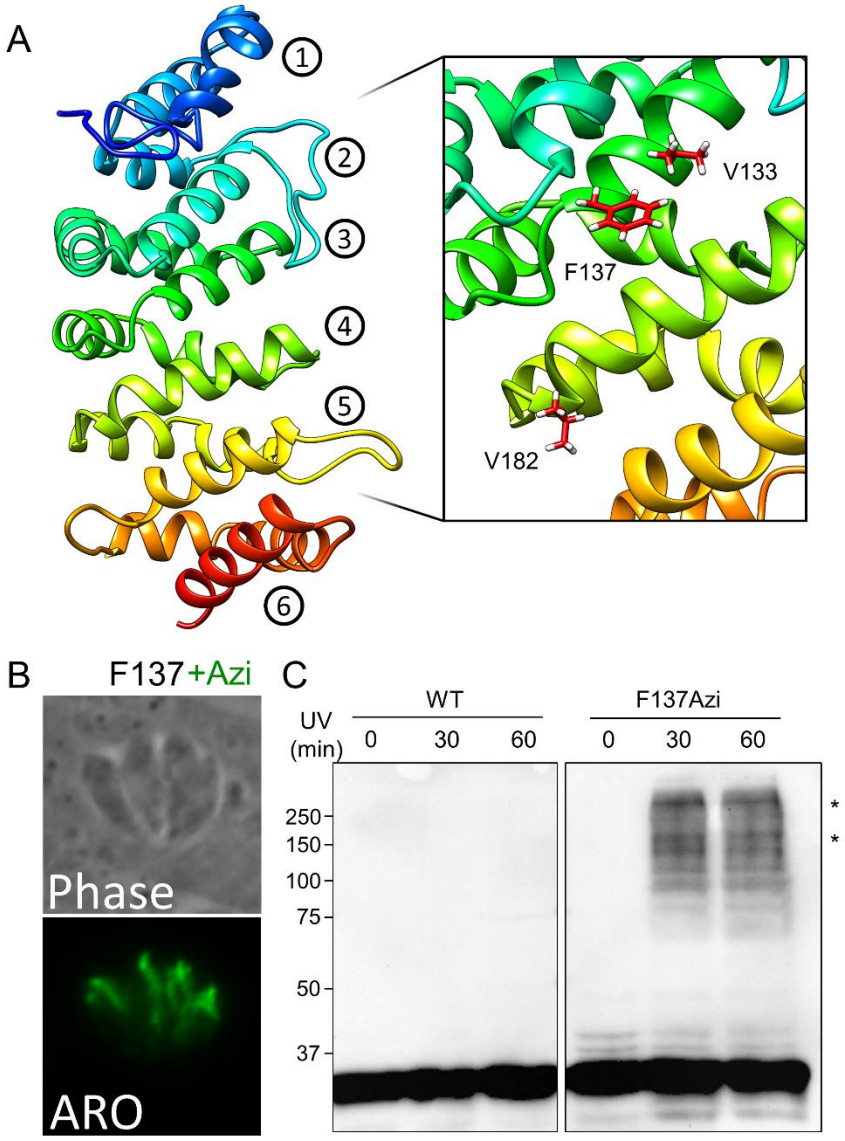

Figure 4-3. TgGT1_279420 localizes to the rhoptries.

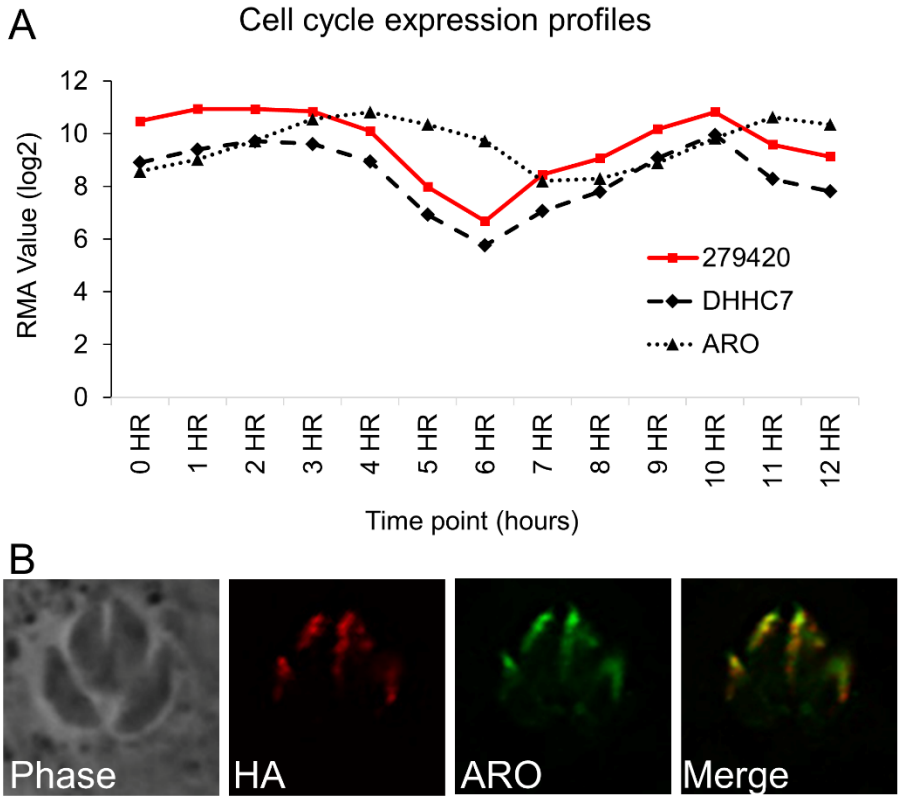

Figure 4-4. A robust Azi-crosslinked product is seen with residue L267 of ARO.

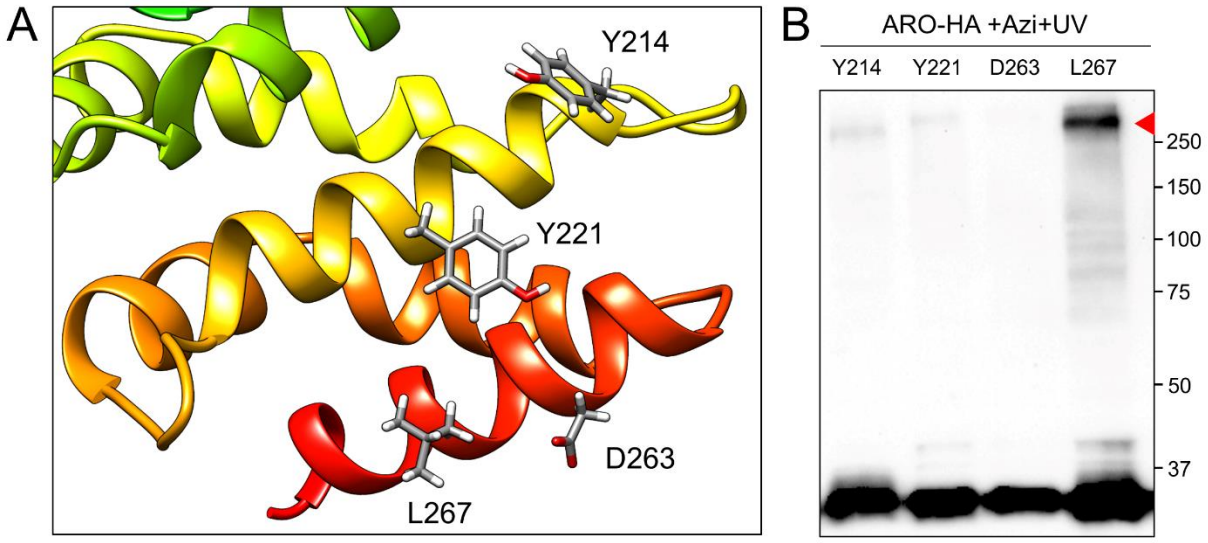

Table 4-5. Primers used in chapter 4.

P1	TgGT1_270865_LICfwd	TACTTCCAATCCAATTTAGCGCATTGAATCCCATCGTG
P2	TgGT1_270865_LICrev	TCCTCCACTTCCAATTTTAGCAGGGTCAATGGGGCGGC
P3	TgGT1_294630_LICfwd	TACTTCCAATCCAATTTAGCTGATATGCGTGCAGGTG
P4	TgGT1_294630_LICrev	TCCTCCACTTCCAATTTTAGCGGCTTCCCGTTCGTCGGTT
P5	TgGT1_279420_LICfwd	TACTTCCAATCCAATTTAGCAAACACCATCAGAATCACTGC
P6	TgGT1_279420_LICrev	TCCTCCACTTCCAATTTTAGCATAGCCGATTTTCCCGTTTTCCG
P7	TgGT1_270865_gRNAfwd	AAGTTGGCGTCAAGTTTAGGCGGGCG
P8	TgGT1_270865_gRNArev	AAAACGCCCGCCTAAACTTGACGCCA
P9	TgGT1_294630_gRNAfwd	AAGTTGAGGTACCTGAGGAGGCAGAG
P10	TgGT1_294630_gRNArev	AAAACTCTGCCTCCTCAGGTACCTCA
P11	BglII-AROcDNA fwd	GATCagatctATGGGGAACCAATGCTGC
P12	AROcDNA-NotI rev	GATCgcggccgcCTCCGACAGCCGGACCAAG
P13	NheI-AROpro fwd	gctagccagtgcacacgcttagcttcg
P14	AROpro-BglII rev	agatctcttctctgtgtgtttgatgcgttg
P15	BsiWI-DHFR fwd	CGTACGcagcacgaaaccttgcattc
P16	DHFR-NheI rev	gctagctcctgcaagtgcatagaagg
P17	ARO Y214stop mut fwd	GACGAATGTCtagACGCAGTTGG
P18	ARO Y214stop mut rev	GCCTCCGGGTTTATGTCA
P19	ARO Y221stop mut fwd	GGAGGCGATCtagCACTTGGAGG
P20	ARO Y221stop mut rev	AACTGCGTGTAGACATTCGTC
P21	ARO D263stop mut fwd	AGACGTCGCAtagGCCGCGAACC
P22	ARO D263stop mut rev	TGGTCTTTGCAGTCTTGCAG
P23	ARO L267stop mut fwd	CGCCGCGAACtagCTCTTGGTCC
P24	ARO L267stop mut rev	TCTGCGACGTCTTGGTCT
P25	ARO T7lic fwd	tacttccaatccaatgcaGGGAACCAATGCTGCGCAG
P26	ARO T7lic rev	TTATCCACTTCCAATGTTATTACTCCGACAGCCGGACCAAG
P27	279420 T7lic fwd	tacttccaatccaatgcaCAGCTGGGTCCATGGGAAAC
P28	279420 T7lic rev	TTATCCACTTCCAATGTTATTAATAGCCGATTTTCCCGTTTTCCG

CHAPTER 5:

Conclusion and Future Directions

Toxoplasma gondii is considered to be one of the most successful protozoan parasites due to its high prevalence and worldwide distribution (Blader et al., 2015). In addition to posing potentially fatal complications in immunocompromised individuals and developing fetuses, this organism also serves as a model organism for studying related parasites belonging to the phylum Apicomplexa due to its ease of culture and genetic tractability. The development of an array of reverse genetic tools in *T. gondii* has led to a robust platform for rapid identification and functional analyses of interesting genes. However, less tools are available for studying the protein associations driving the processes that are important for growth and infection. To expand the repertoire for examining macromolecular protein complexes, we have implemented a photoactivatable UAA crosslinking system for capturing interactions in the native cellular environment.

The apicomplexan IMC is an essential organelle that governs replication, motility, and intracellular invasion (Harding & Meissner, 2014). The composition of this intricate structure has only recently been understood with the application of high-throughput protein identification techniques such as proximity-dependent biotin labeling, yet the exact organization of these proteins needed to construct an intact IMC remains unknown (Chen et al., 2015, 2017). The evidence shown in this dissertation that ILP1 directly binds to IMC1, IMC3, IMC6, and IMC27 is the first demonstration of the precise protein-protein interactions that organize the cytoskeletal component of this organelle. We selected ILP1 due to the distinct EF-hand and coiled-coil regions in its sequence. While we were confident that the coiled-coil domain would be involved in protein binding, we were intrigued to discover that the degenerate EF-hand domain also interacts robustly with the alveolin IMC1, suggesting a multifactorial role of ILP1 in IMC assembly. Both coiled-

coil and degenerate EF-hand domains are relatively unexplored in *T. gondii* biology and promise to be interesting regions to target using Azi crosslinking.

There are a number of other interesting candidates to investigate using this technology. To complement our data showing that ILP1 binds to the IMC3 C-terminus and IMC6 N-terminus, site-specific UAA crosslinking using these regions as bait would enable us to identify the specific location within these domains that bind to the ILP1 coiled-coils, therefore revealing the binding interfaces on both sides of the interaction. IMC4 and IMC10 are the remaining alveolins that localize to the IMC body, and we would also like to determine how they interact with the other components of the intermediate filaments (Dubey et al., 2017). The coiled-coil region of IMC1 situated inside the alveolin repeat domain is unique among the alveolins and represents an ideal location to target for crosslinking. We anticipate that truncation mutants will serve as good pilot studies to define minimal regions that can be used for Azi mutagenesis.

Another interesting family of IMC proteins are the GAPMs. These multiple transmembrane domain proteins in the IMC membrane have been implicated in maintaining the integrity of the subpellicular microtubules and therefore likely have a role in binding to the accompanying IMC cytoskeleton (Harding et al., 2019). As the majority of the protein sequence is embedded in the membrane, it should be relatively easy to generate multiple Azi mutants at residues exposed towards the cytoplasm. Similarly, it would be straightforward to attempt crosslinking within the IMC lumen to make the first attempt at understanding an organellar subcompartment that remains enigmatic.

Our application towards the rhoptry tethering complex demonstrates that this technology is not limited to the IMC. Although more work needs to be done, the robust upshift seen with the ARO L267 is promising and may finally lead to a mechanism for this important phenomenon. The

conoid is another structure worth investigation. In addition to the degenerate EF-hand CaM3, a recent screen revealed multiple conoid-specific proteins with coiled-coil domains (Long et al., 2017a). Other than its core microtubule structure, the specific roles of accessory proteins and how they are organized to function in relation to micronemal and rhoptry release signaling has yet to be determined.

In conclusion, we have applied a photoactivated unnatural amino acid crosslinking system to capture robust and specific protein interactions in *Toxoplasma gondii*. These covalently bound partners can be identified using a candidate approach or *de novo* using mass spectrometric analysis. This technology brings a new approach to the molecular toolkit that will benefit our understanding of *T. gondii* and apicomplexan cell biology. As the first application of photocrosslinking in a protozoan system, this may also be readily adapted for the study of protein-protein interactions in other eukaryotic pathogenic organisms.

REFERENCES

Agop-Nersesian, C., Egarter, S., Langsley, G., Foth, B. J., Ferguson, D. J. P., & Meissner, M. (2010). Biogenesis of the Inner Membrane Complex Is Dependent on Vesicular Transport by the Alveolate Specific GTPase Rab11B. *PLOS Pathogens*, *6*(7), e1001029. https://doi.org/10.1371/journal.ppat.1001029

Ajioka, J. W., Boothroyd, J. C., Brunk, B. P., Hehl, A., Hillier, L., Manger, I. D., Marra, M., Overton, G. C., Roos, D. S., Wan, K.-L., et al. (1998). Gene Discovery by EST Sequencing in Toxoplasma gondii Reveals Sequences Restricted to the Apicomplexa. *Genome Research*, *8*(1), 18–28. https://doi.org/10.1101/gr.8.1.18

Aloush, N., Schvartz, T., König, A. I., Cohen, S., Brozgol, E., Tam, B., Nachmias, D., Ben-David, O., Garini, Y., Elia, N., et al. (2018). Live Cell Imaging of Bioorthogonally Labelled Proteins Generated With a Single Pyrrolysine tRNA Gene. *Scientific Reports*, *8*. https://doi.org/10.1038/s41598-018-32824-1

Anderson-White, B. R., Beck, J. R., Chen, C.-T., Meissner, M., Bradley, P. J., & Gubbels, M.-J. (2012). Cytoskeleton assembly in Toxoplasma gondii cell division. *International Review of Cell and Molecular Biology*, *298*, 1–31. https://doi.org/10.1016/B978-0-12-394309-5.00001-8

Anderson-White, B. R., Ivey, F. D., Cheng, K., Szatanek, T., Lorestani, A., Beckers, C. J., Ferguson, D. J. P., Sahoo, N., & Gubbels, M.-J. (2011). A family of intermediate filament-like proteins is sequentially assembled into the cytoskeleton of Toxoplasma gondii. *Cellular Microbiology*, *13*(1), 18–31. https://doi.org/10.1111/j.1462-5822.2010.01514.x

Attias, M., Miranda, K., & De Souza, W. (2019). Development and fate of the residual body of Toxoplasma gondii. *Experimental Parasitology*, *196*, 1–11. https://doi.org/10.1016/j.exppara.2018.11.004

Bähler, M., & Rhoads, A. (2002). Calmodulin signaling via the IQ motif. *FEBS Letters*, *513*(1), 107–113. https://doi.org/10.1016/S0014-5793(01)03239-2

Barragan, A., Brossier, F., & Sibley, L. D. (2005). Transepithelial migration of Toxoplasma gondii involves an interaction of intercellular adhesion molecule 1 (ICAM-1) with the parasite adhesin MIC2. *Cellular Microbiology*, *7*(4), 561–568. https://doi.org/10.1111/j.1462-5822.2005.00486.x

Barragan, A., & Sibley, L. D. (2002). Transepithelial Migration of Toxoplasma gondii Is Linked to Parasite Motility and Virulence. *Journal of Experimental Medicine*, *195*(12), 1625–1633. https://doi.org/10.1084/jem.20020258

Bastin, P., Bagherzadeh, Z., Matthews, K. R., & Gull, K. (1996). A novel epitope tag system to study protein targeting and organelle biogenesis in Trypanosoma brucei. *Molecular and Biochemical Parasitology*, *77*(2), 235–239.

Baum, J., Richard, D., Healer, J., Rug, M., Krnajski, Z., Gilberger, T.-W., Green, J. L., Holder, A. A., & Cowman, A. F. (2006). A conserved molecular motor drives cell invasion and

gliding motility across malaria life cycle stages and other apicomplexan parasites. *The Journal of Biological Chemistry*, *281*(8), 5197–5208. https://doi.org/10.1074/jbc.M509807200

Beck, J. R., Chen, A. L., Kim, E. W., & Bradley, P. J. (2014). RON5 Is Critical for Organization and Function of the Toxoplasma Moving Junction Complex. *PLoS Pathog*, *10*(3), e1004025. https://doi.org/10.1371/journal.ppat.1004025

Beck, J. R., Fung, C., Straub, K. W., Coppens, I., Vashisht, A. A., Wohlschlegel, J. A., & Bradley, P. J. (2013). A Toxoplasma Palmitoyl Acyl Transferase and the Palmitoylated Armadillo Repeat Protein TgARO Govern Apical Rhoptry Tethering and Reveal a Critical Role for the Rhoptries in Host Cell Invasion but Not Egress. *PLoS Pathog*, *9*(2), e1003162. https://doi.org/10.1371/journal.ppat.1003162

Beck, J. R., Rodriguez-Fernandez, I. A., Leon, J. C. de, Huynh, M.-H., Carruthers, V. B., Morrissette, N. S., & Bradley, P. J. (2010). A Novel Family of Toxoplasma IMC Proteins Displays a Hierarchical Organization and Functions in Coordinating Parasite Division. *PLOS Pathogens*, *6*(9), e1001094. https://doi.org/10.1371/journal.ppat.1001094

Bedouelle, H. (1990). Recognition of tRNA(Tyr) by tyrosyl-tRNA synthetase. *Biochimie*, *72*(8), 589–598.

Behnke, M. S., Fentress, S. J., Mashayekhi, M., Li, L. X., Taylor, G. A., & Sibley, L. D. (2012). The Polymorphic Pseudokinase ROP5 Controls Virulence in Toxoplasma gondii by Regulating the Active Kinase ROP18. *PLOS Pathogens*, *8*(11), e1002992. https://doi.org/10.1371/journal.ppat.1002992

Behnke, M. S., Khan, A., Wootton, J. C., Dubey, J. P., Tang, K., & Sibley, L. D. (2011). Virulence differences in Toxoplasma mediated by amplification of a family of polymorphic pseudokinases. *Proceedings of the National Academy of Sciences of the United States of America*, *108*(23), 9631–9636. https://doi.org/10.1073/pnas.1015338108

Behnke, M. S., Wootton, J. C., Lehmann, M. M., Radke, J. B., Lucas, O., Nawas, J., Sibley, L. D., & White, M. W. (2010). Coordinated progression through two subtranscriptomes underlies the tachyzoite cycle of Toxoplasma gondii. *PloS One*, *5*(8), e12354. https://doi.org/10.1371/journal.pone.0012354

Benchimol, M. (2004). Trichomonads under Microscopy. *Microscopy and Microanalysis: The Official Journal of Microscopy Society of America, Microbeam Analysis Society, Microscopical Society of Canada*, *10*(5), 528–550. https://doi.org/10.1017/S1431927604040905

Bender, K. W., Zielinski, R. E., & Huber, S. C. (2018). Revisiting paradigms of Ca2+ signaling protein kinase regulation in plants. *Biochemical Journal*, *475*(1), 207–223. https://doi.org/10.1042/BCJ20170022

Beraki, T., Hu, X., Broncel, M., Young, J. C., O'Shaughnessy, W. J., Borek, D., Treeck, M., & Reese, M. L. (2019). Divergent kinase regulates membrane ultrastructure of the

Toxoplasma parasitophorous vacuole. *Proceedings of the National Academy of Sciences*, *116*(13), 6361–6370. https://doi.org/10.1073/pnas.1816161116

Berry, M. J., Banu, L., Harney, J. W., & Larsen, P. R. (1993). Functional characterization of the eukaryotic SECIS elements which direct selenocysteine insertion at UGA codons. *The EMBO Journal*, *12*(8), 3315–3322.

Besteiro, S., Dubremetz, J.-F., & Lebrun, M. (2011). The moving junction of apicomplexan parasites: a key structure for invasion. *Cellular Microbiology*, *13*(6), 797–805. https://doi.org/10.1111/j.1462-5822.2011.01597.x

Black, M. W., & Boothroyd, J. C. (2000). Lytic Cycle of Toxoplasma gondii. *Microbiology and Molecular Biology Reviews*, *64*(3), 607–623.

Blader, I., Coleman, B., Chen, C.-T., & Gubbels, M.-J. (2015). The lytic cycle of Toxoplasma gondii: 15 years later. *Annual Review of Microbiology*, *69*, 463–485. https://doi.org/10.1146/annurev-micro-091014-104100

Blader, I. J., & Koshy, A. A. (2014). Toxoplasma gondii Development of Its Replicative Niche: in Its Host Cell and Beyond. *Eukaryotic Cell*, *13*(8), 965–976. https://doi.org/10.1128/EC.00081-14

Boothroyd, J. C., & Dubremetz, J.-F. (2008). Kiss and spit: the dual roles of Toxoplasma rhoptries. *Nature Reviews Microbiology*, *6*(1), 79–88. https://doi.org/10.1038/nrmicro1800

Boothroyd, J. C., & Grigg, M. E. (2002). Population biology of Toxoplasma gondii and its relevance to human infection: do different strains cause different disease? *Current Opinion in Microbiology*, *5*(4), 438–442.

Boucher, L. E., & Bosch, J. (2015). The apicomplexan glideosome and adhesins -- structures and function. *Journal of Structural Biology*, *190*(2), 93–114. https://doi.org/10.1016/j.jsb.2015.02.008

Bradley, P. J., Ward, C., Cheng, S. J., Alexander, D. L., Coller, S., Coombs, G. H., Dunn, J. D., Ferguson, D. J., Sanderson, S. J., Wastling, J. M., et al. (2005). Proteomic Analysis of Rhoptry Organelles Reveals Many Novel Constituents for Host-Parasite Interactions in Toxoplasma gondii. *Journal of Biological Chemistry*, *280*(40), 34245–34258. https://doi.org/10.1074/jbc.M504158200

Breinich, M. S., Ferguson, D. J. P., Foth, B. J., van Dooren, G. G., Lebrun, M., Quon, D. V., Striepen, B., Bradley, P. J., Frischknecht, F., Carruthers, V. B., et al. (2009). An alveolate specific dynamin is required for the biogenesis of specialised secretory organelles in Toxoplasma gondii. *Current Biology : CB*, *19*(4), 277–286. https://doi.org/10.1016/j.cub.2009.01.039

Brossier, F., Jewett, T. J., Sibley, L. D., & Urban, S. (2005). A spatially localized rhomboid protease cleaves cell surface adhesins essential for invasion by Toxoplasma. *Proceedings*

of the National Academy of Sciences of the United States of America, *102*(11), 4146–4151. https://doi.org/10.1073/pnas.0407918102

Brown, J. R., Schwartz, C. L., Heumann, J. M., Dawson, S. C., & Hoenger, A. (2016). A detailed look at the cytoskeletal architecture of the Giardia lamblia ventral disc. *Journal of Structural Biology*, *194*(1), 38–48. https://doi.org/10.1016/j.jsb.2016.01.011

Bullen, H. E., Jia, Y., Yamaryo-Botté, Y., Bisio, H., Zhang, O., Jemelin, N. K., Marq, J.-B., Carruthers, V., Botté, C. Y., & Soldati-Favre, D. (2016). Phosphatidic Acid-Mediated Signaling Regulates Microneme Secretion in Toxoplasma. *Cell Host & Microbe*, *19*(3), 349–360. https://doi.org/10.1016/j.chom.2016.02.006

Bullen, H. E., Tonkin, C. J., O'Donnell, R. A., Tham, W.-H., Papenfuss, A. T., Gould, S., Cowman, A. F., Crabb, B. S., & Gilson, P. R. (2009). A novel family of Apicomplexan glideosome-associated proteins with an inner membrane-anchoring role. *The Journal of Biological Chemistry*, *284*(37), 25353–25363. https://doi.org/10.1074/jbc.M109.036772

Burg, J. L., Perelman, D., Kasper, L. H., Ware, P. L., & Boothroyd, J. C. (1988). Molecular analysis of the gene encoding the major surface antigen of Toxoplasma gondii. *Journal of Immunology (Baltimore, Md.: 1950)*, *141*(10), 3584–3591.

Cabrera, A., Herrmann, S., Warszta, D., Santos, J. M., John Peter, A. T., Kono, M., Debrouver, S., Jacobs, T., Spielmann, T., Ungermann, C., et al. (2012). Dissection of Minimal Sequence Requirements for Rhoptry Membrane Targeting in the Malaria Parasite. *Traffic*, *13*(10), 1335–1350. https://doi.org/10.1111/j.1600-0854.2012.01394.x

Caldas, L. A., de Souza, W., & Attias, M. (2010). Microscopic analysis of calcium ionophore activated egress of Toxoplasma gondii from the host cell. *Veterinary Parasitology*, *167*(1), 8–18. https://doi.org/10.1016/j.vetpar.2009.09.051

Carey, K. L., Westwood, N. J., Mitchison, T. J., & Ward, G. E. (2004). A small-molecule approach to studying invasive mechanisms of Toxoplasma gondii. *Proceedings of the National Academy of Sciences*, *101*(19), 7433–7438. https://doi.org/10.1073/pnas.0307769101

Carruthers, V. B., & Sibley, L. D. (1999). Mobilization of intracellular calcium stimulates microneme discharge in Toxoplasma gondii. *Molecular Microbiology*, *31*(2), 421–428. https://doi.org/10.1046/j.1365-2958.1999.01174.x

Carruthers, V. B., & Suzuki, Y. (2007). Effects of Toxoplasma gondii Infection on the Brain. *Schizophrenia Bulletin*, *33*(3), 745–751. https://doi.org/10.1093/schbul/sbm008

Carruthers, V. B., & Tomley, F. M. (2008). Receptor-ligand interaction and invasion: Microneme proteins in apicomplexans. *Sub-Cellular Biochemistry*, *47*, 33–45.

Cesbron-Delauw, M. F. (1994). Dense-granule organelles of Toxoplasma gondii: their role in the host-parasite relationship. *Parasitology Today (Personal Ed.)*, *10*(8), 293–296.

Chang, L., Dykes, E. J., Li, J., Moreno, S. N. J., & Triana, M. A. H. (2019). Characterization of Two EF-hand Domain-containing Proteins from Toxoplasma gondii. *Journal of Eukaryotic Microbiology*, *66*(2), 343–353. https://doi.org/10.1111/jeu.12675

Charron, A. J., & Sibley, L. D. (2004). Molecular Partitioning during Host Cell Penetration by Toxoplasma gondii. *Traffic*, *5*(11), 855–867. https://doi.org/10.1111/j.1600-0854.2004.00228.x

Chazin, W. J. (2011). Relating Form and Function of EF-hand Calcium Binding Proteins. *Accounts of Chemical Research*, *44*(3), 171–179. https://doi.org/10.1021/ar100110d

Chen, A. L., Kim, E. W., Toh, J. Y., Vashisht, A. A., Rashoff, A. Q., Van, C., Huang, A. S., Moon, A. S., Bell, H. N., Bentolila, L. A., et al. (2015). Novel Components of the Toxoplasma Inner Membrane Complex Revealed by BioID. *MBio*, *6*(1), e02357-14. https://doi.org/10.1128/mBio.02357-14

Chen, A. L., Moon, A. S., Bell, H. N., Huang, A. S., Vashisht, A. A., Toh, J. Y., Lin, A. H., Nadipuram, S. M., Kim, E. W., Choi, C. P., et al. (2017). Novel insights into the composition and function of the Toxoplasma IMC sutures. *Cellular Microbiology*, *19*(4). https://doi.org/10.1111/cmi.12678

Chen, S., Schultz, P. G., & Brock, A. (2007). An Improved System for the Generation and Analysis of Mutant Proteins Containing Unnatural Amino Acids in Saccharomyces cerevisiae. *Journal of Molecular Biology*, *371*(1), 112–122. https://doi.org/10.1016/j.jmb.2007.05.017

Chin, J. W., Cropp, T. A., Anderson, J. C., Mukherji, M., Zhang, Z., & Schultz, P. G. (2003). An Expanded Eukaryotic Genetic Code. *Science*, *301*(5635), 964–967. https://doi.org/10.1126/science.1084772

Coers, J., & Haldar, A. K. (2015). Ubiquitination of pathogen-containing vacuoles promotes host defense to Chlamydia trachomatis and Toxoplasma gondii. *Communicative & Integrative Biology*, *8*(6). https://doi.org/10.1080/19420889.2015.1115163

Coin, I., Katritch, V., Sun, T., Xiang, Z., Siu, F. Y., Beyermann, M., Stevens, R. C., & Wang, L. (2013). Genetically encoded chemical probes in cells reveal the binding path of urocortin-I to CRF class B GPCR. *Cell*, *155*(6), 1258–1269. https://doi.org/10.1016/j.cell.2013.11.008

Coin, I., Perrin, M. H., Vale, W. W., & Wang, L. (2011). Photocrosslinkers incorporated into G-protein coupled receptors in mammalian cells: a ligand comparison. *Angewandte Chemie (International Ed. in English)*, *50*(35), 8077–8081. https://doi.org/10.1002/anie.201102646

Coleman, B. I., Saha, S., Sato, S., Engelberg, K., Ferguson, D. J. P., Coppens, I., Lodoen, M. B., & Gubbels, M.-J. (2018). A Member of the Ferlin Calcium Sensor Family Is Essential for Toxoplasma gondii Rhoptry Secretion. *MBio*, *9*(5), e01510-18. https://doi.org/10.1128/mBio.01510-18

Cox, J., & Mann, M. (2008). MaxQuant enables high peptide identification rates, individualized p.p.b.-range mass accuracies and proteome-wide protein quantification. *Nature Biotechnology*, *26*(12), 1367–1372. https://doi.org/10.1038/nbt.1511

Daher, W., Plattner, F., Carlier, M.-F., & Soldati-Favre, D. (2010). Concerted Action of Two Formins in Gliding Motility and Host Cell Invasion by Toxoplasma gondii. *PLoS Pathogens*, *6*(10). https://doi.org/10.1371/journal.ppat.1001132

de Souza Giassi, K., Costa, A. N., Apanavicius, A., Teixeira, F. B., Fernandes, C. J. C., Helito, A. S., & Kairalla, R. A. (2014). Tomographic findings of acute pulmonary toxoplasmosis in immunocompetent patients. *BMC Pulmonary Medicine*, *14*. https://doi.org/10.1186/1471-2466-14-185

Denessiouk, K., Permyakov, S., Denesyuk, A., Permyakov, E., & Johnson, M. S. (2014). Two Structural Motifs within Canonical EF-Hand Calcium-Binding Domains Identify Five Different Classes of Calcium Buffers and Sensors. *PLoS ONE*, *9*(10). https://doi.org/10.1371/journal.pone.0109287

Donald, R. G., Carter, D., Ullman, B., & Roos, D. S. (1996). Insertional Tagging, Cloning, and Expression of the Toxoplasma gondii Hypoxanthine-Xanthine-Guanine Phosphoribosyltransferase Gene USE AS A SELECTABLE MARKER FOR STABLE TRANSFORMATION. *Journal of Biological Chemistry*, *271*(24), 14010–14019. https://doi.org/10.1074/jbc.271.24.14010

Donald, R. G., & Roos, D. S. (1993). Stable molecular transformation of Toxoplasma gondii: a selectable dihydrofolate reductase-thymidylate synthase marker based on drug-resistance mutations in malaria. *Proceedings of the National Academy of Sciences of the United States of America*, *90*(24), 11703–11707.

Donald, R. G., & Roos, D. S. (1995). Insertional mutagenesis and marker rescue in a protozoan parasite: cloning of the uracil phosphoribosyltransferase locus from Toxoplasma gondii. *Proceedings of the National Academy of Sciences of the United States of America*, *92*(12), 5749–5753.

Drozdetskiy, A., Cole, C., Procter, J., & Barton, G. J. (2015). JPred4: a protein secondary structure prediction server. *Nucleic Acids Research*, *43*(W1), W389-394. https://doi.org/10.1093/nar/gkv332

Dubey, J. P. (2003). Review of Neospora caninum and neosporosis in animals. *The Korean Journal of Parasitology*, *41*(1), 1–16.

Dubey, J. P. (2009). History of the discovery of the life cycle of Toxoplasma gondii. *International Journal for Parasitology*, *39*(8), 877–882.

Dubey, J. P., Lindsay, D. S., & Speer, C. A. (1998). Structures of Toxoplasma gondii Tachyzoites, Bradyzoites, and Sporozoites and Biology and Development of Tissue Cysts. *Clinical Microbiology Reviews*, *11*(2), 267–299.

Dubey, R., Harrison, B., Dangoudoubiyam, S., Bandini, G., Cheng, K., Kosber, A., Agop-Nersesian, C., Howe, D. K., Samuelson, J., Ferguson, D. J. P., et al. (2017). Differential Roles for Inner Membrane Complex Proteins across Toxoplasma gondii and Sarcocystis neurona Development. *MSphere*, *2*(5). https://doi.org/10.1128/mSphere.00409-17

Dubois, D. J., & Soldati-Favre, D. (2019). Biogenesis and secretion of micronemes in Toxoplasma gondii. *Cellular Microbiology*, *21*(5), e13018. https://doi.org/10.1111/cmi.13018

Dubremetz, J. F., Achbarou, A., Bermudes, D., & Joiner, K. A. (1993). Kinetics and pattern of organelle exocytosis during Toxoplasma gondii/host-cell interaction. *Parasitology Research*, *79*(5), 402–408.

Dunn, J. D., Ravindran, S., Kim, S.-K., & Boothroyd, J. C. (2008). The Toxoplasma gondii dense granule protein GRA7 is phosphorylated upon invasion and forms an unexpected association with the rhoptry proteins ROP2 and ROP4. *Infection and Immunity*, *76*(12), 5853–5861. https://doi.org/10.1128/IAI.01667-07

El Hajj, H., Demey, E., Poncet, J., Lebrun, M., Wu, B., Galéotti, N., Fourmaux, M. N., Mercereau-Puijalon, O., Vial, H., Labesse, G., et al. (2006). The ROP2 family of Toxoplasma gondii rhoptry proteins: proteomic and genomic characterization and molecular modeling. *Proteomics*, *6*(21), 5773–5784. https://doi.org/10.1002/pmic.200600187

Evan, G. I., Lewis, G. K., Ramsay, G., & Bishop, J. M. (1985). Isolation of monoclonal antibodies specific for human c-myc proto-oncogene product. *Molecular and Cellular Biology*, *5*(12), 3610–3616.

Fentress, S. J., Behnke, M. S., Dunay, I. R., Mashayekhi, M., Rommereim, L. M., Fox, B. A., Bzik, D. J., Taylor, G. A., Turk, B. E., Lichti, C. F., et al. (2010). Phosphorylation of Immunity-Related GTPases by a Toxoplasma gondii-Secreted Kinase Promotes Macrophage Survival and Virulence. *Cell Host & Microbe*, *8*(6), 484–495. https://doi.org/10.1016/j.chom.2010.11.005

Ferguson, S. M., & De Camilli, P. (2012). Dynamin, a membrane-remodelling GTPase. *Nature Reviews Molecular Cell Biology*, *13*(2), 75–88. https://doi.org/10.1038/nrm3266

Fleckenstein, M. C., Reese, M. L., Könen-Waisman, S., Boothroyd, J. C., Howard, J. C., & Steinfeldt, T. (2012). A Toxoplasma gondii Pseudokinase Inhibits Host IRG Resistance Proteins. *PLOS Biology*, *10*(7), e1001358. https://doi.org/10.1371/journal.pbio.1001358

Fleet, G. W. J., Porter, R. R., & Knowles, J. R. (1969). Affinity Labelling of Antibodies with Aryl Nitrene as Reactive Group. *Nature*, *224*(5218), 511. https://doi.org/10.1038/224511a0

Flegr, J., Prandota, J., Sovičková, M., & Israili, Z. H. (2014). Toxoplasmosis – A Global Threat. Correlation of Latent Toxoplasmosis with Specific Disease Burden in a Set of 88 Countries. *PLoS ONE*, *9*(3). https://doi.org/10.1371/journal.pone.0090203

Foth, B. J., Goedecke, M. C., & Soldati, D. (2006). New insights into myosin evolution and classification. *Proceedings of the National Academy of Sciences of the United States of America*, *103*(10), 3681–3686. https://doi.org/10.1073/pnas.0506307103

Francia, M. E., Jordan, C. N., Patel, J. D., Sheiner, L., Demerly, J. L., Fellows, J. D., de Leon, J. C., Morrissette, N. S., Dubremetz, J.-F., & Striepen, B. (2012). Cell Division in Apicomplexan Parasites Is Organized by a Homolog of the Striated Rootlet Fiber of Algal Flagella. *PLoS Biology*, *10*(12). https://doi.org/10.1371/journal.pbio.1001444

Francia, M. E., & Striepen, B. (2014). Cell division in apicomplexan parasites. *Nature Reviews Microbiology*, *12*(2), 125–136. https://doi.org/10.1038/nrmicro3184

Frénal, K., Dubremetz, J.-F., Lebrun, M., & Soldati-Favre, D. (2017). Gliding motility powers invasion and egress in Apicomplexa. *Nature Reviews Microbiology*, *15*(11), 645–660. https://doi.org/10.1038/nrmicro.2017.86

Frénal, K., Kemp, L. E., & Soldati-Favre, D. (2014a). Emerging roles for protein S-palmitoylation in Toxoplasma biology. *International Journal for Parasitology*, *44*(2), 121–131. https://doi.org/10.1016/j.ijpara.2013.09.004

Frénal, K., Marq, J.-B., Jacot, D., Polonais, V., & Soldati-Favre, D. (2014b). Plasticity between MyoC- and MyoA-Glideosomes: An Example of Functional Compensation in Toxoplasma gondii Invasion. *PLoS Pathogens*, *10*(11). https://doi.org/10.1371/journal.ppat.1004504

Frénal, K., Polonais, V., Marq, J.-B., Stratmann, R., Limenitakis, J., & Soldati-Favre, D. (2010). Functional Dissection of the Apicomplexan Glideosome Molecular Architecture. *Cell Host & Microbe*, *8*(4), 343–357. https://doi.org/10.1016/j.chom.2010.09.002

Frénal, K., Tay, C. L., Mueller, C., Bushell, E. S., Jia, Y., Graindorge, A., Billker, O., Rayner, J. C., & Soldati-Favre, D. (2013). Global Analysis of Apicomplexan Protein S-Acyl Transferases Reveals an Enzyme Essential for Invasion. *Traffic (Copenhagen, Denmark)*, *14*(8), 895–911. https://doi.org/10.1111/tra.12081

Furumoto, T., Ogawa, N., Hata, S., & Izui, K. (1996). Plant calcium-dependent protein kinase-related kinases (CRKs) do not require calcium for their activities. *FEBS Letters*, *396*(2–3), 147–151. https://doi.org/10.1016/0014-5793(96)01090-3

Gajria, B., Bahl, A., Brestelli, J., Dommer, J., Fischer, S., Gao, X., Heiges, M., Iodice, J., Kissinger, J. C., Mackey, A. J., et al. (2008). ToxoDB: an integrated Toxoplasma gondii database resource. *Nucleic Acids Research*, *36*(suppl_1), D553–D556. https://doi.org/10.1093/nar/gkm981

Garces, R. G., Gillon, W., & Pai, E. F. (2007). Atomic model of human Rcd-1 reveals an armadillo-like-repeat protein with in vitro nucleic acid binding properties. *Protein Science: A Publication of the Protein Society*, *16*(2), 176–188. https://doi.org/10.1110/ps.062600507

Gaskins, E., Gilk, S., DeVore, N., Mann, T., Ward, G., & Beckers, C. (2004). Identification of the membrane receptor of a class XIV myosin in Toxoplasma gondii. *The Journal of Cell Biology*, *165*(3), 383–393. https://doi.org/10.1083/jcb.200311137

Ghosh, A., Uthaiah, R., Howard, J., Herrmann, C., & Wolf, E. (2004). Crystal Structure of IIGP1: A Paradigm for Interferon-Inducible p47 Resistance GTPases. *Molecular Cell*, *15*(5), 727–739. https://doi.org/10.1016/j.molcel.2004.07.017

Gold, D. A., Kaplan, A. D., Lis, A., Bett, G. C. L., Rosowski, E. E., Cirelli, K. M., Bougdour, A., Sidik, S. M., Beck, J. R., Lourido, S., et al. (2015). The Toxoplasma Dense Granule Proteins GRA17 and GRA23 Mediate the Movement of Small Molecules between the Host and the Parasitophorous Vacuole. *Cell Host & Microbe*, *17*(5), 642–652. https://doi.org/10.1016/j.chom.2015.04.003

González Del Carmen, M., Mondragón, M., González, S., & Mondragón, R. (2009). Induction and regulation of conoid extrusion in Toxoplasma gondii. *Cellular Microbiology*, *11*(6), 967–982. https://doi.org/10.1111/j.1462-5822.2009.01304.x

Gould, S. B., Tham, W.-H., Cowman, A. F., McFadden, G. I., & Waller, R. F. (2008). Alveolins, a New Family of Cortical Proteins that Define the Protist Infrakingdom Alveolata. *Molecular Biology and Evolution*, *25*(6), 1219–1230. https://doi.org/10.1093/molbev/msn070

Graham, T. A., Clements, W. K., Kimelman, D., & Xu, W. (2002). The Crystal Structure of the β-Catenin/ICAT Complex Reveals the Inhibitory Mechanism of ICAT. *Molecular Cell*, *10*(3), 563–571. https://doi.org/10.1016/S1097-2765(02)00637-8

Graindorge, A., Frénal, K., Jacot, D., Salamun, J., Marq, J. B., & Soldati-Favre, D. (2016). The Conoid Associated Motor MyoH Is Indispensable for Toxoplasma gondii Entry and Exit from Host Cells. *PLOS Pathogens*, *12*(1), e1005388. https://doi.org/10.1371/journal.ppat.1005388

Grant, I. H., Gold, J. W., Rosenblum, M., Niedzwiecki, D., & Armstrong, D. (1990). Toxoplasma gondii serology in HIV-infected patients: the development of central nervous system toxoplasmosis in AIDS. *AIDS (London, England)*, *4*(6), 519–521.

Gubbels, M.-J., & Duraisingh, M. T. (2012). Evolution of apicomplexan secretory organelles. *International Journal for Parasitology*, *42*(12), 1071–1081. https://doi.org/10.1016/j.ijpara.2012.09.009

Gubbels, M.-J., Vaishnava, S., Boot, N., Dubremetz, J.-F., & Striepen, B. (2006). A MORN-repeat protein is a dynamic component of the Toxoplasma gondii cell division apparatus. *Journal of Cell Science*, *119*(11), 2236–2245. https://doi.org/10.1242/jcs.02949

Guérin, A., Corrales, R. M., Parker, M. L., Lamarque, M. H., Jacot, D., Hajj, H. E., Soldati-Favre, D., Boulanger, M. J., & Lebrun, M. (2017). Efficient invasion by Toxoplasma depends on the subversion of host protein networks. *Nature Microbiology*, *2*(10), 1358. https://doi.org/10.1038/s41564-017-0018-1

Håkansson, S., Charron, A. J., & Sibley, L. D. (2001). Toxoplasma evacuoles: a two-step process of secretion and fusion forms the parasitophorous vacuole. *The EMBO Journal*, *20*(12), 3132–3144. https://doi.org/10.1093/emboj/20.12.3132

Håkansson, S., Morisaki, H., Heuser, J., & Sibley, L. D. (1999). Time-Lapse Video Microscopy of Gliding Motility inToxoplasma gondii Reveals a Novel, Biphasic Mechanism of Cell Locomotion. *Molecular Biology of the Cell*, *10*(11), 3539–3547. https://doi.org/10.1091/mbc.10.11.3539

Harding, C. R., Egarter, S., Gow, M., Jiménez-Ruiz, E., Ferguson, D. J. P., & Meissner, M. (2016). Gliding Associated Proteins Play Essential Roles during the Formation of the Inner Membrane Complex of Toxoplasma gondii. *PLOS Pathogens*, *12*(2), e1005403. https://doi.org/10.1371/journal.ppat.1005403

Harding, C. R., Gow, M., Kang, J. H., Shortt, E., Manalis, S. R., Meissner, M., & Lourido, S. (2019). Alveolar proteins stabilize cortical microtubules in Toxoplasma gondii. *Nature Communications*, *10*(1), 401. https://doi.org/10.1038/s41467-019-08318-7

Harding, C. R., & Meissner, M. (2014). The inner membrane complex through development of Toxoplasma gondii and Plasmodium. *Cellular Microbiology*, *16*(5), 632–641. https://doi.org/10.1111/cmi.12285

Hartmann, J., Hu, K., He, C. Y., Pelletier, L., Roos, D. S., & Warren, G. (2006). Golgi and centrosome cycles in Toxoplasma gondii. *Molecular and Biochemical Parasitology*, *145*(1), 125–127. https://doi.org/10.1016/j.molbiopara.2005.09.015

Heaslip, A. T., Dzierszinski, F., Stein, B., & Hu, K. (2010a). TgMORN1 Is a Key Organizer for the Basal Complex of Toxoplasma gondii. *PLoS Pathogens*, *6*(2). https://doi.org/10.1371/journal.ppat.1000754

Heaslip, A. T., Leung, J. M., Carey, K. L., Catti, F., Warshaw, D. M., Westwood, N. J., Ballif, B. A., & Ward, G. E. (2010b). A Small-Molecule Inhibitor of T. gondii Motility Induces the Posttranslational Modification of Myosin Light Chain-1 and Inhibits Myosin Motor Activity. *PLOS Pathogens*, *6*(1), e1000720. https://doi.org/10.1371/journal.ppat.1000720

Heaslip, A. T., Nelson, S. R., & Warshaw, D. M. (2016). Dense granule trafficking in Toxoplasma gondii requires a unique class 27 myosin and actin filaments. *Molecular Biology of the Cell*, *27*(13), 2080–2089. https://doi.org/10.1091/mbc.E15-12-0824

Heintzelman, M. B., & Schwartzman, J. D. (1997). A novel class of unconventional myosins from Toxoplasma gondii11Edited by J. Karn. *Journal of Molecular Biology*, *271*(1), 139–146. https://doi.org/10.1006/jmbi.1997.1167

Heredero-Bermejo, I., Varberg, J. M., Charvat, R., Jacobs, K., Garbuz, T., Sullivan, W. J., & Arrizabalaga, G. (2019). TgDrpC, an atypical dynamin-related protein in Toxoplasma gondii, is associated with vesicular transport factors and parasite division. *Molecular Microbiology*, *111*(1), 46–64. https://doi.org/10.1111/mmi.14138

Hermanson, G. T. (2013). *Bioconjugate Techniques*. Academic Press.

Herm-Götz, A., Weiss, S., Stratmann, R., Fujita-Becker, S., Ruff, C., Meyhöfer, E., Soldati, T., Manstein, D. J., Geeves, M. A., & Soldati, D. (2002). Toxoplasma gondii myosin A and its light chain: a fast, single-headed, plus-end-directed motor. *The EMBO Journal*, *21*(9), 2149–2158. https://doi.org/10.1093/emboj/21.9.2149

Hill, D. E., Chirukandoth, S., & Dubey, J. P. (2005). Biology and epidemiology of Toxoplasma gondii in man and animals. *Animal Health Research Reviews*, *6*(1), 41–61. https://doi.org/10.1079/AHR2005100

Ho, C.-M., Beck, J. R., Lai, M., Cui, Y., Goldberg, D. E., Egea, P. F., & Zhou, Z. H. (2018). Malaria parasite translocon structure and mechanism of effector export. *Nature*, *561*(7721), 70–75. https://doi.org/10.1038/s41586-018-0469-4

Hoffmann, J.-E., Plass, T., Nikić, I., Aramburu, I. V., Koehler, C., Gillandt, H., Lemke, E. A., & Schultz, C. (2015). Highly Stable trans-Cyclooctene Amino Acids for Live-Cell Labeling. *Chemistry – A European Journal*, *21*(35), 12266–12270. https://doi.org/10.1002/chem.201501647

Holland, G. N. (2003). Ocular toxoplasmosis: a global reassessment: . Part I: epidemiology and course of disease. *American Journal of Ophthalmology*, *136*(6), 973–988. https://doi.org/10.1016/j.ajo.2003.09.040

Holland, G. N., Lewis, K. G., & O'Connor, G. R. (2002). Ocular Toxoplasmosis: A 50th Anniversary Tribute to the Contributions of Helenor Campbell Wilder Foerster. *Archives of Ophthalmology*, *120*(8), 1081–1084. https://doi.org/10.1001/archopht.120.8.1081

Howe, D. K., & Sibley, L. D. (1995). Toxoplasma gondii comprises three clonal lineages: correlation of parasite genotype with human disease. *The Journal of Infectious Diseases*, *172*(6), 1561–1566.

Hu, K. (2008). Organizational Changes of the Daughter Basal Complex during the Parasite Replication of Toxoplasma gondii. *PLoS Pathogens*, *4*(1). https://doi.org/10.1371/journal.ppat.0040010

Hu, K., Johnson, J., Florens, L., Fraunholz, M., Suravajjala, S., DiLullo, C., Yates, J., Roos, D. S., & Murray, J. M. (2006). Cytoskeletal Components of an Invasion Machine—The Apical Complex of Toxoplasma gondii. *PLOS Pathogens*, *2*(2), e13. https://doi.org/10.1371/journal.ppat.0020013

Hu, K., Mann, T., Striepen, B., Beckers, C. J. M., Roos, D. S., & Murray, J. M. (2002). Daughter Cell Assembly in the Protozoan Parasite Toxoplasma gondii. *Molecular Biology of the Cell*, *13*(2), 593–606. https://doi.org/10.1091/mbc.01-06-0309

Hui, R., El Bakkouri, M., & Sibley, L. D. (2015). Designing selective inhibitors for calcium-dependent protein kinases in apicomplexans. *Trends in Pharmacological Sciences*, *36*(7), 452–460. https://doi.org/10.1016/j.tips.2015.04.011

Huynh, M.-H., & Carruthers, V. B. (2009). Tagging of Endogenous Genes in a Toxoplasma gondii Strain Lacking Ku80. *Eukaryotic Cell*, *8*(4), 530–539. https://doi.org/10.1128/EC.00358-08

Ibba, M., & Söll, D. (1999). Quality Control Mechanisms During Translation. *Science*, *286*(5446), 1893–1897. https://doi.org/10.1126/science.286.5446.1893

Jacot, D., Daher, W., & Soldati-Favre, D. (2013). Toxoplasma gondii myosin F, an essential motor for centrosomes positioning and apicoplast inheritance. *The EMBO Journal*, *32*(12), 1702–1716. https://doi.org/10.1038/emboj.2013.113

Jacot, D., Tosetti, N., Pires, I., Stock, J., Graindorge, A., Hung, Y.-F., Han, H., Tewari, R., Kursula, I., & Soldati-Favre, D. (2016). An Apicomplexan Actin-Binding Protein Serves as a Connector and Lipid Sensor to Coordinate Motility and Invasion. *Cell Host & Microbe*, *20*(6), 731–743. https://doi.org/10.1016/j.chom.2016.10.020

Jacquet, A., Coulon, L., De Nève, J., Daminet, V., Haumont, M., Garcia, L., Bollen, A., Jurado, M., & Biemans, R. (2001). The surface antigen SAG3 mediates the attachment of Toxoplasma gondii to cell-surface proteoglycans. *Molecular and Biochemical Parasitology*, *116*(1), 35–44.

Jena, B. P. (2009). Porosome: the secretory portal in cells. *Biochemistry*, *48*(19), 4009–4018. https://doi.org/10.1021/bi9002698

Johnson, T. M., Rajfur, Z., Jacobson, K., & Beckers, C. J. (2007). Immobilization of the Type XIV Myosin Complex in Toxoplasma gondii. *Molecular Biology of the Cell*, *18*(8), 3039–3046. https://doi.org/10.1091/mbc.E07-01-0040

Joiner, K. A., & Roos, D. S. (2002). Secretory traffic in the eukaryotic parasite Toxoplasma gondii: less is more. *J Cell Biol*, *157*(4), 557–563. https://doi.org/10.1083/jcb.200112144

Jones, D. H., Cellitti, S. E., Hao, X., Zhang, Q., Jahnz, M., Summerer, D., Schultz, P. G., Uno, T., & Geierstanger, B. H. (2009). Site-specific labeling of proteins with NMR-active unnatural amino acids. *Journal of Biomolecular NMR*, *46*(1), 89. https://doi.org/10.1007/s10858-009-9365-4

Jones, J. L., & Dubey, J. P. (2010). Waterborne toxoplasmosis--recent developments. *Experimental Parasitology*, *124*(1), 10–25. https://doi.org/10.1016/j.exppara.2009.03.013

Jones, J. L., Kruszon-Moran, D., Wilson, M., McQuillan, G., Navin, T., & McAuley, J. B. (2001). Toxoplasma gondii Infection in the United States: Seroprevalence and Risk Factors. *American Journal of Epidemiology*, *154*(4), 357–365. https://doi.org/10.1093/aje/154.4.357

Jones, J. L., & Roberts, J. M. (2012). Toxoplasmosis Hospitalizations in the United States, 2008, and Trends, 1993–2008. *Clinical Infectious Diseases*, *54*(7), e58–e61. https://doi.org/10.1093/cid/cir990

Jones, L. A., Alexander, J., & Roberts, C. W. (2006). Ocular toxoplasmosis: in the storm of the eye. *Parasite Immunology*, *28*(12), 635–642. https://doi.org/10.1111/j.1365-3024.2006.00874.x

Jung, C., Lee, C. Y.-F., & Grigg, M. E. (2004). The SRS superfamily of Toxoplasma surface proteins. *International Journal for Parasitology*, *34*(3), 285–296. https://doi.org/10.1016/j.ijpara.2003.12.004

Kafsack, B. F. C., Pena, J. D. O., Coppens, I., Ravindran, S., Boothroyd, J. C., & Carruthers, V. B. (2009). Rapid Membrane Disruption by a Perforin-Like Protein Facilitates Parasite Exit from Host Cells. *Science (New York, N.Y.)*, *323*(5913), 530–533. https://doi.org/10.1126/science.1165740

Katris, N. J., Dooren, G. G. van, McMillan, P. J., Hanssen, E., Tilley, L., & Waller, R. F. (2014). The Apical Complex Provides a Regulated Gateway for Secretion of Invasion Factors in Toxoplasma. *PLOS Pathogens*, *10*(4), e1004074. https://doi.org/10.1371/journal.ppat.1004074

Kelley, L. A., Mezulis, S., Yates, C. M., Wass, M. N., & Sternberg, M. J. E. (2015). The Phyre2 web portal for protein modeling, prediction and analysis. *Nature Protocols*, *10*(6), 845–858. https://doi.org/10.1038/nprot.2015.053

Kessler, H., Herm-Götz, A., Hegge, S., Rauch, M., Soldati-Favre, D., Frischknecht, F., & Meissner, M. (2008). Microneme protein 8 – a new essential invasion factor in Toxoplasma gondii. *Journal of Cell Science*, *121*(7), 947–956. https://doi.org/10.1242/jcs.022350

Khaminets, A., Hunn, J. P., Könen-Waisman, S., Zhao, Y. O., Preukschat, D., Coers, J., Boyle, J. P., Ong, Y.-C., Boothroyd, J. C., Reichmann, G., et al. (2010). Coordinated loading of IRG resistance GTPases on to the Toxoplasma gondii parasitophorous vacuole. *Cellular Microbiology*, *12*(7), 939–961. https://doi.org/10.1111/j.1462-5822.2010.01443.x

Khan, A., Dubey, J. P., Su, C., Ajioka, J. W., Rosenthal, B. M., & Sibley, L. D. (2011). Genetic analyses of atypical Toxoplasma gondii strains reveal a fourth clonal lineage in North America. *International Journal for Parasitology*, *41*(6), 645–655. https://doi.org/10.1016/j.ijpara.2011.01.005

Khan, A., Taylor, S., Su, C., Mackey, A. J., Boyle, J., Cole, R., Glover, D., Tang, K., Paulsen, I. T., Berriman, M., et al. (2005). Composite genome map and recombination parameters derived from three archetypal lineages of Toxoplasma gondii. *Nucleic Acids Research*, *33*(9), 2980–2992. https://doi.org/10.1093/nar/gki604

Khurana, S., & Batra, N. (2016). Toxoplasmosis in organ transplant recipients: Evaluation, implication, and prevention. *Tropical Parasitology*, *6*(2), 123–128. https://doi.org/10.4103/2229-5070.190814

Kilpatrick, A. M., Honts, J. E., Sleister, H. M., & Fowler, C. A. (2016). Solution NMR structures of the C-domain of Tetrahymena cytoskeletal protein Tcb2 reveal distinct calcium-

induced structural rearrangements. *Proteins*, *84*(11), 1748–1756. https://doi.org/10.1002/prot.25111

Kim, E. W., Nadipuram, S. M., Tetlow, A. L., Barshop, W. D., Liu, P. T., Wohlschlegel, J. A., & Bradley, P. J. (2016). The Rhoptry Pseudokinase ROP54 Modulates Toxoplasma gondii Virulence and Host GBP2 Loading. *MSphere*, *1*(2), e00045-16. https://doi.org/10.1128/mSphere.00045-16

Kim, K., & Boothroyd, J. C. (1995). Toxoplasma gondii: stable complementation of sag1 (p30) mutants using SAG1 transfection and fluorescence-activated cell sorting. *Experimental Parasitology*, *80*(1), 46–53. https://doi.org/10.1006/expr.1995.1006

Kim, K., Soldati, D., & Boothroyd, J. C. (1993). Gene replacement in Toxoplasma gondii with chloramphenicol acetyltransferase as selectable marker. *Science (New York, N.Y.)*, *262*(5135), 911–914.

Kissinger, J. C., Gajria, B., Li, L., Paulsen, I. T., & Roos, D. S. (2003). ToxoDB: accessing the Toxoplasma gondii genome. *Nucleic Acids Research*, *31*(1), 234–236.

Kivaria, F. M. (2006). Estimated direct economic costs associated with tick-borne diseases on cattle in Tanzania. *Tropical Animal Health and Production*, *38*(4), 291–299.

Konrad, C., Wek, R. C., & Sullivan, W. J. (2011). A GCN2-Like Eukaryotic Initiation Factor 2 Kinase Increases the Viability of Extracellular Toxoplasma gondii Parasites. *Eukaryotic Cell*, *10*(11), 1403–1412. https://doi.org/10.1128/EC.05117-11

Koonin, E. V., & Novozhilov, A. S. (2017). Origin and Evolution of the Universal Genetic Code. *Annual Review of Genetics*, *51*(1), 45–62. https://doi.org/10.1146/annurev-genet-120116-024713

Kremer, K., Kamin, D., Rittweger, E., Wilkes, J., Flammer, H., Mahler, S., Heng, J., Tonkin, C. J., Langsley, G., Hell, S. W., et al. (2013). An Overexpression Screen of Toxoplasma gondii Rab-GTPases Reveals Distinct Transport Routes to the Micronemes. *PLoS Pathogens*, *9*(3). https://doi.org/10.1371/journal.ppat.1003213

Krishnamurthy, S., Deng, B., Rio, R. del, Buchholz, K. R., Treeck, M., Urban, S., Boothroyd, J., Lam, Y.-W., & Ward, G. E. (2016). Not a Simple Tether: Binding of Toxoplasma gondii AMA1 to RON2 during Invasion Protects AMA1 from Rhomboid-Mediated Cleavage and Leads to Dephosphorylation of Its Cytosolic Tail. *MBio*, *7*(5), e00754-16. https://doi.org/10.1128/mBio.00754-16

Krishnamurthy, S., & Saeij, J. P. J. (2018). Toxoplasma Does Not Secrete the GRA16 and GRA24 Effectors Beyond the Parasitophorous Vacuole Membrane of Tissue Cysts. *Frontiers in Cellular and Infection Microbiology*, *8*. https://doi.org/10.3389/fcimb.2018.00366

Lamarque, M. H., Roques, M., Kong-Hap, M., Tonkin, M. L., Rugarabamu, G., Marq, J.-B., Penarete-Vargas, D. M., Boulanger, M. J., Soldati-Favre, D., & Lebrun, M. (2014).

Plasticity and redundancy among AMA–RON pairs ensure host cell entry of Toxoplasma parasites. *Nature Communications*, *5*, 4098. https://doi.org/10.1038/ncomms5098

Lebrun, M., Carruthers, V. B., & Cesbron-Delauw, M.-F. (2014). Chapter 12 - Toxoplasma Secretory Proteins and Their Roles in Cell Invasion and Intracellular Survival. In L. M. Weiss & K. Kim (Eds.), *Toxoplasma Gondii (Second Edition)* (pp. 389–453). Boston: Academic Press. https://doi.org/10.1016/B978-0-12-396481-6.00012-X

Lemke, E. A. (2011). Site-Specific Labeling of Proteins for Single-Molecule FRET Measurements Using Genetically Encoded Ketone Functionalities. In S. S. Mark (Ed.), *Bioconjugation Protocols: Strategies and Methods* (pp. 3–15). Totowa, NJ: Humana Press. https://doi.org/10.1007/978-1-61779-151-2_1

Leung, J. M., He, Y., Zhang, F., Hwang, Y.-C., Nagayasu, E., Liu, J., Murray, J. M., & Hu, K. (2017). Stability and function of a putative microtubule-organizing center in the human parasite Toxoplasma gondii. *Molecular Biology of the Cell*, *28*(10), 1361–1378. https://doi.org/10.1091/mbc.e17-01-0045

Lim, D., Gold, D. A., Julien, L., Rosowski, E. E., Niedelman, W., Yaffe, M. B., & Saeij, J. P. J. (2013). Structure of the Toxoplasma gondii ROP18 kinase domain reveals a second ligand binding pocket required for acute virulence. *The Journal of Biological Chemistry*, *288*(48), 34968–34980. https://doi.org/10.1074/jbc.M113.523266

Lim, L., & McFadden, G. I. (2010). The evolution, metabolism and functions of the apicoplast. *Philosophical Transactions of the Royal Society B: Biological Sciences*, *365*(1541), 749–763. https://doi.org/10.1098/rstb.2009.0273

Lindsay, D. S., & Dubey, J. P. (2011). Toxoplasma gondii: the changing paradigm of congenital toxoplasmosis. *Parasitology*, *138*(14), 1829–1831. https://doi.org/10.1017/S0031182011001478

Ling, Y. M., Shaw, M. H., Ayala, C., Coppens, I., Taylor, G. A., Ferguson, D. J. P., & Yap, G. S. (2006). Vacuolar and plasma membrane stripping and autophagic elimination of Toxoplasma gondii in primed effector macrophages. *The Journal of Experimental Medicine*, *203*(9), 2063–2071. https://doi.org/10.1084/jem.20061318

Liu, D. R., & Schultz, P. G. (1999). Progress toward the evolution of an organism with an expanded genetic code. *Proceedings of the National Academy of Sciences*, *96*(9), 4780–4785. https://doi.org/10.1073/pnas.96.9.4780

Liu, J., Wetzel, L., Zhang, Y., Nagayasu, E., Ems-McClung, S., Florens, L., & Hu, K. (2013). Novel thioredoxin-like proteins are components of a protein complex coating the cortical microtubules of Toxoplasma gondii. *Eukaryotic Cell*, *12*(12), 1588–1599. https://doi.org/10.1128/EC.00082-13

Liu, W., Brock, A., Chen, S., Chen, S., & Schultz, P. G. (2007). Genetic incorporation of unnatural amino acids into proteins in mammalian cells. *Nature Methods*, *4*(3), 239–244. https://doi.org/10.1038/nmeth1016

Long, S., Anthony, B., Drewry, L. L., & Sibley, L. D. (2017a). A conserved ankyrin repeat-containing protein regulates conoid stability, motility and cell invasion in Toxoplasma gondii. *Nature Communications*, *8*(1), 2236. https://doi.org/10.1038/s41467-017-02341-2

Long, S., Brown, K. M., Drewry, L. L., Anthony, B., Phan, I. Q. H., & Sibley, L. D. (2017b). Calmodulin-like proteins localized to the conoid regulate motility and cell invasion by Toxoplasma gondii. *PLOS Pathogens*, *13*(5), e1006379. https://doi.org/10.1371/journal.ppat.1006379

Long, S., Wang, Q., & Sibley, L. D. (2016). Analysis of Noncanonical Calcium-Dependent Protein Kinases in Toxoplasma gondii by Targeted Gene Deletion Using CRISPR/Cas9. *Infection and Immunity*, *84*(5), 1262–1273. https://doi.org/10.1128/IAI.01173-15

Lorestani, A., Ivey, F. D., Thirugnanam, S., Busby, M. A., Marth, G. T., Cheeseman, I. M., & Gubbels, M.-J. (2012). Targeted proteomic dissection of Toxoplasma cytoskeleton sub-compartments using MORN1. *Cytoskeleton (Hoboken, N.J.)*, *69*(12), 1069–1085. https://doi.org/10.1002/cm.21077

Lourido, S., Tang, K., & Sibley, L. D. (2012). Distinct signalling pathways control Toxoplasma egress and host-cell invasion. *The EMBO Journal*, *31*(24), 4524–4534. https://doi.org/10.1038/emboj.2012.299

Lovett, J. L., & Sibley, L. D. (2003). Intracellular calcium stores in Toxoplasma gondii govern invasion of host cells. *Journal of Cell Science*, *116*(14), 3009–3016. https://doi.org/10.1242/jcs.00596

Luft, B. J., & Remington, J. S. (1992). Toxoplasmic Encephalitis in AIDS. *Clinical Infectious Diseases*, *15*(2), 211–222.

Lupas, A. (1997). Predicting coiled-coil regions in proteins. *Current Opinion in Structural Biology*, *7*(3), 388–393.

Lupas, A., & Bassler, J. (2017). Coiled Coils - A Model System for the 21st Century. *Trends in Biochemical Sciences*, *42*(2), 130–140. https://doi.org/10.1016/j.tibs.2016.10.007

Macino, G., Coruzzi, G., Nobrega, F. G., Li, M., & Tzagoloff, A. (1979). Use of the UGA terminator as a tryptophan codon in yeast mitochondria. *Proceedings of the National Academy of Sciences of the United States of America*, *76*(8), 3784–3785.

Mackintosh, C. L., Beeson, J. G., & Marsh, K. (2004). Clinical features and pathogenesis of severe malaria. *Trends in Parasitology*, *20*(12), 597–603. https://doi.org/10.1016/j.pt.2004.09.006

Maldonado, Y. A., Read, J. S., & Diseases, C. on I. (2017). Diagnosis, Treatment, and Prevention of Congenital Toxoplasmosis in the United States. *Pediatrics*, *139*(2), e20163860. https://doi.org/10.1542/peds.2016-3860

Mann, T., & Beckers, C. (2001). Characterization of the subpellicular network, a filamentous membrane skeletal component in the parasite Toxoplasma gondii. *Molecular and Biochemical Parasitology*, *115*(2), 257–268.

Mann, T., Gaskins, E., & Beckers, C. (2002). Proteolytic Processing of TgIMC1 during Maturation of the Membrane Skeleton of Toxoplasma gondii. *Journal of Biological Chemistry*, *277*(43), 41240–41246. https://doi.org/10.1074/jbc.M205056200

Marino, N. D., Panas, M. W., Franco, M., Theisen, T. C., Naor, A., Rastogi, S., Buchholz, K. R., Lorenzi, H. A., & Boothroyd, J. C. (2018). Identification of a novel protein complex essential for effector translocation across the parasitophorous vacuole membrane of Toxoplasma gondii. *PLoS Pathogens*, *14*(1). https://doi.org/10.1371/journal.ppat.1006828

Marra, C. M. (2018). Chapter 9 - Central nervous system infection with Toxoplasma gondii. In B. J. Brew (Ed.), *Handbook of Clinical Neurology* (Vol. 152, pp. 117–122). Elsevier. https://doi.org/10.1016/B978-0-444-63849-6.00009-8

Martinez-Sanz, J., Kateb, F., Assairi, L., Blouquit, Y., Bodenhausen, G., Abergel, D., Mouawad, L., & Craescu, C. T. (2010). Structure, dynamics and thermodynamics of the human centrin 2/hSfi1 complex. *Journal of Molecular Biology*, *395*(1), 191–204. https://doi.org/10.1016/j.jmb.2009.10.041

McLeod, R., Boyer, K. M., Lee, D., Mui, E., Wroblewski, K., Karrison, T., Noble, A. G., Withers, S., Swisher, C. N., Heydemann, P. T., et al. (2012). Prematurity and Severity Are Associated With Toxoplasma gondii Alleles (NCCCTS, 1981–2009). *Clinical Infectious Diseases: An Official Publication of the Infectious Diseases Society of America*, *54*(11), 1595–1605. https://doi.org/10.1093/cid/cis258

Mehnert, M., Sommer, T., & Jarosch, E. (2014). Der1 promotes movement of misfolded proteins through the endoplasmic reticulum membrane. *Nature Cell Biology*, *16*(1), 77–86. https://doi.org/10.1038/ncb2882

Mehta, S., & Sibley, L. D. (2011). Actin depolymerizing factor controls actin turnover and gliding motility in Toxoplasma gondii. *Molecular Biology of the Cell*, *22*(8), 1290–1299. https://doi.org/10.1091/mbc.E10-12-0939

Melo, E. J. L., Attias, M., & De Souza, W. (2000). The Single Mitochondrion of Tachyzoites of Toxoplasma gondii. *Journal of Structural Biology*, *130*(1), 27–33. https://doi.org/10.1006/jsbi.2000.4228

Mercier, C., Dubremetz, J.-F., Rauscher, B., Lecordier, L., Sibley, L. D., & Cesbron-Delauw, M.-F. (2002). Biogenesis of Nanotubular Network in ToxoplasmaParasitophorous Vacuole Induced by Parasite Proteins. *Molecular Biology of the Cell*, *13*(7), 2397–2409. https://doi.org/10.1091/mbc.e02-01-0021

Mineo, J. R., McLeod, R., Mack, D., Smith, J., Khan, I. A., Ely, K. H., & Kasper, L. H. (1993). Antibodies to Toxoplasma gondii major surface protein (SAG-1, P30) inhibit infection of

host cells and are produced in murine intestine after peroral infection. *The Journal of Immunology*, *150*(9), 3951–3964.

Mondragon, R., & Frixione, E. (1996). Ca2+-Dependence of Conoid Extrusion in Toxoplasma gondii Tachyzoites. *Journal of Eukaryotic Microbiology*, *43*(2), 120–127. https://doi.org/10.1111/j.1550-7408.1996.tb04491.x

Montoya, J. G., & Liesenfeld, O. (2004). Toxoplasmosis. *The Lancet*, *363*(9425), 1965–1976. https://doi.org/10.1016/S0140-6736(04)16412-X

Mordue, D. G., Desai, N., Dustin, M., & Sibley, L. D. (1999). Invasion by Toxoplasma gondii Establishes a Moving Junction That Selectively Excludes Host Cell Plasma Membrane Proteins on the Basis of Their Membrane Anchoring. *The Journal of Experimental Medicine*, *190*(12), 1783–1792.

Morisaki, J. H., Heuser, J. E., & Sibley, L. D. (1995). Invasion of Toxoplasma gondii occurs by active penetration of the host cell. *Journal of Cell Science*, *108*(6), 2457–2464.

Morrissette, N. S., & Ajioka, J. W. (2009). The early years of Toxoplasma research: What's past is prologue. *International Journal for Parasitology*, *39*(8), 865–869. https://doi.org/10.1016/j.ijpara.2009.02.010

Morrissette, N. S., & Sibley, L. D. (2002a). Cytoskeleton of Apicomplexan Parasites. *Microbiology and Molecular Biology Reviews*, *66*(1), 21–38. https://doi.org/10.1128/MMBR.66.1.21-38.2002

Morrissette, N. S., & Sibley, L. D. (2002b). Disruption of microtubules uncouples budding and nuclear division in Toxoplasma gondii. *Journal of Cell Science*, *115*(Pt 5), 1017–1025.

Mueller, C., Klages, N., Jacot, D., Santos, J. M., Cabrera, A., Gilberger, T. W., Dubremetz, J.-F., & Soldati-Favre, D. (2013). The Toxoplasma protein ARO mediates the apical positioning of rhoptry organelles, a prerequisite for host cell invasion. *Cell Host & Microbe*, *13*(3), 289–301. https://doi.org/10.1016/j.chom.2013.02.001

Mueller, C., Samoo, A., Hammoudi, P.-M., Klages, N., Kallio, J. P., Kursula, I., & Soldati-Favre, D. (2016). Structural and functional dissection of Toxoplasma gondii armadillo repeats only protein. *Journal of Cell Science*, *129*(5), 1031–1045. https://doi.org/10.1242/jcs.177386

Mueller-Planitz, F. (2015). Crossfinder-assisted mapping of protein crosslinks formed by site-specifically incorporated crosslinkers. *Bioinformatics (Oxford, England)*, *31*(12), 2043–2045. https://doi.org/10.1093/bioinformatics/btv083

Mukai, T., Wakiyama, M., Sakamoto, K., & Yokoyama, S. (2010). Genetic encoding of non-natural amino acids in Drosophila melanogaster Schneider 2 cells. *Protein Science : A Publication of the Protein Society*, *19*(3), 440–448. https://doi.org/10.1002/pro.322

Mukherjee, A., & Sadhukhan, G. C. (2016). Anti-malarial Drug Design by Targeting Apicoplasts: New Perspectives. *Journal of Pharmacopuncture*, *19*(1), 7–15. https://doi.org/10.3831/KPI.2016.19.001

Nadipuram, S. M., Kim, E. W., Vashisht, A. A., Lin, A. H., Bell, H. N., Coppens, I., Wohlschlegel, J. A., & Bradley, P. J. (2016). In Vivo Biotinylation of the Toxoplasma Parasitophorous Vacuole Reveals Novel Dense Granule Proteins Important for Parasite Growth and Pathogenesis. *MBio*, *7*(4), e00808-16. https://doi.org/10.1128/mBio.00808-16

Nagamune, K., Hicks, L. M., Fux, B., Brossier, F., Chini, E. N., & Sibley, L. D. (2008). Abscisic acid controls calcium-dependent egress and development in Toxoplasma gondii. *Nature*, *451*(7175), 207–210. https://doi.org/10.1038/nature06478

Nakamura, Y., Gojobori, T., & Ikemura, T. (2000). Codon usage tabulated from international DNA sequence databases: status for the year 2000. *Nucleic Acids Research*, *28*(1), 292.

Nebl, T., Prieto, J. H., Kapp, E., Smith, B. J., Williams, M. J., Yates 3rd, J. R., Cowman, A. F., & Tonkin, C. J. (2011). Quantitative in vivo Analyses Reveal Calcium-dependent Phosphorylation Sites and Identifies a Novel Component of the Toxoplasma Invasion Motor Complex. *PLOS Pathogens*, *7*(9), e1002222. https://doi.org/10.1371/journal.ppat.1002222

Nichols, B. A., Chiappino, M. L., & O'Connor, G. R. (1983). Secretion from the rhoptries of Toxoplasma gondii during host-cell invasion. *Journal of Ultrastructure Research*, *83*(1), 85–98.

Nichols, B. A., & Chiappino, M. L. (1987). Cytoskeleton of Toxoplasma gondii1. *The Journal of Protozoology*, *34*(2), 217–226. https://doi.org/10.1111/j.1550-7408.1987.tb03162.x

Nicolle, C., & Manceaux, L. (1908). Sur une infection à corps de Leishman (ou organismes voisins) du gondi. *C R Seances Acad Sci*, *147*, 763–766.

Niedelman, W., Gold, D. A., Rosowski, E. E., Sprokholt, J. K., Lim, D., Arenas, A. F., Melo, M. B., Spooner, E., Yaffe, M. B., & Saeij, J. P. J. (2012). The Rhoptry Proteins ROP18 and ROP5 Mediate Toxoplasma gondii Evasion of the Murine, But Not the Human, Interferon-Gamma Response. *PLOS Pathogens*, *8*(6), e1002784. https://doi.org/10.1371/journal.ppat.1002784

Nirenberg, M. (2004). Historical review: Deciphering the genetic code – a personal account. *Trends in Biochemical Sciences*, *29*(1), 46–54. https://doi.org/10.1016/j.tibs.2003.11.009

Nishi, M., Hu, K., Murray, J. M., & Roos, D. S. (2008). Organellar dynamics during the cell cycle of Toxoplasma gondii. *Journal of Cell Science*, *121*(Pt 9), 1559–1568. https://doi.org/10.1242/jcs.021089

Nosala, C., Hagen, K. D., & Dawson, S. C. (2018). “Disc-o-Fever”: Getting Down with Giardia’s Groovy Microtubule Organelle. *Trends in Cell Biology*, *28*(2), 99–112. https://doi.org/10.1016/j.tcb.2017.10.007

Ouologuem, D. T., & Roos, D. S. (2014). Dynamics of the Toxoplasma gondii inner membrane complex. *Journal of Cell Science*, *127*(15), 3320–3330. https://doi.org/10.1242/jcs.147736

Pantoja, R., Rodriguez, E. A., Dibas, M. I., Dougherty, D. A., & Lester, H. A. (2009). Single-Molecule Imaging of a Fluorescent Unnatural Amino Acid Incorporated Into Nicotinic Receptors. *Biophysical Journal*, *96*(1), 226–237. https://doi.org/10.1016/j.bpj.2008.09.034

Paredes-Santos, T. C., de Souza, W., & Attias, M. (2012). Dynamics and 3D organization of secretory organelles of Toxoplasma gondii. *Journal of Structural Biology*, *177*(2), 420–430. https://doi.org/10.1016/j.jsb.2011.11.028

Paul, A. S., Saha, S., Engelberg, K., Jiang, R. H. Y., Coleman, B. I., Kosber, A. L., Chen, C.-T., Ganter, M., Espy, N., Gilberger, T. W., et al. (2015). Parasite calcineurin regulates host cell recognition and attachment by apicomplexans. *Cell Host & Microbe*, *18*(1), 49–60. https://doi.org/10.1016/j.chom.2015.06.003

Peixoto, L., Chen, F., Harb, O. S., Davis, P. H., Beiting, D. P., Brownback, C. S., Ouologuem, D., & Roos, D. S. (2010). Integrative Genomic Approaches Highlight a Family of Parasite-Specific Kinases that Regulate Host Responses. *Cell Host & Microbe*, *8*(2), 208–218. https://doi.org/10.1016/j.chom.2010.07.004

Perdomo, D., Bonhivers, M., & Robinson, D. R. (2016). The Trypanosome Flagellar Pocket Collar and Its Ring Forming Protein-TbBILBO1. *Cells*, *5*(1). https://doi.org/10.3390/cells5010009

Pernas, L., Adomako-Ankomah, Y., Shastri, A. J., Ewald, S. E., Treeck, M., Boyle, J. P., & Boothroyd, J. C. (2014). Toxoplasma Effector MAF1 Mediates Recruitment of Host Mitochondria and Impacts the Host Response. *PLOS Biology*, *12*(4), e1001845. https://doi.org/10.1371/journal.pbio.1001845

Peyron, F., Leod, R. M., Ajzenberg, D., Contopoulos-Ioannidis, D., Kieffer, F., Mandelbrot, L., Sibley, L. D., Pelloux, H., Villena, I., Wallon, M., et al. (2017). Congenital Toxoplasmosis in France and the United States: One Parasite, Two Diverging Approaches. *PLOS Neglected Tropical Diseases*, *11*(2), e0005222. https://doi.org/10.1371/journal.pntd.0005222

Polonais, V., Javier Foth, B., Chinthalapudi, K., Marq, J.-B., Manstein, D. J., Soldati-Favre, D., & Frénal, K. (2011). Unusual anchor of a motor complex (MyoD-MLC2) to the plasma membrane of Toxoplasma gondii. *Traffic (Copenhagen, Denmark)*, *12*(3), 287–300. https://doi.org/10.1111/j.1600-0854.2010.01148.x

Porchet, E., & Torpier, G. (1977). [Freeze fracture study of Toxoplasma and Sarcocystis infective stages (author's transl)]. *Zeitschrift Fur Parasitenkunde (Berlin, Germany)*, *54*(2), 101–124.

Praefcke, G. J. K. (2018). Regulation of innate immune functions by guanylate-binding proteins. *International Journal of Medical Microbiology*, *308*(1), 237–245. https://doi.org/10.1016/j.ijmm.2017.10.013

Reese, M. L., & Boothroyd, J. C. (2009). A helical membrane-binding domain targets the Toxoplasma ROP2 family to the parasitophorous vacuole. *Traffic (Copenhagen, Denmark)*, *10*(10), 1458–1470. https://doi.org/10.1111/j.1600-0854.2009.00958.x

Reese, M. L., Zeiner, G. M., Saeij, J. P. J., Boothroyd, J. C., & Boyle, J. P. (2011). Polymorphic family of injected pseudokinases is paramount in Toxoplasma virulence. *Proceedings of the National Academy of Sciences*, *108*(23), 9625–9630. https://doi.org/10.1073/pnas.1015980108

Ren, J., Wen, L., Gao, X., Jin, C., Xue, Y., & Yao, X. (2008). CSS-Palm 2.0: an updated software for palmitoylation sites prediction. *Protein Engineering, Design & Selection: PEDS*, *21*(11), 639–644. https://doi.org/10.1093/protein/gzn039

Richter, R., Pajak, A., Dennerlein, S., Rozanska, A., Lightowlers, R. N., & Chrzanowska-Lightowlers, Z. M. A. (2010). Translation termination in human mitochondrial ribosomes. *Biochemical Society Transactions*, *38*(6), 1523–1526. https://doi.org/10.1042/BST0381523

Robben, P. M., Mordue, D. G., Truscott, S. M., Takeda, K., Akira, S., & Sibley, L. D. (2004). Production of IL-12 by macrophages infected with Toxoplasma gondii depends on the parasite genotype. *Journal of Immunology (Baltimore, Md.: 1950)*, *172*(6), 3686–3694.

Robert-Gangneux, F., & Dardé, M.-L. (2012). Epidemiology of and Diagnostic Strategies for Toxoplasmosis. *Clinical Microbiology Reviews*, *25*(2), 264–296. https://doi.org/10.1128/CMR.05013-11

Roiko, M. S., Svezhova, N., & Carruthers, V. B. (2014). Acidification Activates Toxoplasma gondii Motility and Egress by Enhancing Protein Secretion and Cytolytic Activity. *PLoS Pathogens*, *10*(11). https://doi.org/10.1371/journal.ppat.1004488

Romano, J. D., Nolan, S. J., Porter, C., Ehrenman, K., Hartman, E. J., Hsia, R., & Coppens, I. (2017). The parasite Toxoplasma sequesters diverse Rab host vesicles within an intravacuolar network. *J Cell Biol*, *216*(12), 4235–4254. https://doi.org/10.1083/jcb.201701108

Rome, M. E., Beck, J. R., Turetzky, J. M., Webster, P., & Bradley, P. J. (2008). Intervacuolar transport and unique topology of GRA14, a novel dense granule protein in Toxoplasma gondii. *Infection and Immunity*, *76*(11), 4865–4875. https://doi.org/10.1128/IAI.00782-08

Roux, K. J., Kim, D. I., Raida, M., & Burke, B. (2012). A promiscuous biotin ligase fusion protein identifies proximal and interacting proteins in mammalian cells. *The Journal of Cell Biology*, *196*(6), 801–810. https://doi.org/10.1083/jcb.201112098

Russell, D. G., & Burns, R. G. (1984). The polar ring of coccidian sporozoites: a unique microtubule-organizing centre. *Journal of Cell Science*, *65*(1), 193–207.

Ryu, Y., & Schultz, P. G. (2006). Efficient incorporation of unnatural amino acids into proteins in Escherichia coli. *Nature Methods*, *3*(4), 263–265. https://doi.org/10.1038/nmeth864

Sabin, A. B. (1941). Toxoplasmic encephalitis in children. *Journal of the American Medical Association*, *116*(9), 801–807. https://doi.org/10.1001/jama.1941.02820090001001

Saeij, J. P. J., Boyle, J. P., Coller, S., Taylor, S., Sibley, L. D., Brooke-Powell, E. T., Ajioka, J. W., & Boothroyd, J. C. (2006). Polymorphic secreted kinases are key virulence factors in toxoplasmosis. *Science (New York, N.Y.)*, *314*(5806), 1780–1783. https://doi.org/10.1126/science.1133690

Saeij, J. P. J., Coller, S., Boyle, J. P., Jerome, M. E., White, M. W., & Boothroyd, J. C. (2007). Toxoplasma co-opts host gene expression by injection of a polymorphic kinase homologue. *Nature*, *445*(7125), 324. https://doi.org/10.1038/nature05395

Sakamoto, K., Hayashi, A., Sakamoto, A., Kiga, D., Nakayama, H., Soma, A., Kobayashi, T., Kitabatake, M., Takio, K., Saito, K., et al. (2002). Site-specific incorporation of an unnatural amino acid into proteins in mammalian cells. *Nucleic Acids Research*, *30*(21), 4692–4699. https://doi.org/10.1093/nar/gkf589

Sakura, T., Sindikubwabo, F., Oesterlin, L. K., Bousquet, H., Slomianny, C., Hakimi, M.-A., Langsley, G., & Tomavo, S. (2016). A Critical Role for Toxoplasma gondii Vacuolar Protein Sorting VPS9 in Secretory Organelle Biogenesis and Host Infection. *Scientific Reports*, *6*, 38842. https://doi.org/10.1038/srep38842

Schumacher, M. A., Carter, D., Scott, D. M., Roos, D. S., Ullman, B., & Brennan, R. G. (1998). Crystal structures of Toxoplasma gondii uracil phosphoribosyltransferase reveal the atomic basis of pyrimidine discrimination and prodrug binding. *The EMBO Journal*, *17*(12), 3219–3232. https://doi.org/10.1093/emboj/17.12.3219

Schumacher, Maria A., Bashor, C. J., Song, M. H., Otsu, K., Zhu, S., Parry, R. J., Ullman, B., & Brennan, R. G. (2002). The structural mechanism of GTP stabilized oligomerization and catalytic activation of the Toxoplasma gondii uracil phosphoribosyltransferase. *Proceedings of the National Academy of Sciences of the United States of America*, *99*(1), 78–83. https://doi.org/10.1073/pnas.012399599

Schwab, J. C., Beckers, C. J., & Joiner, K. A. (1994). The parasitophorous vacuole membrane surrounding intracellular Toxoplasma gondii functions as a molecular sieve. *Proceedings of the National Academy of Sciences of the United States of America*, *91*(2), 509–513.

Sellers, J. R. (2000). Myosins: a diverse superfamily. *Biochimica et Biophysica Acta (BBA) - Molecular Cell Research*, *1496*(1), 3–22. https://doi.org/10.1016/S0167-4889(00)00005-7

Sharman, P. A., Smith, N. C., Wallach, M. G., & Katrib, M. (2010). Chasing the golden egg: vaccination against poultry coccidiosis. *Parasite Immunology*, *32*(8), 590–598. https://doi.org/10.1111/j.1365-3024.2010.01209.x

Shaw, M. K., Roos, D. S., & Tilney, L. G. (1998). Acidic compartments and rhoptry formation in Toxoplasma gondii. *Parasitology*, *117*(5), 435–443. https://doi.org/10.1017/S0031182098003278

Sheffield, H. G. (1970). Schizogony in Toxoplasma gondii: an electron microscope study. *Proceedings of the Helminthological Society of Washington*, *37*(2), 237–242.

Shenoy, A. R., Kim, B.-H., Choi, H.-P., Matsuzawa, T., Tiwari, S., & MacMicking, J. D. (2007). Emerging themes in IFN-γ-induced macrophage immunity by the p47 and p65 GTPase Families. *Immunobiology*, *212*(9–10), 771–784. https://doi.org/10.1016/j.imbio.2007.09.018

Sibley, L. D., Niesman, I. R., Parmley, S. F., & Cesbron-Delauw, M. F. (1995). Regulated secretion of multi-lamellar vesicles leads to formation of a tubulo-vesicular network in host-cell vacuoles occupied by Toxoplasma gondii. *Journal of Cell Science*, *108 (Pt 4)*, 1669–1677.

Sibley, L. D., Khan, A., Ajioka, J. W., & Rosenthal, B. M. (2009). Genetic diversity of Toxoplasma gondii in animals and humans. *Philosophical Transactions of the Royal Society B: Biological Sciences*, *364*(1530), 2749–2761. https://doi.org/10.1098/rstb.2009.0087

Sidik, S. M., Hackett, C. G., Tran, F., Westwood, N. J., & Lourido, S. (2014). Efficient Genome Engineering of Toxoplasma gondii Using CRISPR/Cas9. *PLoS ONE*, *9*(6), e100450. https://doi.org/10.1371/journal.pone.0100450

Sidik, S. M., Huet, D., Ganesan, S. M., Huynh, M.-H., Wang, T., Nasamu, A. S., Thiru, P., Saeij, J. P. J., Carruthers, V. B., Niles, J. C., et al. (2016). A Genome-wide CRISPR Screen in Toxoplasma Identifies Essential Apicomplexan Genes. *Cell*, *166*(6), 1423-1435.e12. https://doi.org/10.1016/j.cell.2016.08.019

Silmon de Monerri, N. C., Yakubu, R. R., Chen, A. L., Bradley, P. J., Nieves, E., Weiss, L. M., & Kim, K. (2015). The Ubiquitin Proteome of Toxoplasma gondii Reveals Roles for Protein Ubiquitination in Cell-Cycle Transitions. *Cell Host & Microbe*, *18*(5), 621–633. https://doi.org/10.1016/j.chom.2015.10.014

Singh, S., Alam, M. M., Pal-Bhowmick, I., Brzostowski, J. A., & Chitnis, C. E. (2010). Distinct External Signals Trigger Sequential Release of Apical Organelles during Erythrocyte Invasion by Malaria Parasites. *PLoS Pathogens*, *6*(2). https://doi.org/10.1371/journal.ppat.1000746

Skariah, S., McIntyre, M. K., & Mordue, D. G. (2010). Toxoplasma gondii: determinants of tachyzoite to bradyzoite conversion. *Parasitology Research*, *107*(2), 253–260. https://doi.org/10.1007/s00436-010-1899-6

Skillman, K. M., Diraviyam, K., Khan, A., Tang, K., Sept, D., & Sibley, L. D. (2011). Evolutionarily Divergent, Unstable Filamentous Actin Is Essential for Gliding Motility in Apicomplexan Parasites. *PLOS Pathogens*, *7*(10), e1002280. https://doi.org/10.1371/journal.ppat.1002280

Sloves, P.-J., Delhaye, S., Mouveaux, T., Werkmeister, E., Slomianny, C., Hovasse, A., Dilezitoko Alayi, T., Callebaut, I., Gaji, R. Y., Schaeffer-Reiss, C., et al. (2012). Toxoplasma Sortilin-like Receptor Regulates Protein Transport and Is Essential for Apical Secretory Organelle Biogenesis and Host Infection. *Cell Host & Microbe*, *11*(5), 515–527. https://doi.org/10.1016/j.chom.2012.03.006

Soldati, D. (1999). The Apicoplast as a Potential Therapeutic Target in Toxoplasma and Other Apicomplexan Parasites. *Parasitology Today*, *15*(1), 5–7. https://doi.org/10.1016/S0169-4758(98)01363-5

Soldati, D., Dubremetz, J. F., & Lebrun, M. (2001). Microneme proteins: structural and functional requirements to promote adhesion and invasion by the apicomplexan parasite Toxoplasma gondii. *International Journal for Parasitology*, *31*(12), 1293–1302. https://doi.org/10.1016/S0020-7519(01)00257-0

Sow, S. O., Muhsen, K., Nasrin, D., Blackwelder, W. C., Wu, Y., Farag, T. H., Panchalingam, S., Sur, D., Zaidi, A. K. M., Faruque, A. S. G., et al. (2016). The Burden of Cryptosporidium Diarrheal Disease among Children < 24 Months of Age in Moderate/High Mortality Regions of Sub-Saharan Africa and South Asia, Utilizing Data from the Global Enteric Multicenter Study (GEMS). *PLOS Neglected Tropical Diseases*, *10*(5), e0004729. https://doi.org/10.1371/journal.pntd.0004729

Splendore, A. (1908). Un nuovo protozoa parassita deconigli incontrato nelle lesioni anatomiche d'une malattia che ricorda in molti punti il Kala-azar dell'uoma. Nota preliminare pel. *Rev Soc Sci Sao Paulo*, *3*, 109–112.

Srinivasan, G., James, C. M., & Krzycki, J. A. (2002). Pyrrolysine Encoded by UAG in Archaea: Charging of a UAG-Decoding Specialized tRNA. *Science*, *296*(5572), 1459–1462. https://doi.org/10.1126/science.1069588

Staros, J. V. (1980). Aryl azide photolabels in biochemistry. *Trends in Biochemical Sciences*, *5*(12), 320–322. https://doi.org/10.1016/0968-0004(80)90140-1

Steinfeldt, T., Könen-Waisman, S., Tong, L., Pawlowski, N., Lamkemeyer, T., Sibley, L. D., Hunn, J. P., & Howard, J. C. (2010). Phosphorylation of Mouse Immunity-Related GTPase (IRG) Resistance Proteins Is an Evasion Strategy for Virulent Toxoplasma gondii. *PLOS Biology*, *8*(12), e1000576. https://doi.org/10.1371/journal.pbio.1000576

Straub, K. W., Peng, E. D., Hajagos, B. E., Tyler, J. S., & Bradley, P. J. (2011). The Moving Junction Protein RON8 Facilitates Firm Attachment and Host Cell Invasion in Toxoplasma gondii. *PLOS Pathogens*, *7*(3), e1002007. https://doi.org/10.1371/journal.ppat.1002007

Suchanek, M., Radzikowska, A., & Thiele, C. (2005). Photo-leucine and photo-methionine allow identification of protein-protein interactions in living cells. *Nature Methods*, *2*(4), 261–268. https://doi.org/10.1038/nmeth752

Takimoto, J. K., Adams, K. L., Xiang, Z., & Wang, L. (2009). Improving orthogonal tRNA-synthetase recognition for efficient unnatural amino acid incorporation and application in mammalian cells. *Molecular BioSystems*, *5*(9), 931–934. https://doi.org/10.1039/b904228h

Tanrikulu, I. C., Schmitt, E., Mechulam, Y., Goddard, W. A., & Tirrell, D. A. (2009). Discovery of Escherichia coli methionyl-tRNA synthetase mutants for efficient labeling of proteins with azidonorleucine in vivo. *Proceedings of the National Academy of Sciences*, *106*(36), 15285–15290. https://doi.org/10.1073/pnas.0905735106

Taylor, G. A., Feng, C. G., & Sher, A. (2007). Control of IFN-γ-mediated host resistance to intracellular pathogens by immunity-related GTPases (p47 GTPases). *Microbes and Infection*, *9*(14), 1644–1651. https://doi.org/10.1016/j.micinf.2007.09.004

Tewari, R., Bailes, E., Bunting, K. A., & Coates, J. C. (2010). Armadillo-repeat protein functions: questions for little creatures. *Trends in Cell Biology*, *20*(8), 470–481. https://doi.org/10.1016/j.tcb.2010.05.003

Tonkin, M. L., Roques, M., Lamarque, M. H., Pugnière, M., Douguet, D., Crawford, J., Lebrun, M., & Boulanger, M. J. (2011). Host Cell Invasion by Apicomplexan Parasites: Insights from the Co-Structure of AMA1 with a RON2 Peptide. *Science*, *333*(6041), 463–467. https://doi.org/10.1126/science.1204988

Tosetti, N., Dos Santos Pacheco, N., Soldati-Favre, D., & Jacot, D. (2019). Three F-actin assembly centers regulate organelle inheritance, cell-cell communication and motility in Toxoplasma gondii. *ELife*, *8*. https://doi.org/10.7554/eLife.42669

Tran, J. Q., de Leon, J. C., Li, C., Huynh, M.-H., Beatty, W., & Morrissette, N. S. (2010). RNG1 is a Late Marker of the Apical Polar Ring in Toxoplasma gondii. *Cytoskeleton (Hoboken, N.J.)*, *67*(9), 586–598. https://doi.org/10.1002/cm.20469

Tran, J. Q., Li, C., Chyan, A., Chung, L., & Morrissette, N. S. (2012). SPM1 Stabilizes Subpellicular Microtubules in Toxoplasma gondii. *Eukaryotic Cell*, *11*(2), 206–216. https://doi.org/10.1128/EC.05161-11

Tremp, A. Z., Al-Khattaf, F. S., & Dessens, J. T. (2017). Palmitoylation of Plasmodium alveolins promotes cytoskeletal function. *Molecular and Biochemical Parasitology*, *213*, 16–21. https://doi.org/10.1016/j.molbiopara.2017.02.003

Tremp, A. Z., Carter, V., Saeed, S., & Dessens, J. T. (2013). Morphogenesis of Plasmodium zoites is uncoupled from tensile strength. *Molecular Microbiology*, *89*(3), 552–564. https://doi.org/10.1111/mmi.12297

Tremp, A. Z., Khater, E. I., & Dessens, J. T. (2008). IMC1b Is a Putative Membrane Skeleton Protein Involved in Cell Shape, Mechanical Strength, Motility, and Infectivity of Malaria Ookinetes. *Journal of Biological Chemistry*, *283*(41), 27604–27611. https://doi.org/10.1074/jbc.M801302200

Tripal, P., Bauer, M., Naschberger, E., Mörtinger, T., Hohenadl, C., Cornali, E., Thurau, M., & Stürzl, M. (2007). Unique features of different members of the human guanylate-binding protein family. *Journal of Interferon & Cytokine Research: The Official Journal of the International Society for Interferon and Cytokine Research*, *27*(1), 44–52. https://doi.org/10.1089/jir.2007.0086

Turetzky, J. M., Chu, D. K., Hajagos, B. E., & Bradley, P. J. (2010). Processing and secretion of ROP13: A unique Toxoplasma effector protein. *International Journal for Parasitology*, *40*(9), 1037–1044. https://doi.org/10.1016/j.ijpara.2010.02.014

Tyler, J. S., & Boothroyd, J. C. (2011). The C-Terminus of Toxoplasma RON2 Provides the Crucial Link between AMA1 and the Host-Associated Invasion Complex. *PLOS Pathogens*, *7*(2), e1001282. https://doi.org/10.1371/journal.ppat.1001282

Vaughan, S., & Gull, K. (2016). Basal body structure and cell cycle-dependent biogenesis in Trypanosoma brucei. *Cilia*, *5*(1), 5. https://doi.org/10.1186/s13630-016-0023-7

Volkmann, K., Pfander, C., Burstroem, C., Ahras, M., Goulding, D., Rayner, J. C., Frischknecht, F., Billker, O., & Brochet, M. (2012). The alveolin IMC1h is required for normal ookinete and sporozoite motility behaviour and host colonisation in Plasmodium berghei. *PloS One*, *7*(7), e41409. https://doi.org/10.1371/journal.pone.0041409

Wals, K., & Ovaa, H. (2014). Unnatural amino acid incorporation in E. coli: current and future applications in the design of therapeutic proteins. *Frontiers in Chemistry*, *2*. https://doi.org/10.3389/fchem.2014.00015

Wan, K.-L., Blackwell, J. M., & Ajioka, J. W. (1996). Toxoplasma gondii expressed sequence tags: insight into tachyzoite gene expression. *Molecular and Biochemical Parasitology*, *75*(2), 179–186. https://doi.org/10.1016/0166-6851(95)02524-3

Wang, J.-L., Huang, S.-Y., Li, T.-T., Chen, K., Ning, H.-R., & Zhu, X.-Q. (2016). Evaluation of the basic functions of six calcium-dependent protein kinases in Toxoplasma gondii using CRISPR-Cas9 system. *Parasitology Research*, *115*(2), 697–702. https://doi.org/10.1007/s00436-015-4791-6

Wang, L. (2017a). Engineering the Genetic Code in Cells and Animals: Biological Considerations and Impacts. *Accounts of Chemical Research*, *50*(11), 2767–2775. https://doi.org/10.1021/acs.accounts.7b00376

Wang, L. (2017b). Genetically encoding new bioreactivity. *New Biotechnology*, *38*(Pt A), 16–25. https://doi.org/10.1016/j.nbt.2016.10.003

Wang, L., Magliery, T. J., Liu, D. R., & Schultz, P. G. (2000). A New Functional Suppressor tRNA/Aminoacyl−tRNA Synthetase Pair for the in Vivo Incorporation of Unnatural Amino Acids into Proteins. *Journal of the American Chemical Society*, *122*(20), 5010–5011. https://doi.org/10.1021/ja000595y

Wang, L., & Schultz, P. G. (2001). A general approach for the generation of orthogonal tRNAs. *Chemistry & Biology*, *8*(9), 883–890.

Wang, L., Xie, J., & Schultz, P. G. (2006). Expanding the Genetic Code. *Annual Review of Biophysics and Biomolecular Structure*, *35*(1), 225–249. https://doi.org/10.1146/annurev.biophys.35.101105.121507

Wang, M., Cao, S., Du, N., Fu, J., Li, Z., Jia, H., & Song, M. (2017). The moving junction protein RON4, although not critical, facilitates host cell invasion and stabilizes MJ members. *Parasitology*, *144*(11), 1490–1497. https://doi.org/10.1017/S0031182017000968

Wang, Q., Parrish, A. R., & Wang, L. (2009). Expanding the Genetic Code for Biological Studies. *Chemistry & Biology*, *16*(3), 323–336. https://doi.org/10.1016/j.chembiol.2009.03.001

Wang, W., Takimoto, J. K., Louie, G. V., Baiga, T. J., Noel, J. P., Lee, K.-F., Slesinger, P. A., & Wang, L. (2007). Genetically encoding unnatural amino acids for cellular and neuronal studies. *Nature Neuroscience*, *10*(8), 1063–1072. https://doi.org/10.1038/nn1932

Wasmuth, J. D., Pszenny, V., Haile, S., Jansen, E. M., Gast, A. T., Sher, A., Boyle, J. P., Boulanger, M. J., Parkinson, J., & Grigg, M. E. (2012). Integrated Bioinformatic and Targeted Deletion Analyses of the SRS Gene Superfamily Identify SRS29C as a Negative Regulator of Toxoplasma Virulence. *MBio*, *3*(6), e00321-12. https://doi.org/10.1128/mBio.00321-12

Wetzel, D. M., Håkansson, S., Hu, K., Roos, D., & Sibley, L. D. (2003). Actin Filament Polymerization Regulates Gliding Motility by Apicomplexan Parasites. *Molecular Biology of the Cell*, *14*(2), 396–406. https://doi.org/10.1091/mbc.E02-08-0458

Wichroski, M. J., Melton, J. A., Donahue, C. G., Tweten, R. K., & Ward, G. E. (2002). Clostridium septicum Alpha-Toxin Is Active against the Parasitic Protozoan Toxoplasma gondii and Targets Members of the SAG Family of Glycosylphosphatidylinositol-Anchored Surface Proteins. *Infection and Immunity*, *70*(8), 4353–4361. https://doi.org/10.1128/IAI.70.8.4353-4361.2002

Wier, G. M., McGreevy, E. M., Brown, M. J., & Boyle, J. P. (2015). New Method for the Orthogonal Labeling and Purification of Toxoplasma gondii Proteins While Inside the Host Cell. *MBio*, *6*(2). https://doi.org/10.1128/mBio.01628-14

Williams, M. J., Alonso, H., Enciso, M., Egarter, S., Sheiner, L., Meissner, M., Striepen, B., Smith, B. J., & Tonkin, C. J. (2015). Two Essential Light Chains Regulate the MyoA Lever Arm To Promote Toxoplasma Gliding Motility. *MBio*, *6*(5). https://doi.org/10.1128/mBio.00845-15

Wolf, A., Cowen, D., & Paige, B. (1939). Human Toxoplasmosis: Occurrence in Infants as an Encephalomyelitis Verification by Transmission to Animals. *Science*, *89*(2306), 226–227. https://doi.org/10.1126/science.89.2306.226

Xie, J., Wang, L., Wu, N., Brock, A., Spraggon, G., & Schultz, P. G. (2004). The site-specific incorporation of p-iodo-L-phenylalanine into proteins for structure determination. *Nature Biotechnology*, *22*(10), 1297–1301. https://doi.org/10.1038/nbt1013

Yamamoto, M., Standley, D. M., Takashima, S., Saiga, H., Okuyama, M., Kayama, H., Kubo, E., Ito, H., Takaura, M., Matsuda, T., et al. (2009). A single polymorphic amino acid on Toxoplasma gondii kinase ROP16 determines the direct and strain-specific activation of Stat3. *The Journal of Experimental Medicine*, *206*(12), 2747–2760. https://doi.org/10.1084/jem.20091703

Yang, J., Roy, A., & Zhang, Y. (2013a). BioLiP: a semi-manually curated database for biologically relevant ligand-protein interactions. *Nucleic Acids Research*, *41*(Database issue), D1096-1103. https://doi.org/10.1093/nar/gks966

Yang, J., Roy, A., & Zhang, Y. (2013b). Protein-ligand binding site recognition using complementary binding-specific substructure comparison and sequence profile alignment. *Bioinformatics (Oxford, England)*, *29*(20), 2588–2595. https://doi.org/10.1093/bioinformatics/btt447

Yang, J., Yan, R., Roy, A., Xu, D., Poisson, J., & Zhang, Y. (2015). The I-TASSER Suite: protein structure and function prediction. *Nature Methods*, *12*(1), 7–8. https://doi.org/10.1038/nmeth.3213

Young, T. S., & Schultz, P. G. (2010). Beyond the Canonical 20 Amino Acids: Expanding the Genetic Lexicon. *Journal of Biological Chemistry*, *285*(15), 11039–11044. https://doi.org/10.1074/jbc.R109.091306

Zhang, M., Wang, C., Otto, T. D., Oberstaller, J., Liao, X., Adapa, S. R., Udenze, K., Bronner, I. F., Casandra, D., Mayho, M., et al. (2018). Uncovering the essential genes of the human malaria parasite Plasmodium falciparum by saturation mutagenesis. *Science*, *360*(6388), eaap7847. https://doi.org/10.1126/science.aap7847